

Appendix A

Comparison of Simulation Results with TETRAD 12.7 and TETRAD 12.7ms

Appendix A

Comparison of Simulation Results with TETRAD 12.7 and TETRAD 12.7ms

This appendix provides a description of two test problems used to demonstrate comparability between TETRAD Version 12.7 and TETRAD Version 12.7ms. The former was the simulator used for the IRA (Becker et al. 1998) and ABRA (Holdren et al. 2002) models. The latter represents a revision of the Version 12.7 that was created to allow component-specific convergence criteria to be applied to decrease the amount of central processing unit time necessary for completing full-scale simulations for the Operable Unit 7-13/14 RI/FS (Shook et al. 2003). Computational gain results in the Version 12.7ms, because a looser convergence criterion can be applied to noncontaminant components. Shook et al. (2003) describes the agreement in results between the previous and revised versions as “in excellent agreement for each problem,” based on a direct comparison of the two sets of results in terms of absolute and normalized agreement. No additional quantitative details are offered on the comparison of the results.

The purpose of this appendix is to graphically demonstrate this equivalence using two problems. One of the problems is the simplest example from the laboratory-directed research and development report. The other uses the U-238 simulation group from the ABRA. Overall, the two-simulation comparison in this appendix shows essentially the same results, demonstrating equivalence between the original Version 12.7 and the revised Version 12.7ms.

A-1. TEST PROBLEM 1: EX3DT

Test Problem 1 (i.e., ex3dt) was created to mimic, in a simplified fashion, the model previously applied with TETRAD 12.7 in the ABRA. The name given to the simulation is ex3dt, which is excerpted from “example 3-dimensional problem with transport.” The ex3dt problem has a simplified grid and lithology that still contain surficial sediment, fractured basalt, and one sedimentary interbed with a centrally-located gap. Transient sources of water are applied at land surface and at depth on one side of the domain. This source undergoes decay to a daughter product.

A summary of physical and chemical processes included in the simulation is given, followed by a detailed problem description. Then simulation results comparing TETRAD 12.7 and 12.7ms are shown. Lastly, the complete TETRAD data deck for the ex3dt problem is included.

A-1.1 Listing of Processes Included in Simulation

- Advection
- Dispersion
- Diffusion
- Adsorption
- Radioactive decay
- Ingrowth.

A-1.2 Three-Dimensional Domain

- 165 m (541.3 ft) in x-horizontal direction, 19 gridblocks with variable grid spacing
- 165 m (541.3 ft) in y-horizontal direction, 19 gridblocks with variable grid spacing
- 61 m (200.1 ft) in the vertical direction, 24 gridblocks with variable grid spacing
- Vertical slice shown in Figure A-1.

A-1.3 Lithology

Two material property zones were simulated as indicated in Figure A-2. The gap in material Type 2 allows water and tracers to move vertically downward.

A-1.4 Hydrologic Properties

Material	1	2
Permeability, X-direction	3,500 mD	1 mD
Permeability, Y-direction	700 mD	1 mD
Porosity	0.48	0.15
van Genuchten alpha	2.0 m^{-1}	1.5 m^{-1}
van Genuchten beta (aka N)	1.8	1.2

A-1.5 General Transport Properties

- Two water-equivalent tracer constituents, a parent and a daughter product
- Half-life of parent (W2 in TETRAD nomenclature) is 34.657 days
- Half-life of daughter (W3) is 346.57 days
- Molecular diffusion is $1.0 \times 10^{-5} \text{ cm}^2/\text{second}$ ($8.64 \times 10^{-5} \text{ m}^2/\text{day}$)
- Tortuosity is uniform and assigned a value of 10
- Dispersion coefficients are 14.4 and 1.4 m for longitudinal and transverse, respectively.

A-1.6 Material-Specific Transport Properties

Material	1	2
Partition coefficient, tracer #1	0 mL/g	1,000 mL/g
Partition coefficient, tracer #2	0 mL/g	500 mL/g

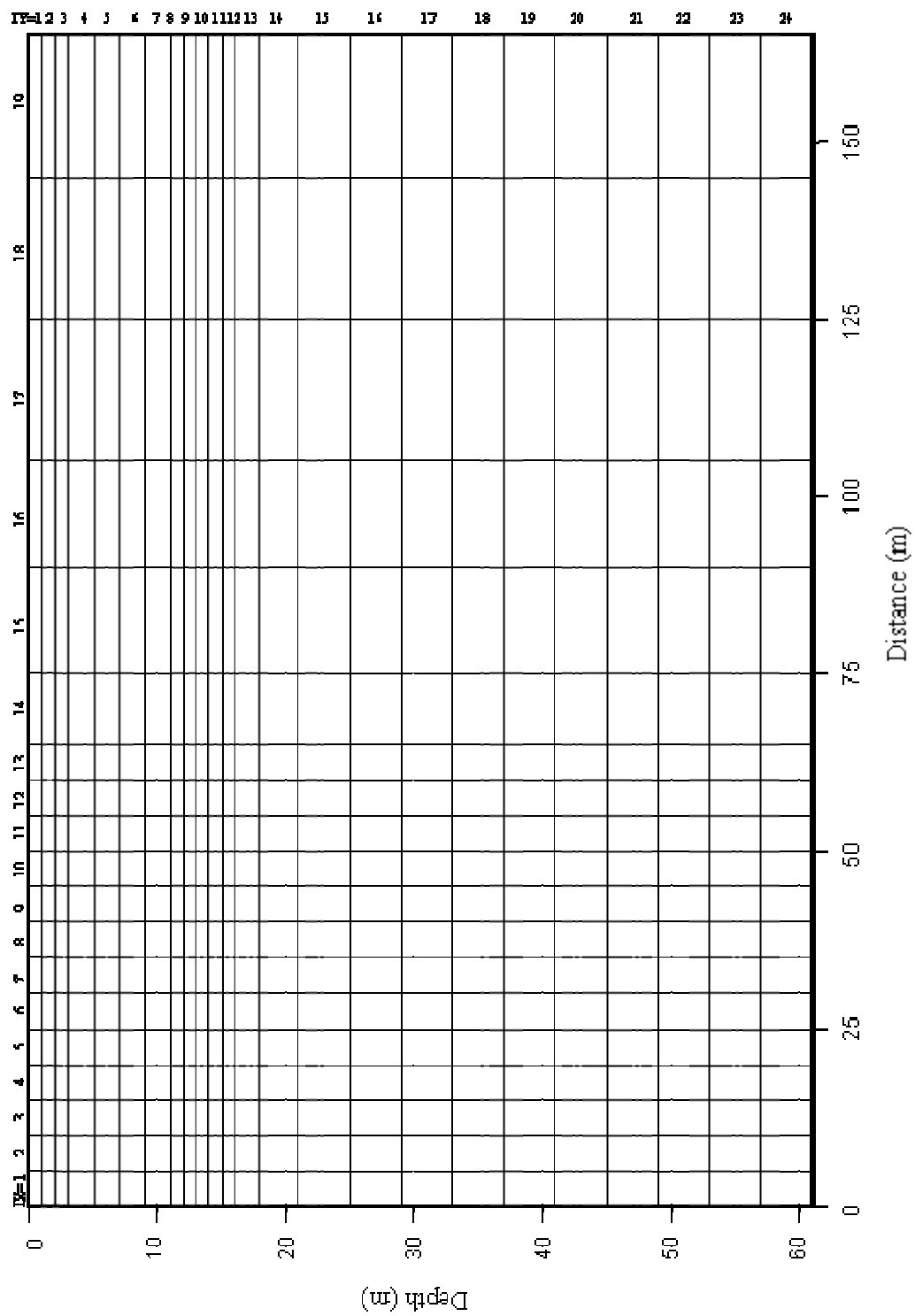


Figure A-1. Simulation domain.

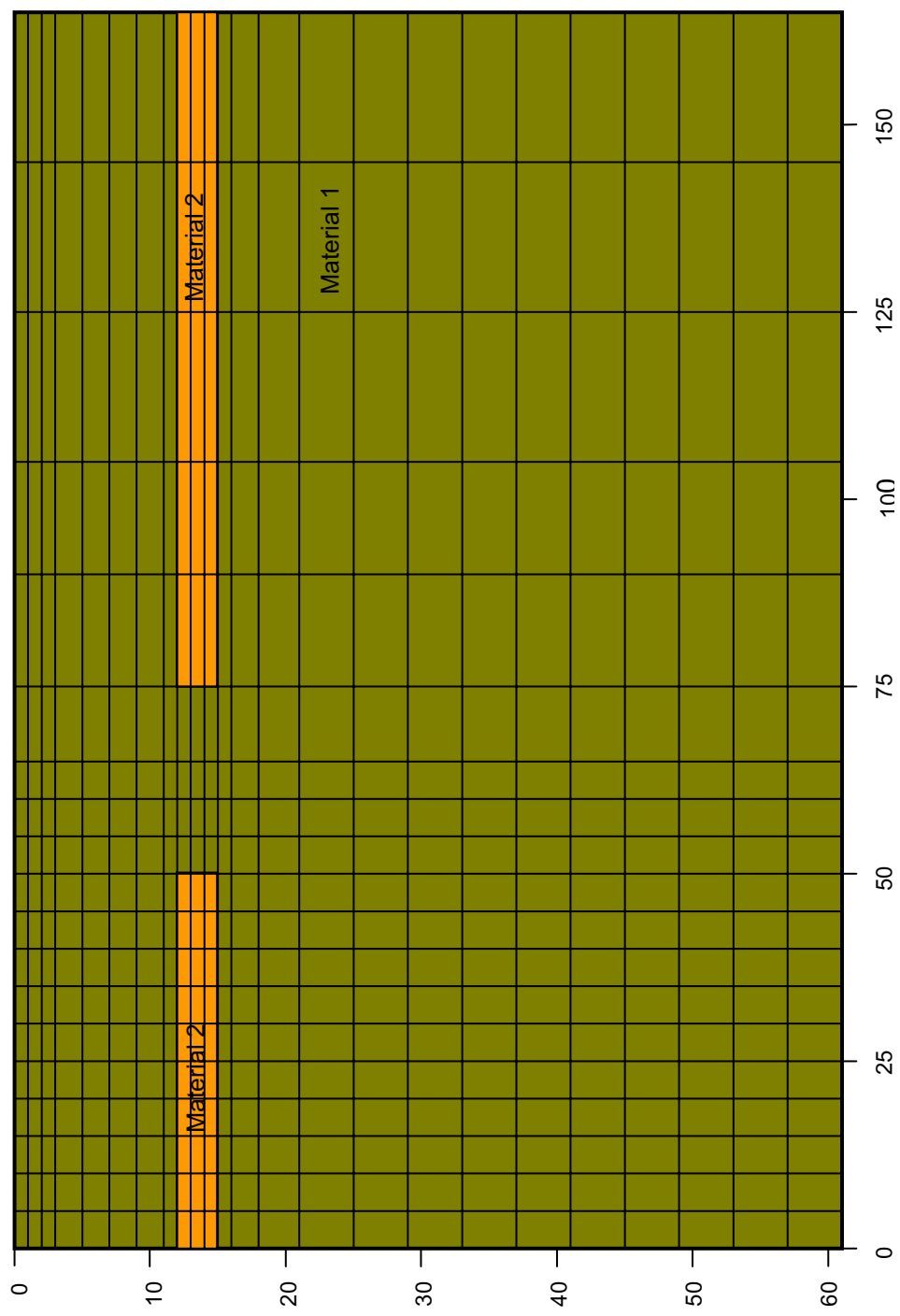


Figure A-2. Lithologic properties.

A-1.7 Boundary Conditions

Surface background infiltration rate is 1 cm/year ($0.02738 \text{ kg/m}^2/\text{day}$).

A head differential of 2 m (6.6 ft) is applied from left to right across the lower 20 m (65.6 ft) (i.e., five gridblocks) of the simulation domain (see Figure A-3).

A-1.8 Transient Water Sources

A water flux is applied to emulate a surface flood at the rate of 100 cm/year ($2.738 \text{ kg/m}^2/\text{day}$) for a 500-day duration from simulation time 1,000 to 1,500 days. This flood applies to the surface over the three gridblocks from 30 to 45 m (98.4 to 147.6 ft). The flooding flux supersedes the background infiltration rate for the time period it is applied.

An additional lateral influx of water is applied at the left edge of the simulation domain as indicated in Figure A-3. This influx consists of water applied at a rate of 1,000 cm/year over the 5-m (16.4-ft) surface of the indicated gridblock for 150 days beginning at simulation day 1,350. This equates to $2,055 \text{ m}^3$ of water being added at depth to the simulation domain over 150 days.

A-1.9 Tracer Loading

The parent tracer is loaded at a constant rate of $1.\text{e-}3 \text{ kg/m}^2/\text{day}$ from simulation time 0 to 1,100 days.

A-1.10 Simulation Results

Simulation results are compared in time histories of the tracer mole fraction of the parent (W2), daughter mole fraction (W3), and water saturation (SW) in Figures A-4, A-5, and A-6, respectively. Tracer mole fractions can be seen to have the “excellent” agreement referred to in Shook et al. (2003). Water saturations also agree almost to the same extent, with the exception of comparison point four, where the TETRAD 12.7 result is slightly greater. This difference was not unexpected because a looser convergence criterion was used for the pure water component; and there was no difference in the transport of the tracers through this region.

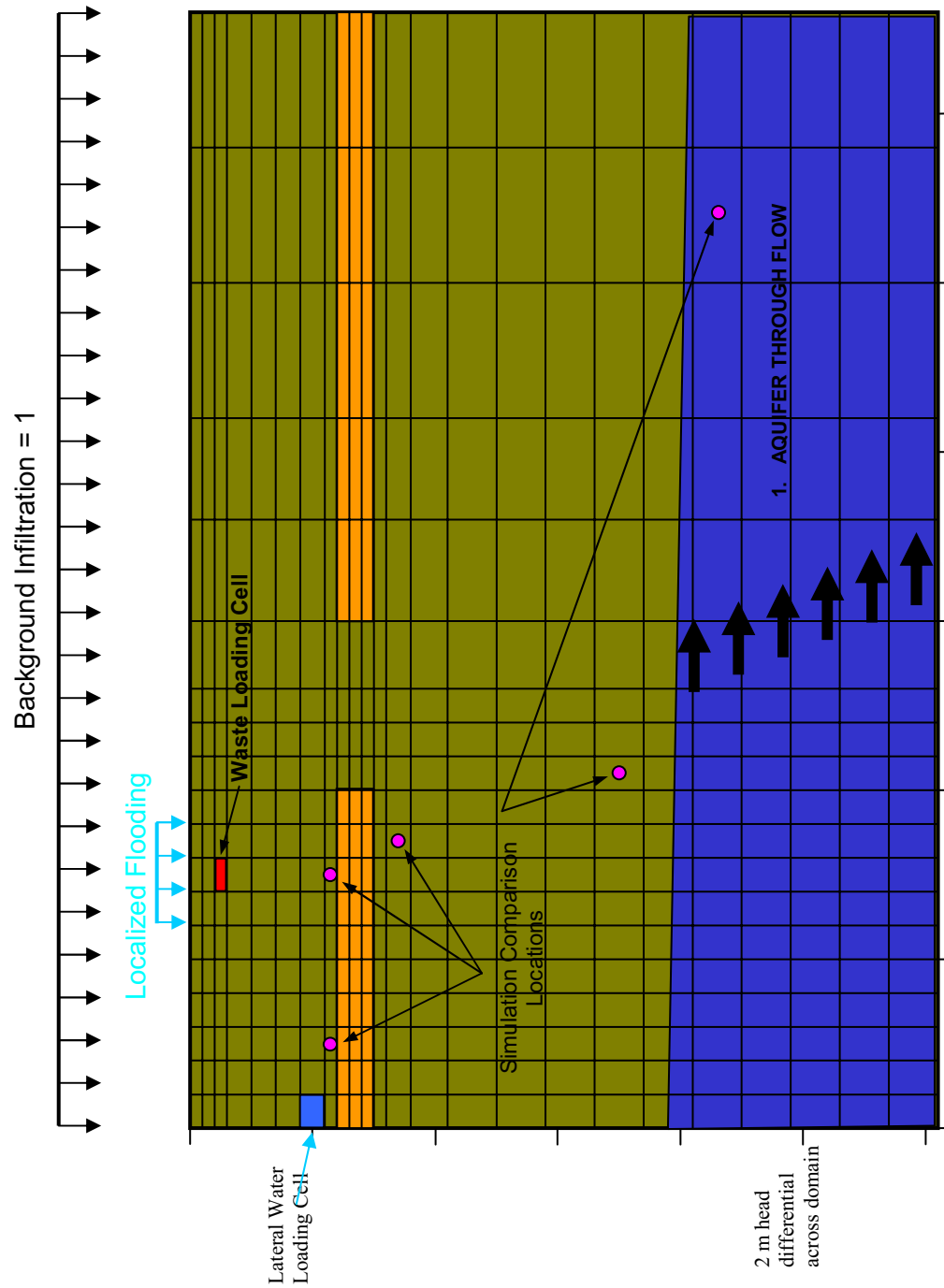


Figure A-3. Boundary conditions.

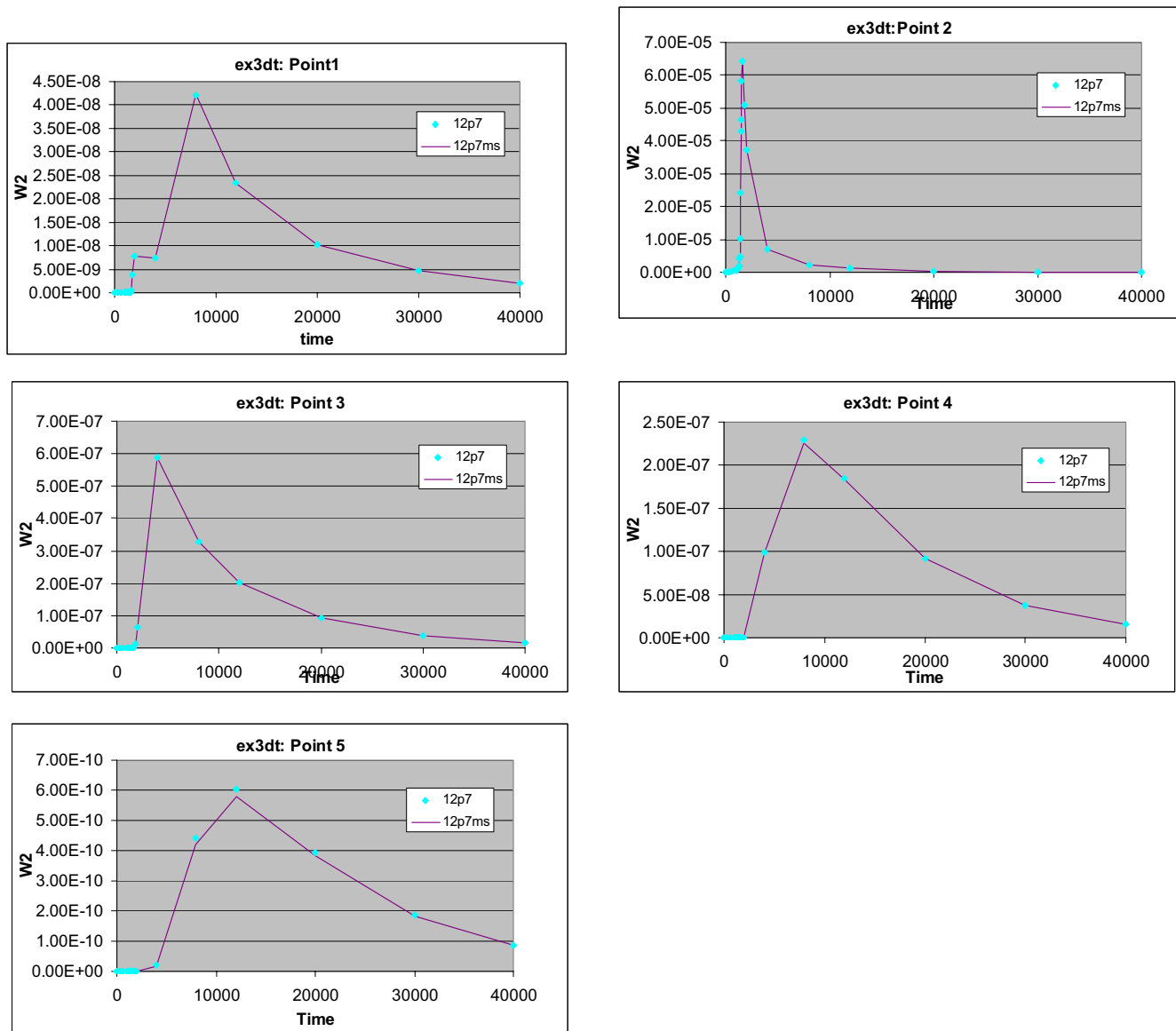


Figure A-4. Comparison of simulated mole fraction of parent (W_2) at comparison points with TETRAD 12.7 and 12.7ms.

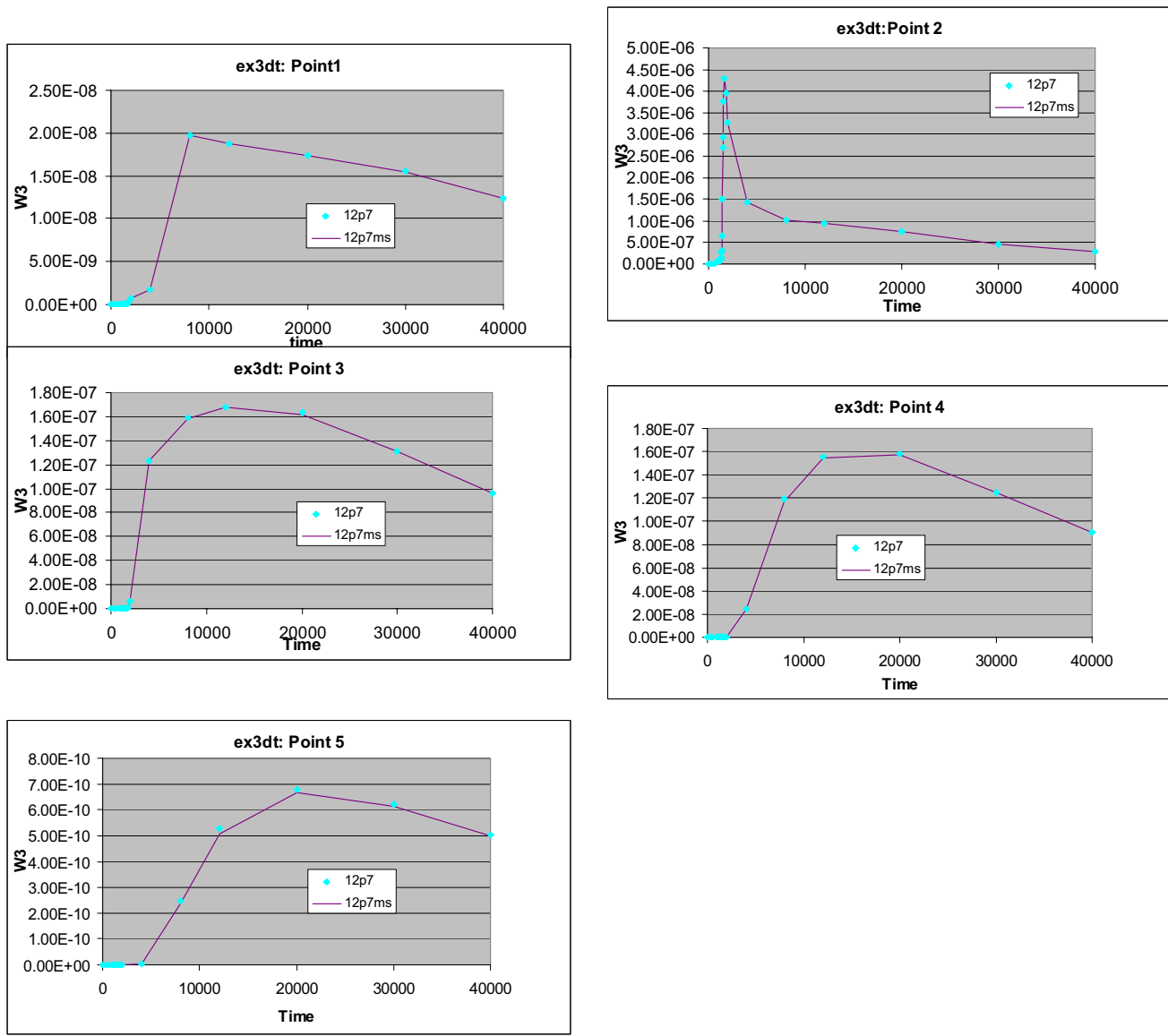


Figure A-5. Comparison of simulated mole fraction of daughter tracer (W_3) at comparison points with TETRAD 12.7 and 12.7ms.

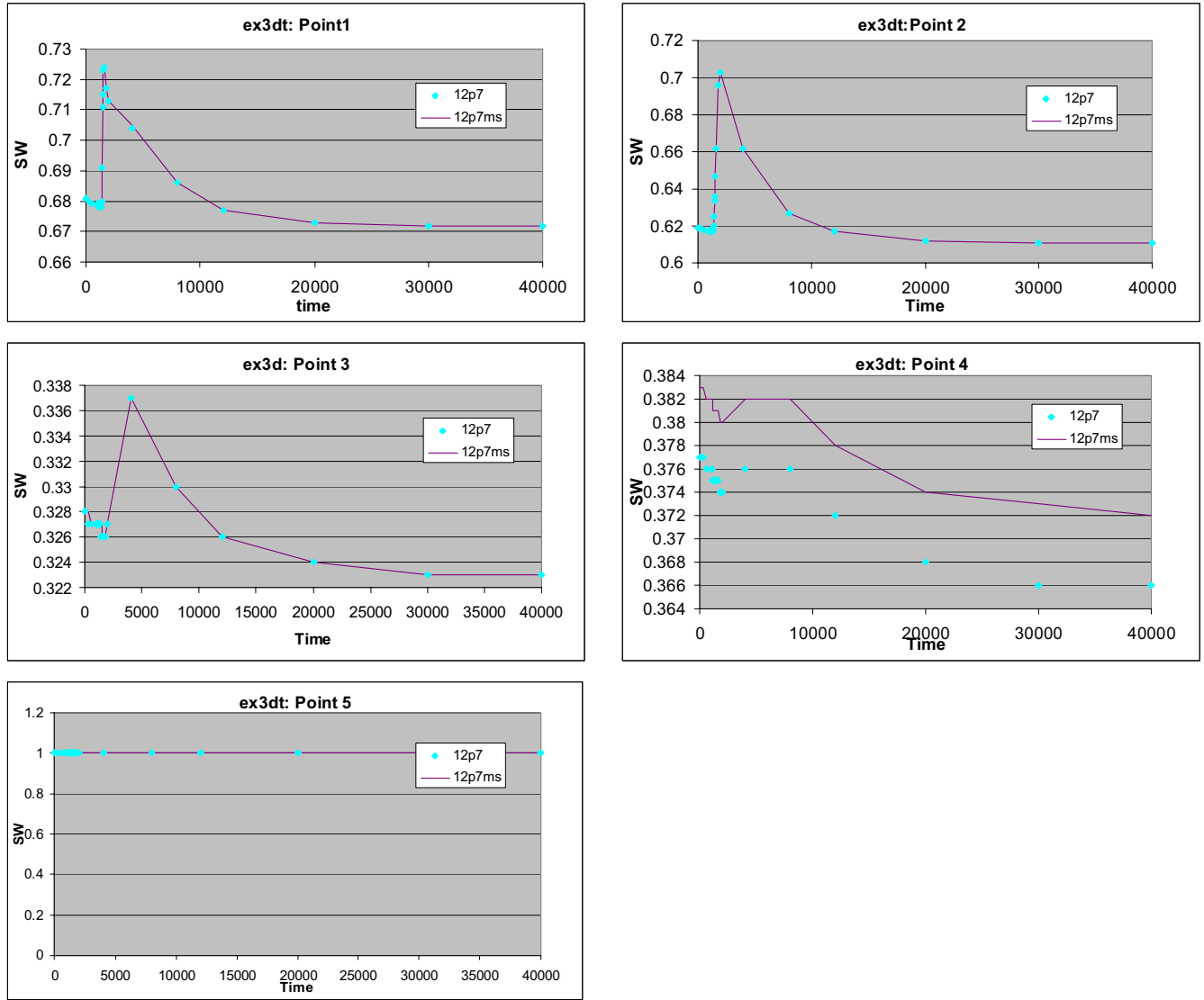


Figure A-6. Comparison of simulated water saturation (SW) at comparison points with TETRAD 12.7 and 12.7ms.

A-1.11 Simulation Deck

The input deck for problem ex3dt is given below. The same simulation deck was used with both the TETRAD 12.7 and 12.7ms data decks, with one exception—the ‘SCALE’ card was not used in the TETRAD 12.7 simulation because it represents loosening of the convergence criterion that can be achieved with the TETRAD 12.7ms simulator.

```
'COMMENT'  '3d variably saturated flow and transport simulation'
'TYPE'      2   5   3   0.   0.
'UNITS'     1   1   0   0
'DIMEN'    19  19  24  20
'PRINT'     0   1   0   2   0
'OUTFUN'    3   1   0   0   0   0   0   0   0
'OUTGEO'    0   0   0   0   0   0   0   0   2   0
```

```

'OUTPROP' 0 0 0 0 0 0 0 0 0 0 0 0
'OUTMISC' 0 0 0 0 0 0 0 0 0 0 0 0
'OUTREF' 3 1 0 0
'EXMBAL' 1
'NEWT' ,7,1.e-7,,,,,,,
'SCALE' 1.e+4 1.0 1.0 1.e+4 1.e+4
'TMSTEP' ,4,,,0.6,,,
'ITER' 60 ,,,,
'DELX' 1
19 5. 5. 5. 5. 5. 5. 5. 5. 5. 5. 5. 10. 15. 15. 20. 20. 20.
'DELY' 1
19 19*5.
'DELZ' 1
24 1. 1. 1. 2. 2. 2. 1. 1. 1. 1. 2. 3. 4. 4. 4. 4. 3. 6. 3. 4. 4. 4.
'FTOPS' 0 0
'COMP' 1.E-7 101.325 0. 20.
'SHIFT' 1.e-5,,,
'PROPERTY'
'VANGEN' 99 1 2.0 1.8 0.0 0.15 0.0 0.1 1.0 0.0 1.0,,, material A
'VANGEN' 99 2 1.5 1.2 0.0 0.25 0.0 0.1 1.0 0.0 1.0,,, material B
'COMMENT' '
'DENCS' 1000. 1000. 1000. 1.22 1584.
1 1 1 2 1
18.02 18.02 18.02 29. 154.
'LIQDEN'
,,0.,101.325,15,,,
,,0.,101.325,15,,,
,,0.,101.325,15,,,
300,,,
1584,,,
'CRITG' 1
,,,
,,,
,,,
3771.8 132.8 .0032
5000. 550. .0018
'LIQVIS'
,,,
,,,
,,,
.5 0.
1. 0.
'GASVIS'
.0181 0. 1. 0. 1.
.0181 0. 1. 0. 1.
.0181 0. 1. 0. 1.
.0181 0. 1. 0. 1.
.0181 0. 1. 0. 1.
'KVAL' 0.0 0.0 0.0 0.001 9.7e-5
1.186e7 -20.96 2.549e-3 3816. 46.13
1.186e7 -20.96 2.549e-3 3816. 46.13
1.186e7 -20.96 2.549e-3 3816. 46.13
8.621e8 0. 0. 3103.4 0.16
9.7 0. 0. 0. 0.
'TEMPMOD' 1 8664 1 15.
'DENRMOD' 1 8664 1 2700.
'WMOD' 1 8664 1 1. 0. 0. 0. 0.

```

```

'YMOD'      1   8664  1   0.  0.  0.    1.  0.
'XMOD'      1   8664  1   0.  0.  0.    .01  .1
'COMMENT'   ' assign porosities'
'PORZLAY'   1 0.48
'PORZLAY'   2 0.48
'PORZLAY'   3 0.48
'PORZLAY'   4 0.48
'PORZLAY'   5 0.48
'PORZLAY'   6 0.48
'PORZLAY'   7 0.48
'PORZLAY'   8 0.48
'PORZLAY'   9 0.15
'PORZLAY'  10 0.15
'PORZLAY'  11 0.15
'PORZLAY'  12 0.48
'PORZLAY'  13 0.48
'PORZLAY'  14 0.48
'PORZLAY'  15 0.48
'PORZLAY'  16 0.48
'PORZLAY'  17 0.48
'PORZLAY'  18 0.48
'PORZLAY'  19 0.48
'PORZLAY'  20 0.48
'PORZLAY'  21 0.48
'PORZLAY'  22 0.48
'PORZLAY'  23 0.48
'PORZLAY'  24 0.48
'COMMENT'   'put a gap in the low perm layer'
'PORMOD' 3051 3054  1 0.48
'PORMOD' 3412 3415  1 0.48
'PORMOD' 3775 3776  1 0.48
'PORMOD' 3070 3073  1 0.48
'PORMOD' 3431 3434  1 0.48
'PORMOD' 3792 3795  1 0.48
'PORMOD' 3089 3092  1 0.48
'PORMOD' 3450 3453  1 0.48
'PORMOD' 3811 3814  1 0.48
'COMMENT'   ' assign permeability'
'PERMZLAY' 1 2*3500.0 700.
'PERMZLAY' 2 2*3500.0 700.
'PERMZLAY' 3 2*3500.0 700.
'PERMZLAY' 4 2*3500.0 700.
'PERMZLAY' 5 2*3500.0 700.
'PERMZLAY' 6 2*3500.0 700.
'PERMZLAY' 7 2*3500.0 700.
'PERMZLAY' 8 2*3500.0 700.
'PERMZLAY' 9 3*1.0
'PERMZLAY' 10 3*1.0
'PERMZLAY' 11 3*1.0
'PERMZLAY' 12 2*3500.0 700.
'PERMZLAY' 13 2*3500.0 700.
'PERMZLAY' 14 2*3500.0 700.
'PERMZLAY' 15 2*3500.0 700.
'PERMZLAY' 16 2*3500.0 700.
'PERMZLAY' 17 2*3500.0 700.
'PERMZLAY' 18 2*3500.0 700.
'PERMZLAY' 19 2*3500.0 700.

```

```

'PERMZLAY' 20 2*3500.0 700.
'PERMZLAY' 21 2*3500.0 700.
'PERMZLAY' 22 2*3500.0 700.
'PERMZLAY' 23 2*3500.0 700.
'PERMZLAY' 24 2*3500.0 700.
'COMMENT'  'put a gap in the low perm layer'
'PERMMOD' 3051 3054 1 3*3500.0 700.
'PERMMOD' 3412 3415 1 3*3500.0 700.
'PERMMOD' 3775 3776 1 3*3500.0 700.
'PERMMOD' 3070 3073 1 3*3500.0 700.
'PERMMOD' 3431 3434 1 3*3500.0 700.
'PERMMOD' 3792 3795 1 3*3500.0 700.
'PERMMOD' 3089 3092 1 3*3500.0 700.
'PERMMOD' 3450 3453 1 3*3500.0 700.
'PERMMOD' 3811 3814 1 3*3500.0 700.
'COMMENT'  ' assign relative permeability tables'
'RKREG'    1 8664 1 1
'RKREG'    2889 3971 1 2      'low perm layer'
'COMMENT'  'put a gap in the low perm layer'
'RKREG'    3051 3054 1 1
'RKREG'    3412 3415 1 1
'RKREG'    3775 3776 1 1
'RKREG'    3070 3073 1 1
'RKREG'    3431 3434 1 1
'RKREG'    3792 3795 1 1
'RKREG'    3089 3092 1 1
'RKREG'    3450 3453 1 1
'RKREG'    3811 3814 1 1
'COMMENT'  ' sorption table with '
'ADSREG'   1 8664 1 1
'ADSREG'   2889 3971 1 2
'COMMENT'  'put a gap in the low perm layer'
'ADSREG'   3051 3054 1 1
'ADSREG'   3412 3415 1 1
'ADSREG'   3775 3776 1 1
'ADSREG'   3070 3073 1 1
'ADSREG'   3431 3434 1 1
'ADSREG'   3792 3795 1 1
'ADSREG'   3089 3092 1 1
'ADSREG'   3450 3453 1 1
'ADSREG'   3811 3814 1 1
'COMMENT'  'assign rad decay half-lives'
'SCRACK'  2 1 1.0 ,,, decay c2=>c3
          0.0 0.0 0.0 2.0e-2           0.0 0.0
'SCRACK'  3 1 1.0 ,,, decay c3=>c1
          0.0 2.0e-3 0.0 0.0           0.0 0.0
'MOLDIFF' 1.0
0.     8.64e-5 8.64e-5    0.     8.64e-5
0.     0.         0.         0.     0.864
0.     0.         0.         0.     0.
'TORMOD'   1 456        1       10.
'DISPER'   14.4 1.4 0. 0. 0. 0.
'ADSORP'   1 1 ,,,,,,,,,,Table 1 for Material 1
0.     0.     1.
0.     0.     1.
0.     0.     1.
0.     0.     1.

```

```

0.      0.      1.
'ADSORP'    1    2    ,,,,,,,,,,,Table 2 for Material 2
0.      0.      1.
1000.    0.      1.
500.     0.      1.
0.      0.      1.
0.      0.      1.
'GVWRITE' -1    0
5 'W2' 'W3' 'SW' 'PW' 'PG'
'COMMENT' 'set initial conditions'
'PRES'      101.325   0.      0.012
'SATMOD'    1    6859    1    0.6  0.0      ,,,, entire vadose zone
'SATMOD'    2889   3971    1    0.001 0.0      ,,,, lowperm interbed
'SATMOD'    3051   3054    1    0.6  0.0      ,,,, interbed gap
'SATMOD'    3412   3415    1    0.6  0.0
'SATMOD'    3775   3776    1    0.6  0.0
'SATMOD'    3070   3073    1    0.6  0.0
'SATMOD'    3431   3434    1    0.6  0.0
'SATMOD'    3792   3795    1    0.6  0.0
'SATMOD'    3089   3092    1    0.6  0.0
'SATMOD'    3450   3453    1    0.6  0.0
'SATMOD'    3811   3814    1    0.6  0.0
'SATMOD'    6860   8664    1    0.0  0.0      ,,,, aquifer
'RECUR'
'TIMEYR'    0
'TIME'     -14000. .001
'TIME'     -13998. -1.
'AQUIFER'  'SSTATE'    1    361    1    3  2    ,,,,,,,,,,,,
'COMMENT' 'aquifers right side boundary'
'AQUIFER'  'SSTATE'    6878    7220    19   1  1    ,,,,,,,,,,,,
'AQUIFER'  'SSTATE'    7239    7581    19   1  1    ,,,,,,,,,,,,
'AQUIFER'  'SSTATE'    7600    7942    19   1  1    ,,,,,,,,,,,,
'AQUIFER'  'SSTATE'    7961    8303    19   1  1    ,,,,,,,,,,,,
'AQUIFER'  'SSTATE'    8322    8664    19   1  1    ,,,,,,,,,,,,
'COMMENT' 'aquifers left side boundary'
'AQUIFER'  'SSTATE'    6860    7202    19   1  1    ,,,,,,,,,,,,
'AQUIFER'  'SSTATE'    7221    7563    19   1  1    ,,,,,,,,,,,,
'AQUIFER'  'SSTATE'    7582    7924    19   1  1    ,,,,,,,,,,,,
'AQUIFER'  'SSTATE'    7943    8285    19   1  1    ,,,,,,,,,,,,
'AQUIFER'  'SSTATE'    8304    8646    19   1  1    ,,,,,,,,,,,,
'COMMENT' 'add del pres = 2 m of water on the left side'
'AQUADDP'    6860    7202    19  19.62
'AQUADDP'    7221    7563    19  19.62
'AQUADDP'    7582    7924    19  19.62
'AQUADDP'    7943    8285    19  19.62
'AQUADDP'    8304    8646    19  19.62
'MFLUX'     1    361   1  3    .02738   0.    0.    0.    0.
'TIME'     -12000. -1.0
'TIME'     -10000. -1.0
'TIME'     -7000.  -1.0
'TIME'     -5000.  -1.0
'TIME'     -3000.  -1.0
'TIME'     -1000.  -1.0
'TIME'     -500.   -1.0
'TIME'      0.    -1.0
'COMMENT' 'begin releasing tracer as component #2'
'MFLUX'    901  901    1  3    0.    1.e-3   0.    0.    0.

```

```

'TIME'    200.    -1.0
'TIME'    400.    -1.0
'TIME'    600.    -1.0
'TIME'    800.    -1.0
'TIME'    1000.   -1.0
'COMMENT' 'localized flood AT SURFACE'
'MFLUX'    159 161    1  3      2.738  0.  0.  0.  0.
'MFLUX'    178 180    1  3      2.738  0.  0.  0.  0.
'MFLUX'    197 199    1  3      2.738  0.  0.  0.  0.
'TIME'    1010.   -1.0
'TIME'    1030.   -1.0
'TIME'    1100.   -1.0
'COMMENT' 'end releasing tracer as component #2'
'MFLUX'    901 901    1  3      0.  0.      0.  0.  0.
'TIME'    1150.   -1.0
'TIME'    1200.   -1.0
'TIME'    1250.   -1.0
'TIME'    1300.   -1.0
'TIME'    1350.   -1.0
'COMMENT' 'lateral influx of water at left boundary'
'MFLUX'  2319 2357    19  3     2.738  0.  0.  0.  0.
'TIME'    1360.   -1.0
'TIME'    1380.   -1.0
'TIME'    1400.   -1.0
'TIME'    1430.   -1.0
'TIME'    1460.   -1.0
'TIME'    1500.   -1.0
'COMMENT' 'return to ambient infiltration at top and no lateral influx'
'MFLUX'    159 161    1  3      .02738  0.  0.  0.  0.
'MFLUX'    178 180    1  3      .02738  0.  0.  0.  0.
'MFLUX'    197 199    1  3      .02738  0.  0.  0.  0.
'COMMENT' 'shut off lateral influx'
'MFLUX'  2319 2357    19  3     0.000   0.  0.  0.  0.
'TIME'    1510.   -1.0
'TIME'    1550.   -1.0
'TIME'    1600.   -1.0
'TIME'    1700.   -1.0
'TIME'    1800.   -1.0
'TIME'    2000.   -1.0
'TIME'    3000.   -1.0
'TIME'    4000.   -1.0
'TIME'    5000.   -1.0
'TIME'    6000.   -1.0
'TIME'    7000.   -1.0
'TIME'    8000.   -1.0
'TIME'    9000.   -1.0
'TIME'   10000.  -1.0
'TIME'   12000.  -1.0
'TIME'   14000.  -1.0
'TIME'   16000.  -1.0
'TIME'   18000.  -1.0
'TIME'   20000.  -1.0
'TIME'   22000.  -1.0
'TIME'   24000.  -1.0
'TIME'   26000.  -1.0
'TIME'   28000.  -1.0
'TIME'   30000.  -1.0

```

```

'TIME' 32000. -1.0
'TIME' 34000. -1.0
'TIME' 36000. -1.0
'TIME' 38000. -1.0
'TIME' 40000. -1.0

```

A-2. TEST PROBLEM 2: B_GRP5

Test Problem 2 (i.e., b_grp5) compares TETRAD 12.7 and 12.7ms when applied to a full-scale SDA problem that was simulated in the ABRA. The TETRAD data deck for the U-238 simulation group (named b_grp5) from the ABRA was used. This data deck is too large to include in this appendix. A complete description of the simulation domain, parameterization, and source loading can be found in the ABRA. The b_grp5 simulation included U-238, U-234, Th-230, Ra-226, and Pb-210. The processes simulated included advection, dispersion, diffusion, adsorption, radioactive decay, and ingrowth. The simulations were performed with a relative convergence criterion of 1×10^{-7} for all components in the TETRAD 12.7 simulation. This same convergence criterion was applied to contaminants in the TETRAD 12.7ms simulation, but was relaxed four orders of magnitude for the pure water, air, and oleic components.

Comparisons in this section are provided as a time history of vertical flux values of components at individual gridblocks at the base of the simulation domain. These individual fluxes are the primary results of the vadose zone model for Operable Unit 7-13/14, because they are then used as input for the aquifer simulations. Figure A-7 shows where flux table comparisons were made with the numbers, indicating the specific flux tables where comparisons might be made.

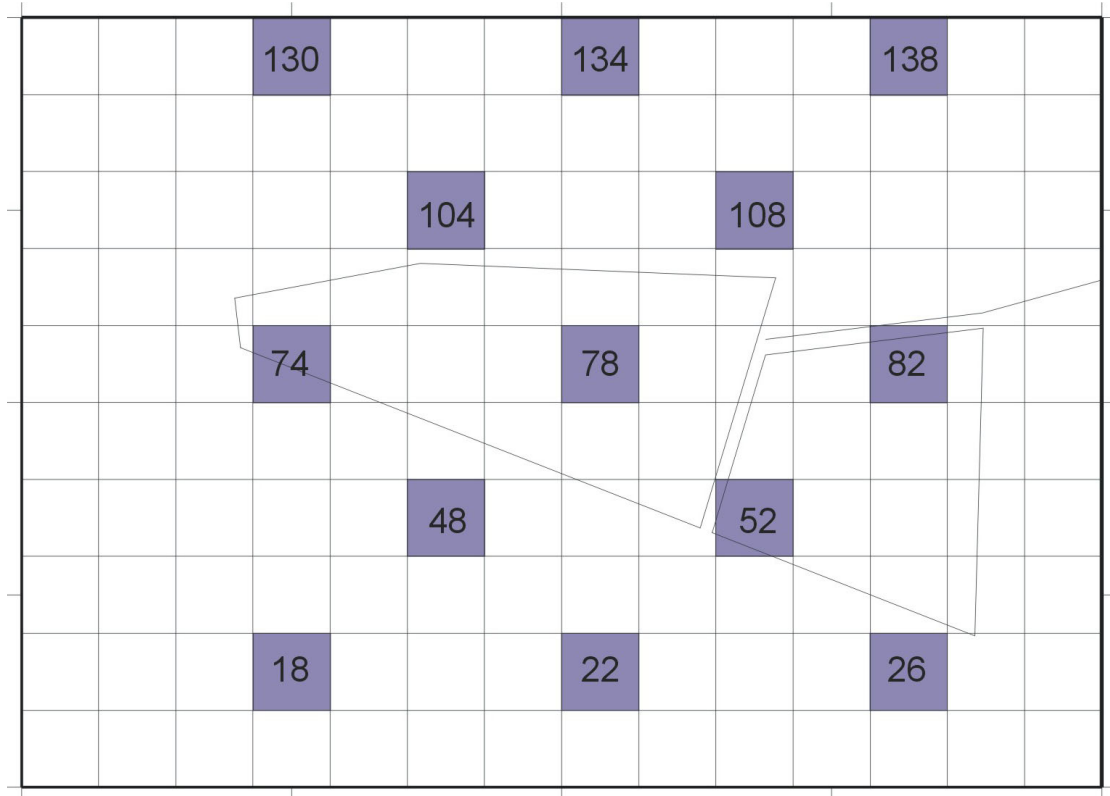


Figure A-7. Locations where fluxes from the Ancillary Basis for Risk Analysis vadose zone model were considered for comparison.

Simulation duration was just over 3,666,000 days or approximately 10,000 years. Figures A-8 through A-18 show time-history comparisons, with the time axis presented in simulation days.

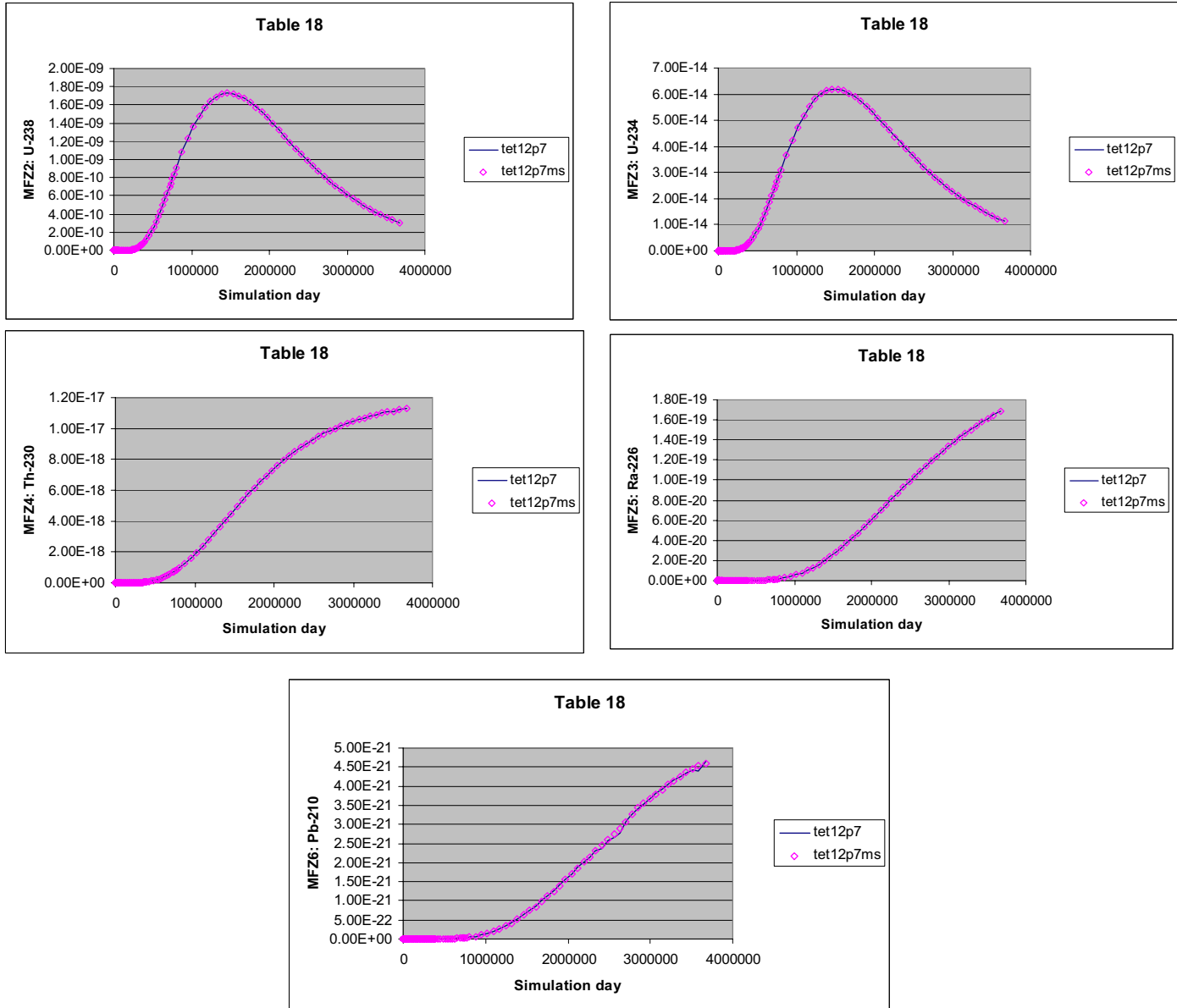


Figure A-8. Simulated flux of uranium-238, uranium-234, thorium-230, radium-228, and lead-210 at grid location 18 with TETRAD 12.7 and 12.7ms.

The first set of results in Figure A-8 shows absolute magnitude of flux for all five contaminants for both TETRAD 12.7 and 12.7ms. The results appear identical. Figure A-9 shows the percentage difference as a function of time, with the percentage calculated by normalized against the TETRAD 12.7 result. These percentage difference results are slightly more interesting and primarily show the effect of dividing by small numbers. All contaminants show a large initial spike in percent difference at very early times as the initial contaminant front advances to the bottom of the simulation domain, resulting in very low concentrations at early times in both simulations. These lead to division by small numbers in the percentage difference calculation that can result in a larger percentage difference due to precision limitations. Lead-210, being the last member of the decay chain, shows the widest degree of variability over the entire simulation period, likely due to the same reason of division by very small numbers as can be seen in the magnitude of the fluxes in Figure A-8.

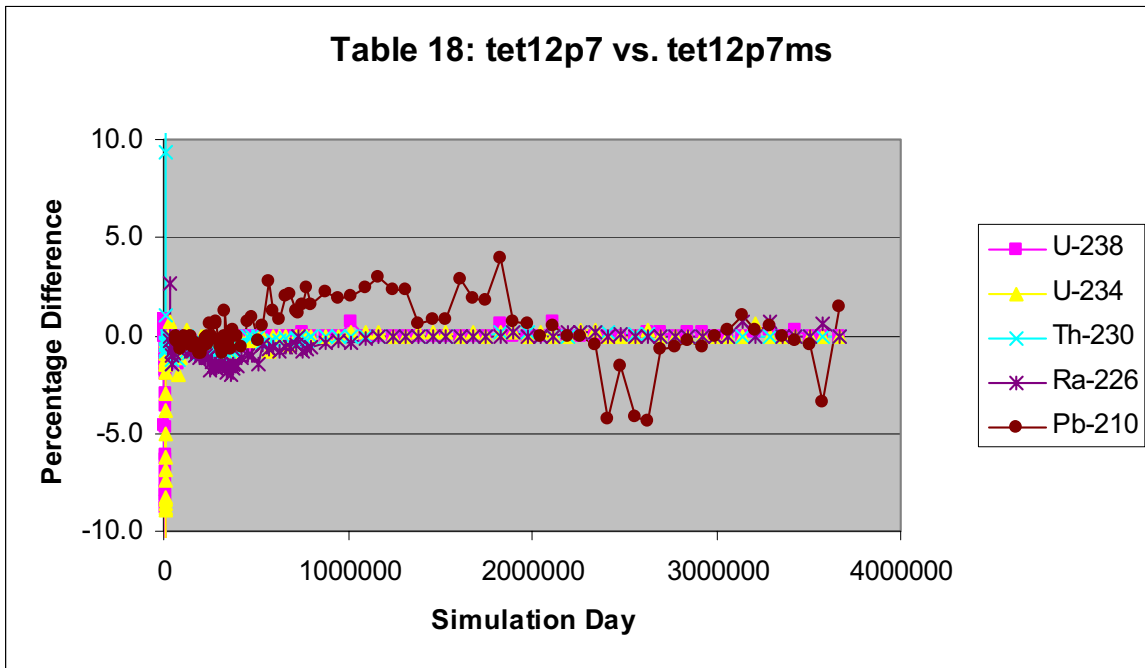


Figure A-9. Percentage difference between TETRAD 12.7 and 12.7ms fluxes as a function of time at grid location 18.

The only other grid location where the full sequence of fluxes from the vadose zone is shown is grid location 78, located directly beneath the SDA. These fluxes are shown in Figure A-10 with the percentage differences shown in Figure A-11. The percentage differences for grid location 78 are similar, but slightly different, from those for grid location 18 (shown previously). Grid 78 results lead to similar conclusions as those for grid 18. The magnitude of the fluxes over time show excellent agreement between TETRAD 12.7 and 12.7ms. The percentage differences also show very early deviation, likely due to precision limitations, with good agreement overall and the Pb-210 showing the most fluctuations over time.

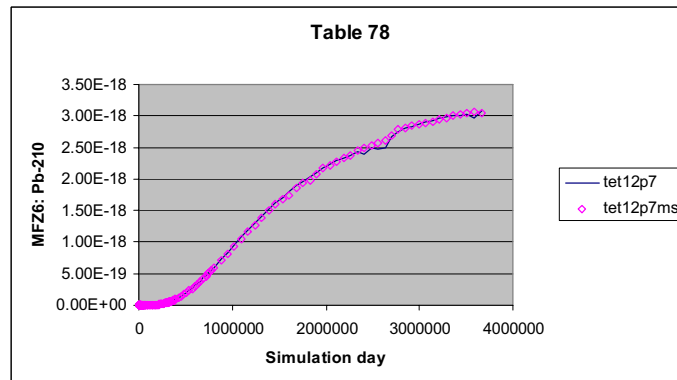
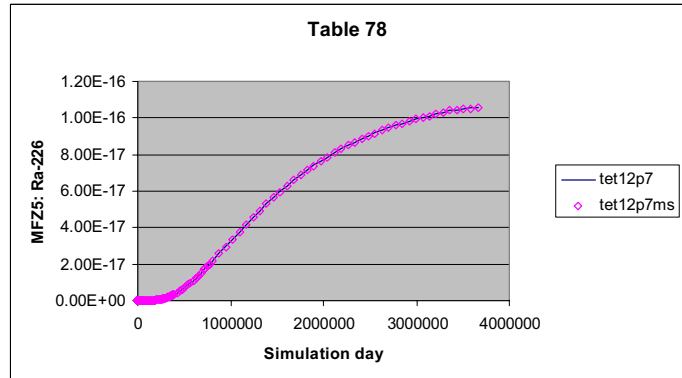
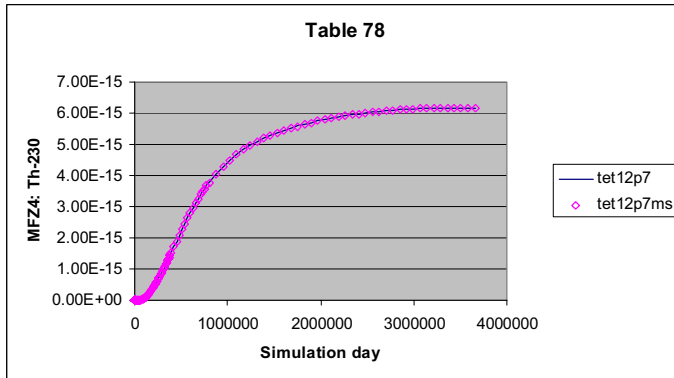
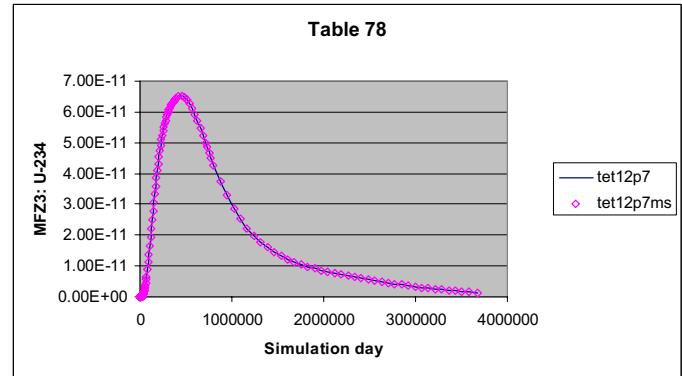
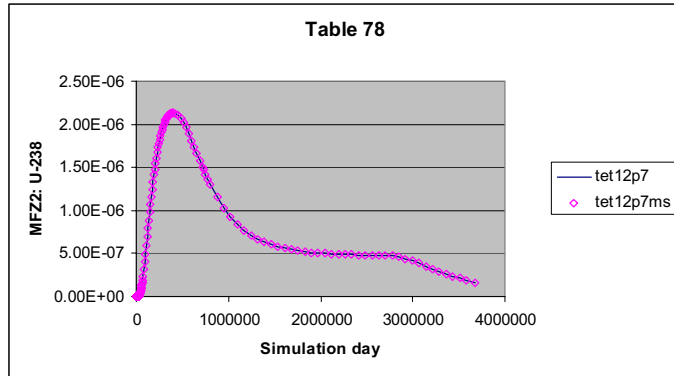


Figure A-10. Simulated flux of uranium-238, uranium-234, thorium-230, radium-228, and lead-210 at grid location 78 with TETRAD 12.7 and 12.7ms.

Table 78: tet12p7 vs. tet12p7ms

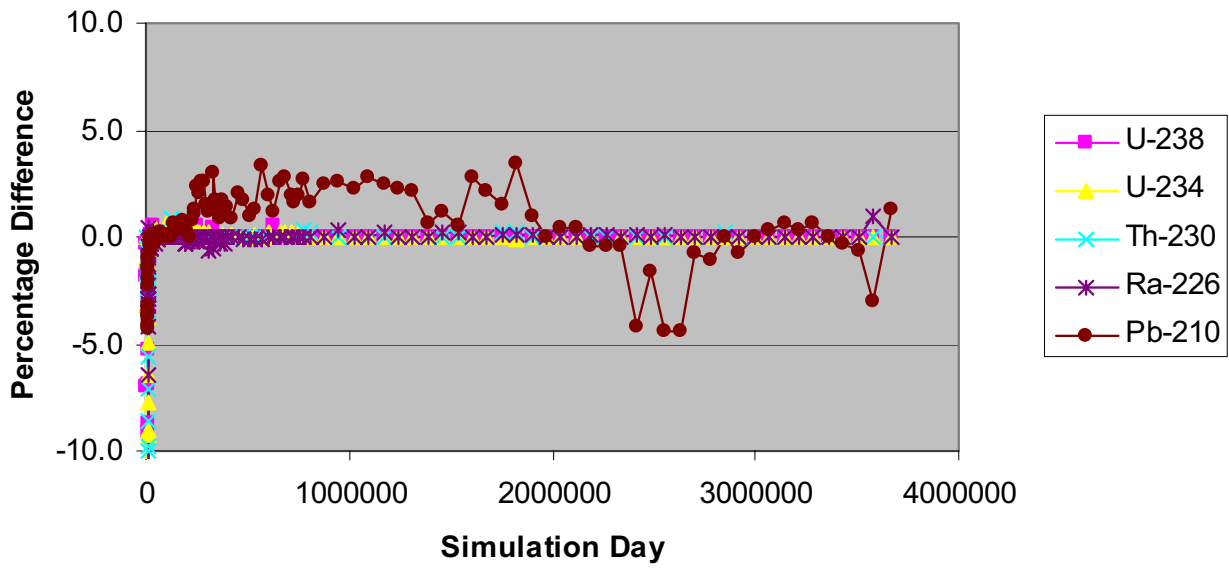
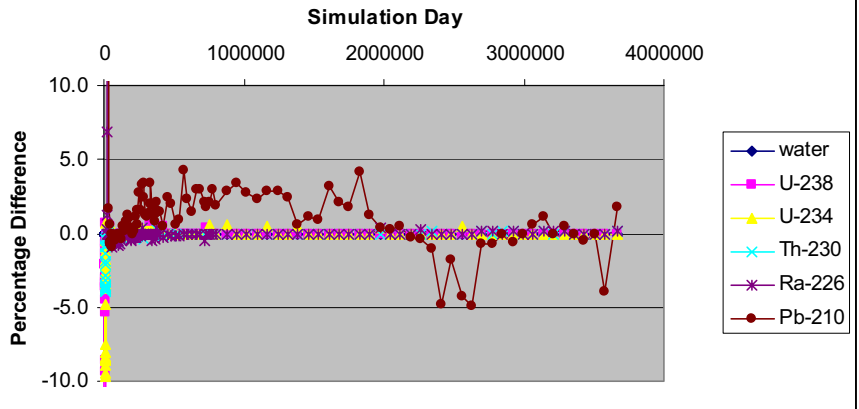


Figure A-11. Percentage difference between TETRAD 12.7 and 12.7ms fluxes as a function of time at grid location 78.

Percentage differences for most of the other indicated comparison locations from Figure A-8 are shown in Figures A-12 and A-13. Figures A-12 and A-13 also show the same result of excellent agreement between the TETRAD 12.7 and 12.7ms simulators.

Table 22: tet12p7 vs. tet12p7ms



**Table 26
: tet12p7 vs. tet12p7ms**

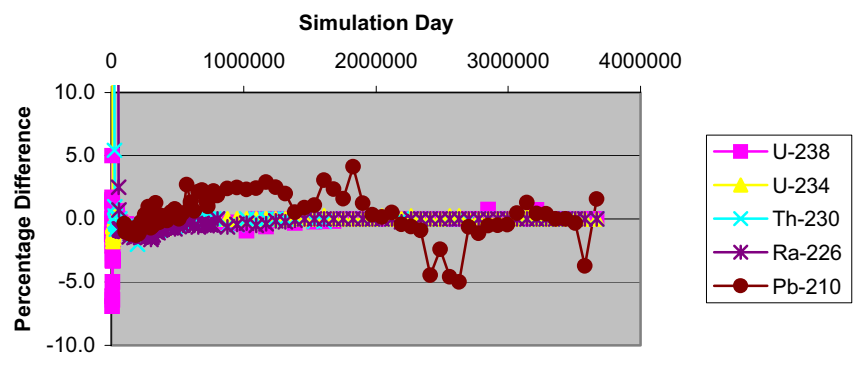


Table 48: tet12p7 vs. tet12p7ms

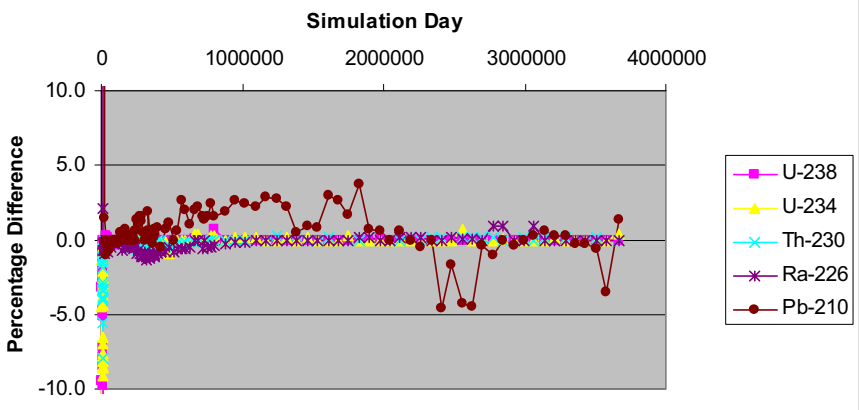


Figure A-12. Percentage difference between TETRAD 12.7 and 12.7ms fluxes as a function of time at grid locations 22, 26, and 48.

Table 52: tet12p7 vs. tet12p7ms

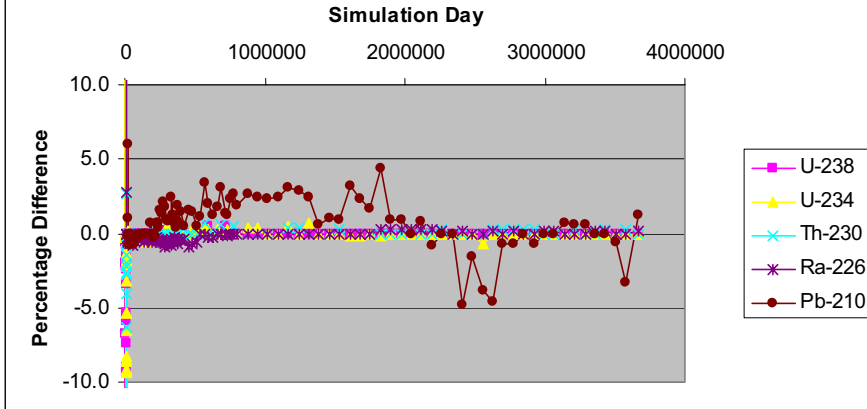


Table 74: tet12p7 vs. tet12p7ms

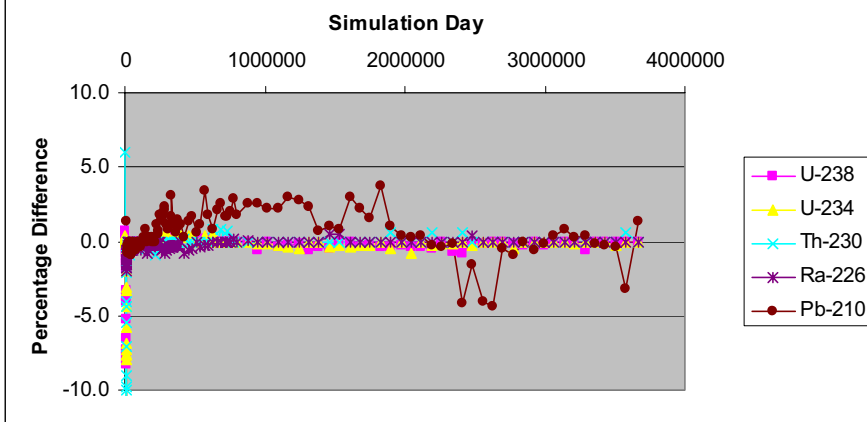


Figure A-13. Percentage difference between TETRAD 12.7 and 12.7ms fluxes as a function of time at grid locations 52 and 74.

A-3. SUMMARY

Overall, this set of simulations for both a simple and complex problem demonstrates equivalence between the TETRAD 12.7 and 12.7ms simulators.

Although it is not the focus of this appendix, the computational times for Problem Number 1 (i.e., ex3dt) were 66 central-processing-unit (CPU) minutes for TETRAD 12.7 and 44 CPU minutes for TETRAD 12.7ms, for a speedup factor of 1.5. The computational times for Problem Number 2 (i.e., b_grp5) were 40,752 CPU minutes for TETRAD 12.7 and 24,914 CPU minutes for TETRAD 12.7ms, for a speedup factor of 1.6.

A-4. REFERENCES

- Becker, B. H., J. D. Burgess, K. J. Holdren, D. K. Jorgensen, S. O. Magnuson, and A. J. Sondrup, 1998, *Interim Risk Assessment and Contaminant Screening for the Waste Area Group 7 Remedial Investigation*, DOE/ID-10569, Rev. 0, U.S. Department of Energy Idaho Operations Office.
- Holdren, K. Jean, Bruce H. Becker, Nancy L. Hampton, L. Don Koeppen, Swen O. Magnuson, T. J. Meyer, Gail L. Olson, and A. Jeffrey Sondrup, 2002, *Ancillary Basis for Risk Analysis of the Subsurface Disposal Area*, INEEL/EXT-02-01125, Rev. 0, Idaho National Engineering and Environmental Laboratory.
- Shook, G. Michael, J. Hope Forsmann, M. Elena Velasquez, and Swen O. Magnuson, 2003, "Improving Numerical Model Efficiency of an Existing, In-House Simulation Model," *Laboratory-Directed Research and Development, FY-2003 Annual Report*, INEEL/EXT-04-01772, Idaho National Engineering and Environmental Laboratory, pp. 197-199.

Appendix B

Description of the Electronic Archive of Simulation Code, Input Files, Simulation Results, Software Management Agreement, and Listing of PV-Wave Processing Codes

Appendix B

Description of the Electronic Archive of Simulation Code, Input Files, Simulation Results, Software Management Agreement, and Listing of PV-Wave Processing Codes

This appendix contains the Software Management Agreement between Idaho Cleanup Project Operable Unit 7-13/14 and the INL Modeling and Measurement Group, a description of the Electronic Data Archive containing a frozen version of the TETRAD simulator, all simulation results for the Operable Unit 7-13/14 RI/BRA and feasibility study, and a listing and description of preprocessing routines used to generate the TETRAD data decks and to post-process the simulation results.

B-1. SOFTWARE MANAGEMENT AGREEMENT BETWEEN THE IDAHO CLEANUP PROJECT WASTE AREA GROUP 7 AND THE MODELING AND MEASUREMENT GROUP

B-1.1 Customer Requirements

The codes and analyses used to generate results that are used to make critical decisions for or by the customer will conform to the quality and documentation required by the customer.

A list of three software management requirements defined by the customer as critical and applicable to modeling activities being performed by the INL Modeling and Measurement Group in support of the Operable Unit 7-13/14 remedial investigation and feasibility study is given below. The work being performed falls under the INL Research and Development General Software Management Plan (PLN-1726 2004).

The following are three key requirements of the Operable Unit 7-13/14 remedial investigation and feasibility study:

1. Reproducibility of final results. Results presented as the final product to the Idaho Cleanup Project for acceptance by regulatory agencies must be reproducible.
2. Verifiability of final results. This will require that simulation results can be qualitatively verified by an expert in the field, using a similar simulation approach. To accomplish this, sufficient detail will be provided on the results generation processes, such that they could be independently verified. Sufficient detail includes an explanation of the predata analysis phase, simulation phase, post-processing phase, and an explanation of the results.
3. Review and approval of results. This requirement complements the second requirement in that accuracy will be verified through a peer and customer review process.

B-1.2 Implementation of Requirements

The INL Modeling and Measurement Group will ensure that the following items are documented and placed in the project file at the time final results are released.

The first and second requirements from Section B-1.1 will be addressed through the following:

- Reference list of commercial software and version used in simulations
- Frozen version of noncommercial software and other routines used to generate results (e.g., electronic backup of Excel spreadsheets and PV-Wave routines)
- Frozen version of input and output results and files throughout data analysis and pre and post-processing stages
- Reference to the operating system and hardware specifications for reproducibility
- Documentation of the simulation and analysis process, including a flow chart or sequence of the data analysis steps that involved use of preprocessing steps, simulation phase, and post-processing phase. This will not include documentation of commercial software, but will include a description of internally written routines in the form of readme files or internal code comments.

The third requirement from Section B-1.1 will be met through the following:

- Internal (i.e., performing organization) peer review of results
 - Any customer-required external reviews
 - Performing organization management approval
 - Customer approval.

B-2. ELECTRONIC DATA ARCHIVE

The primary purpose of the electronic data archive is to document the TETRAD simulator used for Operable Unit 7-13/14 simulations, the simulation input files and results, and the pre and post-processing routines used to manipulate data for simulations. The archive resides on a file server called Schwartz and in a file partition called OU7_13_14.

B-2.1 TETRAD Simulator

The simulator used for all simulations was TETRAD 12.7ms (Shook et al 2003). Executable files for this version of TETRAD are stored in a subdirectory called ou7_13_14\1 Fate & Transport Modeling Archive\TETRAD simulator, frozen version. Since TETRAD is a proprietary code, the source files are not kept in this directory. The complete source files remain under control of the code custodian. The executables were used on an INL personal computer cluster named Squadron, administered by Mr. Alan Marley of the INL. The operating system on the Squadron personal computer cluster was Red Hat Linux release 7.3. The TETRAD source code was compiled on Squadron using the Linux f77 compiler.

Three TETRAD executables are found in the frozen version directory. The file tet12p7ms_off was the primary file used in RI/FS modeling and contains no limitations on output times. The file tet12p7ms_off_162 was used for C-14 simulations and otherwise would have had generated voluminous output every time pressures were imposed downhole during well drilling. Similarly tet12p7ms_off_261 was used for FmR_g11 simulations and had additional output times after Calendar Year 2110 for

evaluating when the VVET system could be shut off. Modifications to the TETRAD code to allow for limiting output to specific times are also included in this directory and are called “modifications for 162 specific output times” and “modifications for 261 specific output times.”

B-2.2 Simulation Input Files and Results

The entire suite of TETRAD simulation results are archived on the Schwartz file server using a Windows Explorer file structure. This file structure is accessed using the Windows XP Professional operating system over the INL network and can be searched using the Windows Search utility. Simulations in the file structure are broken up into groups according to the purpose for which they were performed. Names of the directories identify the purpose. Four directories exist and are named “Simulations, BRA,” “Simulations, FS,” “Simulations, Initial Conditions,” and “Simulations, PA-CA.”

Development of a nomenclature to track simulations was necessary because of the extensive number and types of simulations performed for the RI/BRA and the feasibility study. Unique names were used in naming all input and output files from a simulation group; therefore, the results can be easily retrieved from project archival storage using keyword searches.

Table B-1 provides the nomenclature for the leading character string in the run names. The first letter is always a “B” for a RI/BRA-related simulation or an “F” for a feasibility study simulation. Letters in the remaining positions—two through four—were then used to identify attributes of a sensitivity case. The TETRAD simulator imposes an arbitrary limit of eight characters total for a unique run name. With the last four positions taken up with the group identifier, the unique leading string should only be four characters long to avoid extensive renaming of results, which was necessary in some cases. Table B-2 shows how these conventions were applied to define names for each of the simulation groups. Table B-2 gives the application that was being simulated and a detailed description of the simulation group. The “g*” indicates Groups 1 through 11 as appropriate for each name.

Each simulation group is further divided into up to 10 individual simulations for the groundwater pathway. Each simulation group did not always include all 10 simulations. In each individual simulation, there are two main divisions: one for the DUST source-release simulation and one for the TETRAD simulation. Only the TETRAD portion of this archive for each simulation will be further described in this appendix.

Each individual TETRAD simulation directory for the baseline risk assessment, the feasibility study, and the performance assessment and composite analysis usually is divided into three directories and sometimes four if surface fluxes were used in the risk assessment evaluation. The three standard directories that are always present are: 1) “BINS”—contains the binary TETRAD results for both the vadose zone simulation and the aquifer simulation, 2) “gwp maxc”—groundwater pathway maximum concentration results for anywhere in the aquifer, anywhere outside the SDA fence, and anywhere along the southern INL Site boundary, and 3) “input files”—the complete input files for the vadose zone simulation and for the aquifer simulation. The fourth directory that is sometimes present is called “surface fluxes” and contains post-processed results for the total flux of a contaminant released across the upper surface of the domain as a function of time. The results files from TETRAD were initially in ASCII files created by the grid view subroutine in TETRAD. These results contain requested output from the TETRAD simulator, consisting of values at every gridblock at each time. The ASCII files are post-processed into binary files, thus the name “BINS” for the subdirectory. The binary results files require less disk storage space and are at least an order of magnitude faster for reading into PV-Wave routines for subsequent post-processing. Only the binary results files are saved in the archive, not the original ASCII results files.

Table B-1. Run-naming nomenclature.

Run Descriptor	Run Attribute
Leading B	Baseline risk assessment
Leading F	Feasibility study
Leading a	Aquifer simulation
u	Upper-bound inventory
i	Infiltration
o	Outside the Subsurface Disposal Area
4	Pit 4
n	No
g	Grout
bc	B-C interbed
h	High
l	Low
k	Permeability
mR	Modified Resource Conservation and Recovery Act cap
et	Evapotranspiration cap
p	Partial
f	Full
R	Retrieval, treatment, and disposal
c	Cap
cP	Colloidal plutonium, in the No sorption in the B-C and C-D interbed sensitivity case
U	Uranium
Pa	Performance assessment (always preceded by FmR)

Table B-2. Simulation group names and descriptions.

Simulation Group Name	Application	Description
BASELINE RISK ASSESSMENT		
B_g*	Baseline risk assessment base case	Best-estimate inventories, average infiltration inside the Subsurface Disposal Area = 5.0 cm/year (2.0 in./year), and background infiltration outside the Subsurface Disposal Area = 1.0 cm/year (0.4 in./year)
Bu_g*	Upper-bound inventories	NO ACTION SENSITIVITY: Hold all values constant, as in the baseline risk assessment base case, except as noted.
Bhi_g*	High infiltration in the Subsurface Disposal Area	Upper-bound instead of best-estimate inventories Increased infiltration rate to 23 cm/year (9.1 in./year) assigned uniformly across the Subsurface Disposal Area
Blci_g*	Low background infiltration	Reduce infiltration rate assigned outside the Subsurface Disposal Area boundary from 1.0 to 0.1 cm/year (0.4 to 0.04 in./year)
Bnbc_g*	No B-C interbed	Bounding case where B-C interbed gridblocks replaced with fractured basalt
B4ng_g*	No interim actions	Pit 4 inventory not reduced for the Accelerated Retrieval Project and beryllium blocks not grouted
Bnlk_g	No low-permeability zone in aquifer	Revise low-permeability region in the aquifer from 153 to 712,000 mD
BcP_g*	No sorption in the vadose zone interbeds	Bounding case where sorption of Pu-239 and Pu-240 does not occur in the B-C and C-D interbeds
FEASIBILITY STUDY: All simulations apply best-estimate inventories (remaining or removed) and have an infiltration-reducing cover emplaced that reduces infiltration inside the Subsurface Disposal Area to 0.1 cm/year (0.04 in./year), unless noted otherwise.		
FmR_g*	Modified Resource Conservation and Recovery Act Type C surface barrier	Pad A left in place and incorporated into cover
Fet_g*	Evapotranspiration surface barrier, 0.1 cm/year (0.04 in./year)	Pad A waste transferred to active Low-Level Waste Pit
FgU_g*	In situ grouting	In situ grouting selected areas; and Pad A waste retrieved, treated ex situ, and returned to a pit in the Subsurface Disposal Area
Fpr_g*	Partial retrieval, treatment, and disposal	Remove 1.6 ha (4 acres), targeting volatile organic compounds and transuranic waste; and Pad A retrieved and sent to the Idaho Comprehensive Environmental Response, Compensation, and Liability Act Disposal Facility
Ffr_g*	Full retrieval, treatment, and disposal	Remove all waste, including Pad A waste treated at the Idaho Comprehensive Environmental Response, Compensation, and Liability Act Disposal Facility, and buried outside of the Idaho National Laboratory Site

Table B-2. (continued).

Simulation Group Name	Application	Description
FEASIBILITY STUDY SENSITIVITY		
Feth_g*	Evapotranspiration surface barrier, 1.0 cm/year (0.4 in./year)	Same as evapotranspiration surface barrier, but with higher infiltration through cover of 1.0 cm/year (0.4 in./year)
Frnc_g	Full retrieval, treatment, and disposal with no cap	Same as full retrieval, treatment, and disposal, except no infiltration-reducing cover emplaced; infiltration remains as is in the remedial investigation and baseline risk assessment base case with spatial average of 5.0 cm/year (2.0 in./year)
PERFORMANCE ASSESSMENT		
FmRpa_g*	Performance assessment base case	Same as the Modified Resource Conservation and Recovery Act Type C Surface Barrier, but with only low-level waste sources active
FmRpalo_g*	Performance assessment with low outside infiltration	Same as performance assessment base case, but with 0.1 cm/year (0.04 in./year) background infiltration outside the Subsurface Disposal Area

The “Simulations, Initial Conditions” directory contains initial condition simulation files for the vadose zone domain that were run for three different cases: (1) the base case with a background infiltration rate of 1.0 cm/year (0.4 in./year) applied uniformly over the entire upper surface of the model, (2) the lower background infiltration case, where the background infiltration was assigned as 0.1 cm/year (0.04 in./year), and (3) the no B-C interbed case, which had gridblocks that normally were assigned hydrologic and transport properties of the B-C interbed, but were assigned as fractured basalt instead and used a background infiltration rate of 1.0 cm/year (0.4 in./year) across the upper surface. Each of these initial condition directories contains files for simulations with two, three, four, five, and six water components. The different numbers of components were needed because the simulations groups had one, two, three, four, or five contaminants per group. Each initial condition subdirectory contains input files (“.dat”), output file generated by TETRAD (“.out”) that reports various information during the simulation, TETRAD output files with GV names that contain user-requested results for each gridblock in the base and refined vadose zone simulation domains, and binary RESTART files. These binary RESTART files are used for restarting the dissolved-phase transport simulations from time zero, which corresponds to January 1, 1952. The use of the TETRAD restart capability alleviates the need to repetitively solve for the initial conditions and keeps the transport data decks smaller without all the grid and property assignments.

The dual-continua simulations do not have corresponding initial conditions simulation. Instead, they have the initial condition simulation incorporated into the transport deck.

Table B-3 lists subdirectories in the archive that contain TETRAD simulation results.

Table B-3. Simulation directories in electronic archive.

Baseline Risk Assessment Simulations	Feasibility Study Simulations	Performance Assessment and Composite Analysis Simulations
B_g#	FmR_g#	FmRpa_g#
Bu_g#	Fet_g#	FmRloi_g#
B4ng_g#	Feth_g#	FmRpalo_g#
Bhi_g#	Fpr_g#	anisotropy simulations
Bloi_g#	Ffr_g#	FmRnlk_g#
Bnbc_g#	Frnc_g#	FmRnlkpa_g#
Bnlk_g#	FgU_g#	
BcP_g#		

B-2.3 Pre and Post-Processors

Routines used to pre and post-process data for Operable Unit 7-13/14 simulations were all written in the PV-Wave programming language. PV-Wave, Version 8.0, was used on a Dell Optiplex GX260 personal computer. The preprocessor routines are used in building portions of the TETRAD input decks. The post-processor routines work on results from TETRAD simulations. Both types of routines are archived in subdirectories under the \Schwartz\ou7_13_14\1 Fate & Transport Modeling Archive\TETRAD Pre- & Post-processors subdirectory. This subsection provides tables of the processing files and their specific function.

Table B-4 lists preprocessing routines that were used to generate portions of the TETRAD simulation input decks. Data files necessary to run the routines also are archived and are likewise described. Where common root names occur, the wildcard character “*” is used to abbreviate the names. The PV-Wave routines can be identified in the archive by their “.pro” extension. In general, output results from PV-Wave routines are named with an “.out” extension. These “.out” files were inserted into the TETRAD input files. The PV-Wave routines are generally presented in logical order of use with grid development and property assignments: first, routines to visualize grid, second, property results, and last, boundary condition assignments and source-term loading.

Table B-5 lists post-processing routines that were used to process results from TETRAD simulations. Data files necessary to run the routines are also archived and are likewise described. Where common root names occur, the wildcard character “*” is used to abbreviate the names.

The PV-Wave routines can be identified in the archive by their “.pro” extension. In general, output results from PV-Wave routines are named with an “.out” extension. These “.out” files were inserted into the TETRAD input files. The PV-Wave routines are separated within the archive by their general functional areas.

Table B-4. PV-Wave preprocessing routines.

PV-Wave Routine	Specific Function	Input Data Files	Location of Data Files
t2.pro	Generates base domain conformable vadose zone gridding, assigns lithology types to gridblocks, and populates a binary stratigraphy file with indicators for each gridblock	gridding.params_refl and lithology kriging results that are named S0*top, S0*bottom, AB*top, AB*bottom, BC*top, BC*bottom, CD*top, CD*bottom	gridding\FY04_grid\leecaster_results\no_overlaps
ref_2_from_1.pro	Generates first-level refined grid from base domain	gridding.params_ref2 and results from t2.pro stored in OUT subdirectory	gridding\FY04_grid\OUT
ref_3_from_2.pro	Generates second-level refined grid from first-level refined grid	gridding.params_ref3 and results from ref_2_from_1.pro stored in OUT subdirectory	gridding\FY04_grid\OUT
ftops.pro	Generates top elevations TETRAD FTOPS cards for base domain	grid_coordinates_refl	gridding\FY04_grid\OUT
delmodsp	Generates gridblock vertical thicknesses TETRAD DELMOD cards for base domain	grid_coordinates_refl	gridding\FY04_grid\OUT
permssv.pro	Generates TETRAD PORMOD and PERMMOD cards for porosity and permeability for base and refined single-continua domains	Porosity*BC, Porosity*CD, Ksat*BC, Ksat*CD, grid_coordinates*, STRAT_FLAGS* (from t2.pro)	gridding\FY04_grid\leecaster_results\HydrData and gridding\FY04_grid\OUT
adstreg.pro	Generates TETRAD ADSREG cards for adsorption for base and refined single-continua domains	grid_coordinates*, STRAT_FLAGS*	gridding\FY04_grid\OUT
tormod.pro	Generates TETRAD TORMOD cards for tortuosity for base and refined single-continua domains	grid_coordinates*, STRAT_FLAGS*	gridding\FY04_grid\OUT
sda_BRA_flood_assignment.pro	Generates TETRAD MFREG cards for assigning floods for single-continua domain	grid_coordinates_ref3 and plxy.params	gridding\FY04_grid\OUT

Table B-4. (continued).

PV-Wave Routine	Specific Function	Input Data Files	Location of Data Files
sda_BRA_infiltration_assignment.pro	Generates TETRAD MFREG cards for assigning spatially varying infiltration for single-continua domain	pltxy.params	gridding\FY04_grid
sda_BRA_waste_assignment.pro	Generates TETRAD MFREG cards for assigning spatial and vertical locations for applying all radiological contaminant mass, except tritium and C-14 from source-release model for single-continua domain	grid_coordinates3, STRAT_FLAGS3, and pltxy.params	gridding\FY04_grid\OUT
lith_out.pro	Interrogates either base or refined grids and output TETRAD gridblock indices; used for checking results of other routines	grid_coordinates*, STRAT_FLAGS*	gridding\FY04_grid\OUT
gen_lysimeter_indices.pro	Uses lysimeter locations and depths to generate TETRAD gridblock indices for comparison between simulated and observed concentrations	“Carol Strong SDA Lysimeter Sampling Notebook.pn”, pltxy.params, and grid_coordinates_ref*	gridding\FY04_grid\OUT
comporck.pro	Generates figures showing contours of kriged porosities and permeabilities and also measured data on which kriging was based	BCavgpork.txt, CDavgpork.txt, Porosity*BC, Porosity*CD, Ksat*BC, Ksat*CD, well_coords.list.dat	gridding\FY04_grid\leecaster_results\HydrData, gridding\FY04_grid\DATA
comp_kriged_w_data.pro	Generates figures showing contours of kriged porosities and permeabilities and also measured data on which kriging was based	sda_lith_data_for_well_plotting, well_coords_list, S0*top, S0*bottom, AB*top, AB*bottom, BC*top, BC*bottom, CD*top, CD*bottom	\gridding\FY04_grid\leecaster_results\no_overlaps

Table B-4. (continued).

PV-Wave Routine	Specific Function	Input Data Files	Location of Data Files
persmv_nbc.pro	Generates TETRAD PORMOD and PERMMOD cards for porosity and permeability for case of no B-C interbed for base and refined domains	Porosity*BC, Porosity*CD, Ksat*BC, Ksat*CD, grid_coordinates*, STRAT_FLAGS*	gridding\FY04_grid\leecaster_results\HydrData and gridding\FY04_grid\OUT
adsreg_nbc.pro	Generates TETRAD ADSREG cards for adsorption for case of no B-C interbed base and refined domains	grid_coordinates*, STRAT_FLAGS*	gridding\FY04_grid\OUT
tormod_nbc.pro	Generates TETRAD TORMOD cards for tortuosity for case of no B-C interbed base and refined domains	grid_coordinates*, STRAT_FLAGS*	gridding\FY04_grid\OUT
“14 × 10 × 80 grid values.xls”	Excel file to calculate gridblock numbers for assigning boundary conditions	NA	NA
permssv_frac.pro	Generates TETRAD PORMOD and PERMMOD cards for porosity and permeability for base and refined fracture portion of dual-continua domain	Porosity*BC, Porosity*CD, Ksat*BC, Ksat*CD, grid_coordinates*, STRAT_FLAGS*	gridding\FY04_grid\leecaster_results\HydrData and gridding\dual_FY04_grid\OUT
permssv_matrix.pro	Generates TETRAD PORMOD and PERMMOD cards for porosity and permeability for base and refined matrix portion of dual-continua domain	Porosity*BC, Porosity*CD, Ksat*BC, Ksat*CD, grid_coordinates*, STRAT_FLAGS*	gridding\FY04_grid\leecaster_results\HydrData and gridding\dual_FY04_grid\OUT
adsreg_frac.pro	Generates TETRAD ADSREG cards for adsorption for base and refined fracture portion of dual-continua domain	grid_coordinates*, STRAT_FLAGS*	gridding\dual_FY04_grid\OUT

Table B-4. (continued).

PV-Wave Routine	Specific Function	Input Data Files	Location of Data Files
adsreg_matrix.pro	Generates TETRAD ADSREG cards for adsorption for base and refined matrix portion of dual-continua domain	grid_coordinates*, STRAT_FLAGS*	gridding\dual_FY04_grid\OUT
tormod_frac.pro	Generates TETRAD TORMOD cards for tortuosity for base and refined fracture portion of dual-continua domain	grid_coordinates*, STRAT_FLAGS*	gridding\dual_FY04_grid\OUT
tormod_matrix.pro	Generates TETRAD TORMOD cards for tortuosity for base and refined matrix portion of dual-continua domain	grid_coordinates*, STRAT_FLAGS*	gridding\dual_FY04_grid\OUT
sda_dual_flood_assignment.pro	Generates TETRAD MFREG cards for assigning floods for dual-continua domains	grid_coordinates_ref3 and pltxy.params	gridding\dual_FY04_grid\OUT
sda_dual_infiltration_assignment.pro	Generates TETRAD MFREG cards for assigning spatially varying infiltration for dual-continua domain	pltxy.params	gridding\dual_FY04_grid
sda_dual_waste_H3_C14_assignment.pro	Generates TETRAD MFREG cards for assigning spatial and vertical locations for applying tritium and C-14 contaminant mass from source-release model for dual-continua domain	grid_coordinates3, STRAT_FLAGS3, and pltxy.params	gridding\dual_FY04_grid\OUT
sda_dual_waste_VOCS_assignment.pro	Generates TETRAD MFREG cards for assigning spatial and vertical locations for applying volatile organic compound contaminant mass from source-release model for dual-continua domain	grid_coordinates3, STRAT_FLAGS3, and pltxy.params	gridding\dual_FY04_grid\OUT

Table B-4. (continued).

PV-Wave Routine	Specific Function	Input Data Files	Location of Data Files
almod_matrix.pro	Generates TETRAD ALMOD cards for sediment portions of matrix dual-continua domain	grid_coordinates*, STRAT_FLAGS*	gridding\dual_FY04_grid\OUT
gen_face_aquifers.pro	Generates TETRAD AQUIFER cards for side faces of dual-continua domain	None	NA
gen_face_diffbcs.pro	Generates TETRAD DIFFBC cards for side faces of dual-continua domain	None	NA
gen_tvbcs.pro	Generates TETRAD AQUADDP cards for time-varying surface atmospheric pressure boundary conditions in dual-continua domain	grid_coordinates*	gridding\dual_FY04_grid\OUT
permssv_frac_nbc.pro	Generates TETRAD PORMOD and PERMMOD cards for porosity and permeability for base and refined fracture portion of dual-continua domain for case of no B-C interbed	Porosity*BC, Porosity*CD, Ksat*BC, Ksat*CD, grid_coordinates*, STRAT_FLAGS*	gridding\FY04_grid\leecaster_results\HydrData and gridding\dual_FY04_grid\OUT
permssv_matrix_nbc.pro	Generates TETRAD PORMOD and PERMMOD cards for porosity and permeability for base and refined matrix portion of dual-continua domain for case of no B-C interbed	Porosity*BC, Porosity*CD, Ksat*BC, Ksat*CD, grid_coordinates*, STRAT_FLAGS*	gridding\FY04_grid\leecaster_results\HydrData and gridding\dual_FY04_grid\OUT
adsreg_frac_nbc.pro	Generates TETRAD ADSREG cards for adsorption for base and refined fracture portion of dual-continua domain for case of no B-C interbed	grid_coordinates*, STRAT_FLAGS*	gridding\dual_FY04_grid\OUT

Table B-4. (continued).

PV-Wave Routine	Specific Function	Input Data Files	Location of Data Files
adsreg_matrix_nbc.pro	Generates TETRAD ADSREG cards for adsorption for base and refined matrix portion of dual-continua domain for case of no B-C interbed	grid_coordinates*, STRAT_FLAGS*	gridding\dual_FY04_grid\OUT
tormod_frac_nbc.pro	Generates TETRAD TORMOD cards for tortuosity for base and refined fracture portion of dual-continua domain for case of no B-C interbed	grid_coordinates*, STRAT_FLAGS*	gridding\dual_FY04_grid\OUT
tormod_matrix.pro	Generates TETRAD TORMOD cards for tortuosity for base and refined matrix portion of dual-continua domain for case of no B-C interbed	grid_coordinates*, STRAT_FLAGS*	gridding\dual_FY04_grid\OUT
gen_INJ_I_C_AQUADDP.pro	Generates TETRAD time-varying boundary conditions with downhole bottom pressures assigned for positive pressure well drilling	pltxy.params, air_drilled_wells_coords_list.dat, grid_coordinates*	gridding\dual_FY04_grid\air_drilling, gridding\dual_FY04_grid\OUT
comb.pro	General program to create TETRAD MFFLUXT cards for releasing contaminant mass from the source-release model into the vadose zone model; group.info contains scale factors for upscaling DUST source-release results for use in TETRAD	group.info and DUST source-release output files	src_loading\bra_input and all subdirectories of this directory
int_fluxes.pro	Integrate total mass out of the revised source-release files for checking against inventories input to source-release model	group.info and g*.inp_tet	src_loading\bra_input and source release directories

Table B-5. PV-Wave post-processing routines.

PV-Wave Routine	Specific Function	Input Data Files	Location of Data Files
gvo.pro, gvoall.pro	Converts TETRAD Gridview ASCII files into binary format. Gvoall.pro converts all grid view files in a subdirectory.	TETRAD ASCII Gridview files	Temporary storage directory
conaq.pro	Contours aquifer domain results.	group.info, binary results files	src_loading\bra_input
conct.pro	Extracts maximum concentration as a function of time from either anywhere in the aquifer model or outside the Subsurface Disposal Area fence. Used to hand off model concentrations for calculating equivalent risk.	group.info, binary results files	src_loading\bra_input
consmax.pro	Plan view contouring of vadose zone simulation results for saturation, capillary pressure, or vertical water flux by maximum within a lithologic zone, or by single slice through domain. Optimally superimposes monitoring results.	STRAT_FLAGS_*, pltxy.params	gridding\dual_fy04_grid\OUT, gridding\dual_fy04_grid
convers.pro	Cross section contouring for vadose zone contaminant concentrations. Field monitoring results are superimposed at lysimeter/perched water monitoring locations. Also, optionally overlays lithology by shading sediment gridblocks.	STRAT_FLAGS_*, group.info, binary results files, Koeppen monitoring results spreadsheet converted to ASCII text files, 'Carol Strong SDA Lysimeter Sampling Notebook.prn'	gridding\dual_fy04_grid\OUT, src_loading\bra_input, \monitoring data (under the pre and post-processors directory), gridding\FY04_grid\
cvtst_lyst.pro	Time history plotting of simulated contaminant concentration as a function of time at vadose zone monitoring locations. Overlays monitoring results from specific lysimeter and perched water monitoring locations.	group.info, binary results files, Koeppen monitoring results spreadsheet converted to ASCII text files, vzlocs.param	src_loading\bra_input, \monitoring data (under the pre and post-processors directory), postprocessing directorymmn

Table B-5. (continued).

PV-Wave Routine	Specific Function	Input Data Files	Location of Data Files
plt_aq_conc.pro	Time history plotting of simulated contaminant concentration as a function of time at aquifer well locations. Overlays monitoring results from specific aquifer water monitoring locations.	group.info, binary results files Koeppen monitoring results spreadsheet converted to ASCII text files pltaq.params, all_well_coordinate_list, sda_well_list	src_loading\bra_input \monitoring data (under the pre and post-processors directory) processing\aq_well_locs\
plt_aq_pro.pro	Plots vertical profiles of simulated concentration in the aquifer for selected contaminants.	binary results files	—
times_ic.pro	Plots water saturation as a function of time during initialization period to allow determination of quasi steady-state conditions.	binary results files	—
vzflux.pro	Reads vadose zone model results and creates input files for loading time history of water and contaminant flux into corresponding gridblocks of the aquifer model. Also generates graphics file with time history flux for each gridblock.	binary results files	—
C14_inst_BRA.pro	Creates time history plot of C-14 contaminant flux through land surface, and creates an ASCII file of contaminant flux as a function of time for use in risk calculation.	binary results files	—
VOC_inst_BRA.pro	Creates time history plot of volatile organic compound contaminant flux through land surface, and creates an ASCII file of contaminant flux as a function of time for use in risk calculation.	binary results files	—
coniso.pro	Creates plan view contour plots of risk over time for a spatially-consistent receptor, using superposition to combine risks from an arbitrary number of contaminants.	*_input_files, table_conv_factors_BRA_FY05 tetrad_scale_fac_BRA_FY05	postprocessing\isopleth

B-3. REFERENCES

PLN-1726, 2004, "Research and Development General Software Management Plan," Rev. 0, Idaho National Engineering and Environmental Laboratory, Idaho Completion Project.

Shook, G. Michael, J. Hope Forsmann, M. Elena Velasquez, and Swen O. Magnuson, 2003, "Improving Numerical Model Efficiency of an Existing, In-House Simulation Model," *Laboratory-Directed Research and Development, FY-2003 Annual Report*, INEEL/EXT-04-01772, Idaho National Engineering and Environmental Laboratory, pp. 197-199.

Appendix C

Aquifer Model Domain Extension

Appendix C

Aquifer Model Domain Extension

This appendix contains a complete letter report from Mike Rohe to S. O. Magnuson and T. J. Meyers, March 9, 2004 which was titled “OU 7-13/14 ABRA Saturated Groundwater Model Update.” This letter report documented the expansion of the Operable Unit 7-13/14 aquifer model domain.

C-1. INTRODUCTION

The original Operable Unit 7-13/14 ABRA saturated groundwater model (Holdren et al. 2002) was used to prepare cumulative risk contours resulting from simulation of eight groundwater contaminant groups. The downgradient end of the resulting cumulative risk contour line for 10^{-5} total risk exceeded the original saturated model domain. To capture the entire contour line within model boundaries, the domain was extended in the downgradient direction of groundwater flow. This letter report describes the effort required to expand the domain and reports the results of re-running the model. The model is fully saturated and based on the TETRAD numerical reservoir simulation code (Vinsome and Shook 1993). PV-Wave, an environmental analysis and visualization software (Visual Numerics 2001), was used to prepare model input and to process results.

C-2. DOMAIN EXTENSION

In the INL Site vicinity, groundwater in the Snake River Plain aquifer flows primarily south-southwest with some localized variation. Initially, the saturated model domain was extended only in the southern direction. The domain was expanded to 300% in this direction. After examining the results of contouring water levels in the extended domain, particularly in the southwestern portion of the domain, it was determined that the domain should also be extended in the west direction. The domain was increased to 200% in this direction, making the new domain three times the original north-south length and two times the original east-west length. The northeast corners of both the original and extended models are located in the same position since the domain extension only occurred to the south and west directions. The original and extended domains are shown in Figure C-1.

The original ABRA saturated model consisted of seven layers of grid cells sized 1,000 feet (304.8 m) per side with variable vertical thickness (Holdren et al. 2002). Each layer contained 34 columns and 27 rows of cells yielding 918 cells per layer and a total of 6,426 grid cells in the model. The original domain was a rectangle 6.4 mi (10.4 km) in the east-west direction and 5.1 mi (8.2 km) in the north-south direction covering an area of 33 mi² (85 km²). The new domain retains the 1,000-ft (304.8 m) sided grid cells but now contains 68 columns and 81 rows per layer, seven layers, yielding 5,508 cells per layer for a total of 38,556 grid cells. The new domain is 12.9 mi (20.7 km) in the east-west direction and 15.3 mi (24.7 km) in the north-south direction covering an area of 198 mi² (512 km²).

The refined grid area from the original model was maintained in the new model. This refinement matches the RWMC vadose zone model footprint onto the aquifer and is 7,000 ft (2134 m) by 5,000 ft (1,524 m) covering an area of 1.25 mi² (3.25 km²). In the refined area, the grid cells are 500 ft (152.4 m) per side.

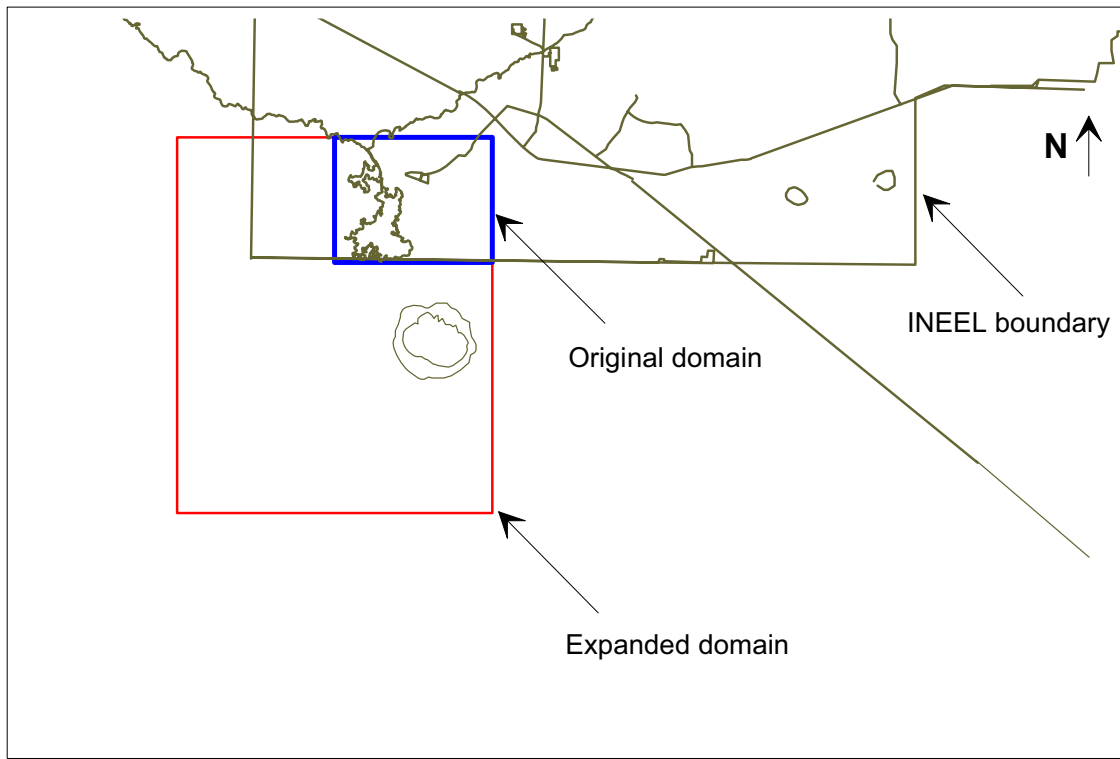


Figure C-1. Extended model domain compared to original Operable Unit 7-13/14 saturated groundwater model domain.

C-3. WATER-TABLE CONTOUR MAPS

Water-table maps were prepared using the Surfer mapping program (Golden Software 2000) to reveal groundwater flow characteristics and to supply fixed head values for boundary nodes in the new model domain. The original groundwater model used 77 aquifer wells in the vicinity of, or upgradient of, the RWMC to establish boundary heads. The new expanded domain model excludes 22 of these wells; these were mostly upgradient wells in close proximity or wells with missing data for fall 2003. These were replaced with 22 wells located mostly south of the RWMC in the extended domain.

The water-table contour map developed for the original ABRA saturated model covered 17 mi (27.4 km) by 13 mi (21.3 km) or 226 mi² (585 km²) in area. The extended domain model required additional wells that cover a territory 52 mi (84.1 km) by 32 mi (51.8 km), for an area of 1,683 mi² (4,359 km²). The expansion in model domain and mapped water-table area included a much larger change in hydraulic head than in the original model. The larger change in hydraulic head has an important effect on modeled water-table elevation and modeled velocities in the new model.

Groundwater elevation data were compiled for fall 2003 and range from September to November water levels. These data were assumed to represent a steady state condition. Borehole deviation correction factors were applied to water level data in those wells with available deviation logs. The resulting groundwater potentiometric contour map is shown in Figure C-2.

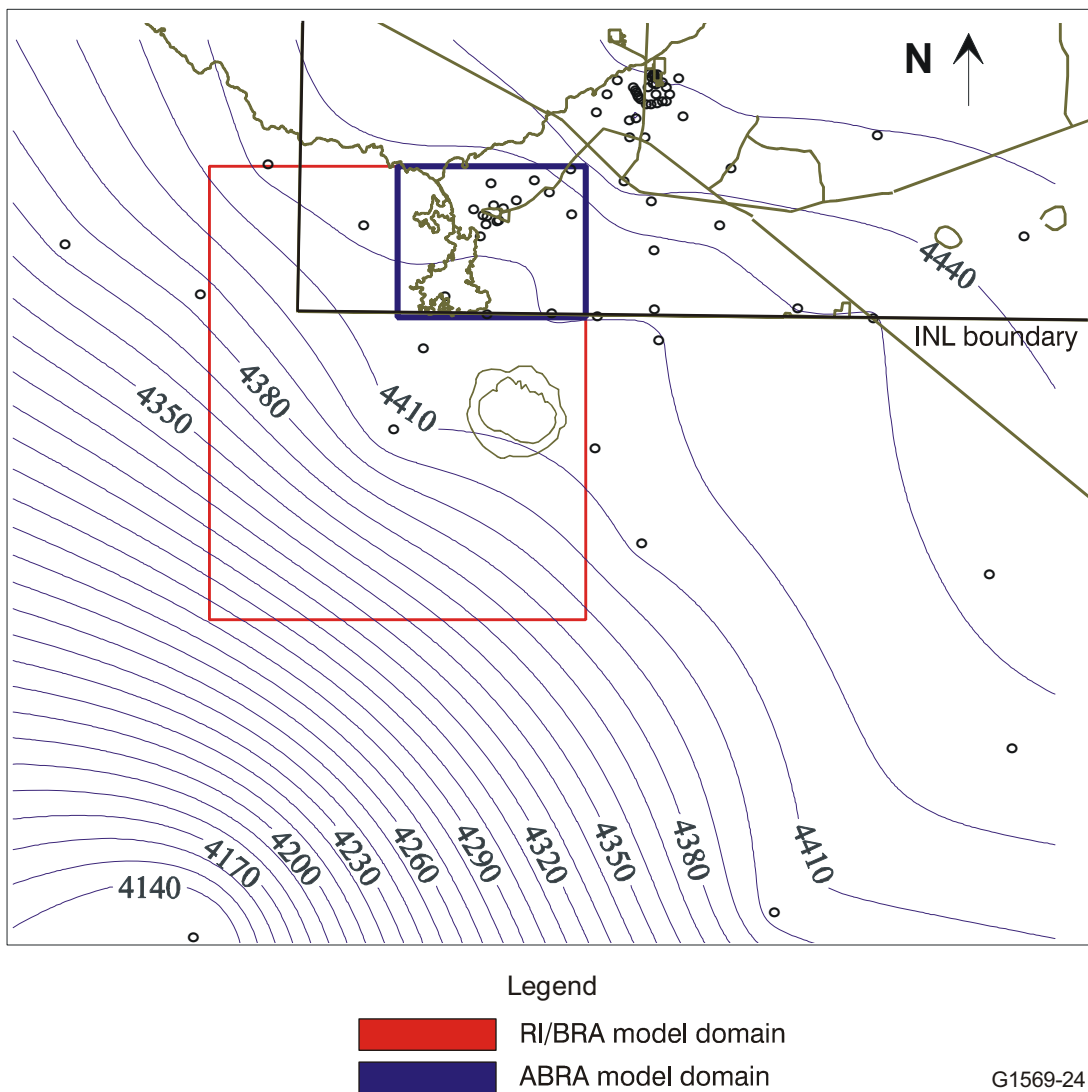


Figure C-2. Remedial investigation/baseline risk assessment-model domain with interpolated fall 2003 water-table contours (feet). Symbols indicate locations used for interpolation.

Additional water-table contour maps were prepared for fall (September through November) of 2001 and 2002. These were prepared using information from 94 and 95 aquifer wells, respectively. Figure C-3 compares the fall 2001 and 2002 maps with a contour map prepared for the extended domain using only the original model's 77 aquifer wells and water level data for fall 2000. The same extent is shown for all three maps and covers an area larger than either model domain. In the original model domain, the groundwater flow direction appears mostly southerly (Figure C-5 through C-37, Holdren et al. 2002). Yet, when expanded to the new domain, the fall 2000 water – map (Figure C-3a) agrees with the later maps (Figure C-3b and C-3c); the groundwater flow direction becomes more southwesterly due to a rapid decrease in water-table elevation.

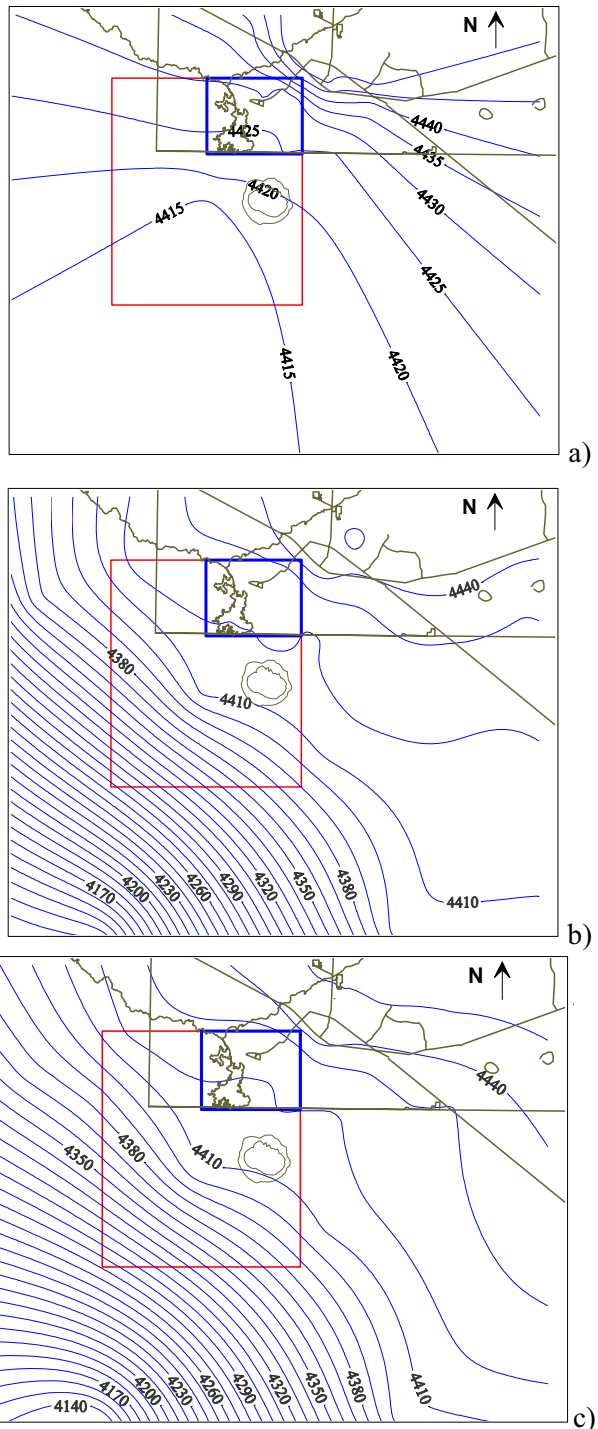


Figure C-3. Comparison of contour maps: (a) original 77 wells from fall 2000; (b) 94 wells in fall 2001; and (c) 95 wells in fall 2002 (original and extended model domains).

C-4. BOUNDARY CONDITIONS

Boundary conditions for the extended domain model were established as prescribed head conditions assuming steady-state conditions. Hydraulic head values were interpolated from the fall 2003 water-table contour map at each perimeter boundary node position using a PV-Wave program. The water-table map indicates a general southwest direction of flow. Figure C-4 shows the fall 2003 water-table map superimposed onto the new model domain. Also shown are the measured water level elevations at their respective locations.

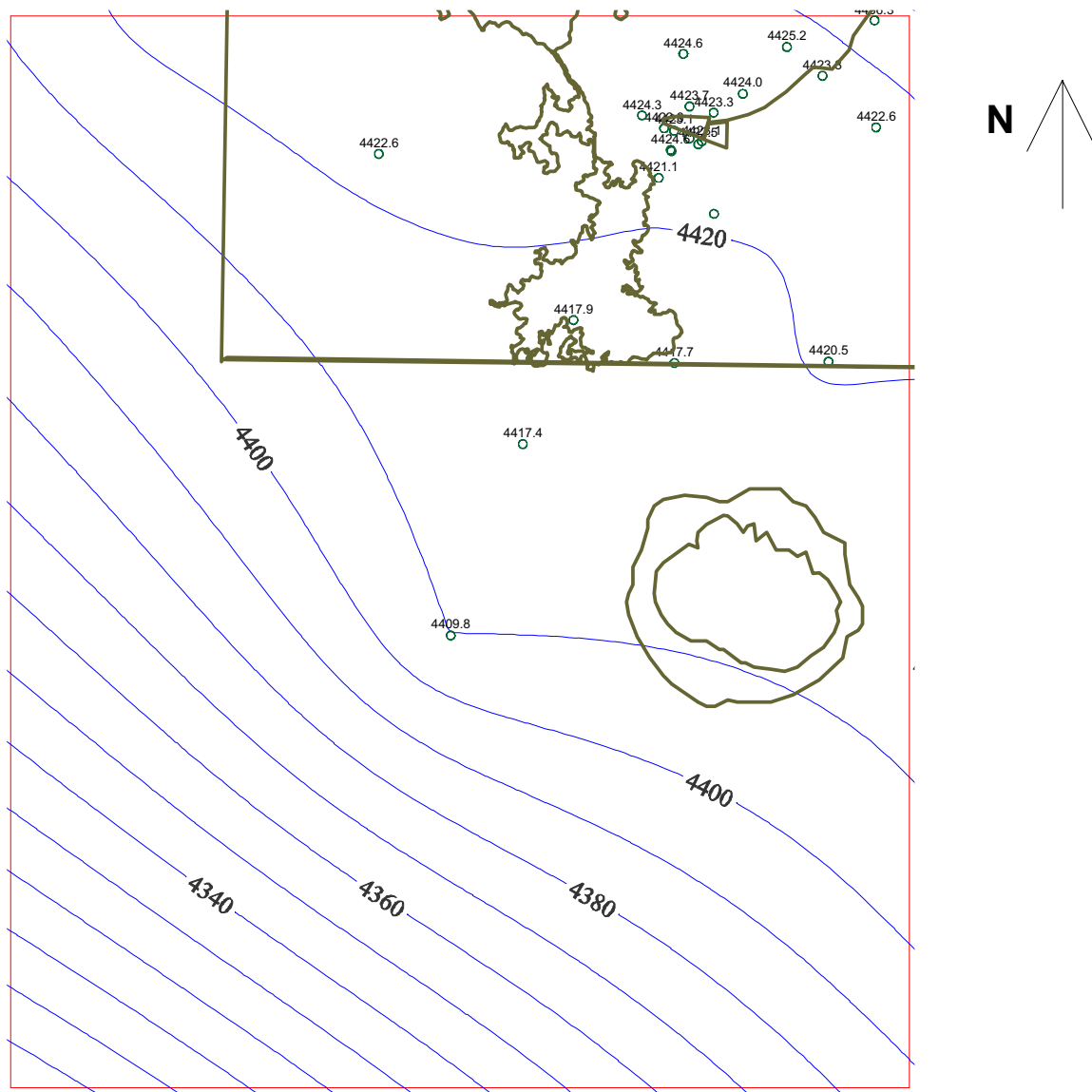


Figure C-4. Model domain with fall 2003 water-table contours.

The hydraulic head relief from the northeast corner to the southwest corner of the new domain is 157 ft (48 m) and extends over a distance of 20 mi (32.2 km). The resulting average hydraulic gradient is 7.8 ft/mi (0.0015 m/m). However, in the vicinity of the RWMC, the gradient is much lower and ranges

approximately 2 to 4 ft/mi (0.0004 to 0.0008). Only in the southwest portion of the domain does the large drop in hydraulic head in measured wells produce a gradient of approximately 13 ft/mi (0.002).

C-5. PERMEABILITY ZONES

The original ABRA saturated model contained three distinct permeability zones that were based in part on the 1994 Waste Area Group-10 regional aquifer modeling effort (McCarthy et al. 1995) as well as calibration required to match modeled heads to fall 2000 measured heads. The three zones had values of 153; 9,300; 712,000 mD (millidarcies) and are labeled as such in Figure C-5. The 153 mD zone was the lowest permeability zone and was located immediately downgradient of RWMC.

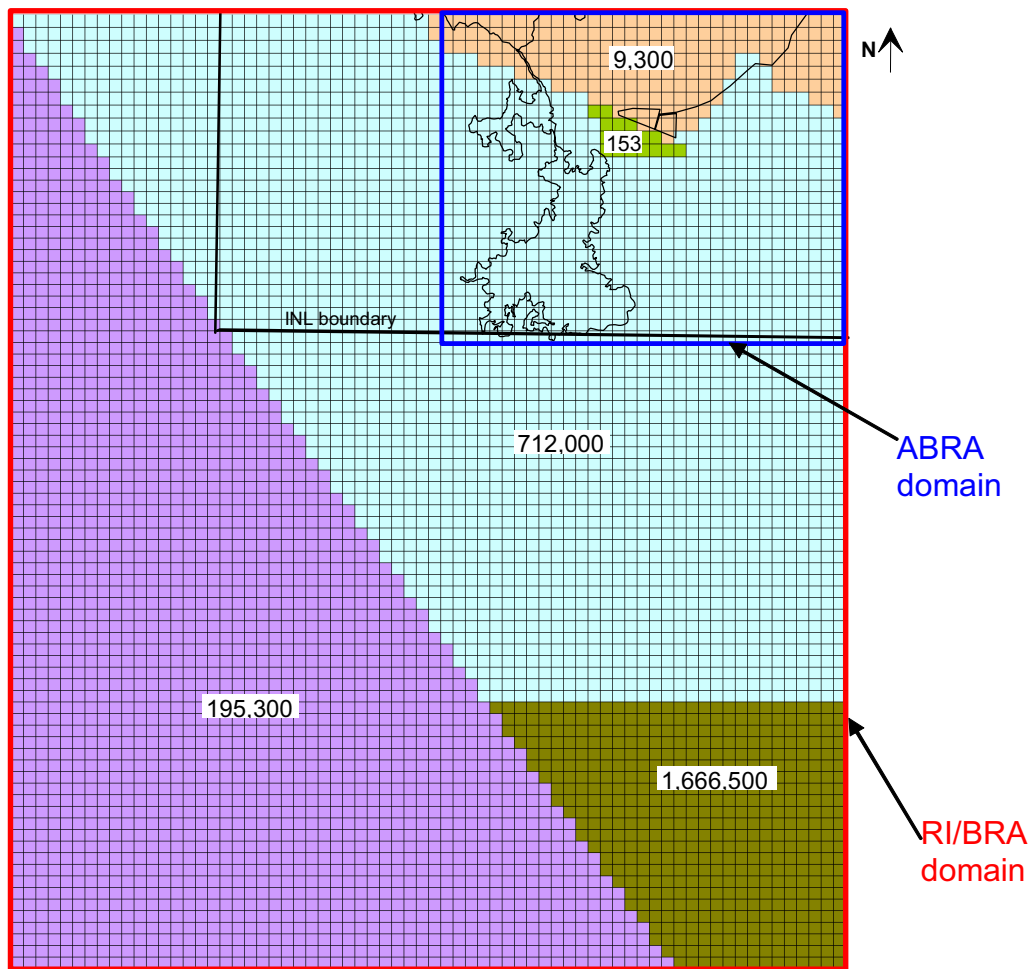


Figure C-5. Permeability zones in the extended remedial investigation/baseline risk assessment aquifer-model domain (values shown in mD).

Initially, the new model was run with only the three permeability zones from the original model. Permeability assigned to the extended domain was a uniform 712,000 mD. To be more consistent with Waste Area Group-10 groundwater modeling efforts, the extended domain was revised to incorporate portions of two additional permeability zones from the 1994 Waste Area Group-10 regional groundwater model. Zones 12 and 55, from Figure C-3 through C-16 of the report describing the 1994 Waste Area

Group-10 model (McCarthy et al. 1995), are downgradient of RWMC and are assigned constant permeability values of 195,300 and 1,666,350 mD, respectively (see Figure C-5).

C-6. MODELED VELOCITIES

The average linear velocity, also called superficial velocity, is a function of head gradient and permeability. The average linear velocity is the Darcian velocity divided by the porosity of the aquifer matrix. A uniform porosity of 0.062 was assumed for the entire domain. Figures C-6 through C-11 show the refined area and the original ABRA saturated model domain for three cases. These figures demonstrate the effect of boundary conditions and permeability on simulated average linear velocity. The figures show vectors representing the magnitude and direction of average linear velocity calculated at each grid cell. The magnitude of the average linear velocity is expressed in units of m/yr.

abra.GV1: Avg Lin Vel (m/yr) in layer 1 at sim day = 15000.

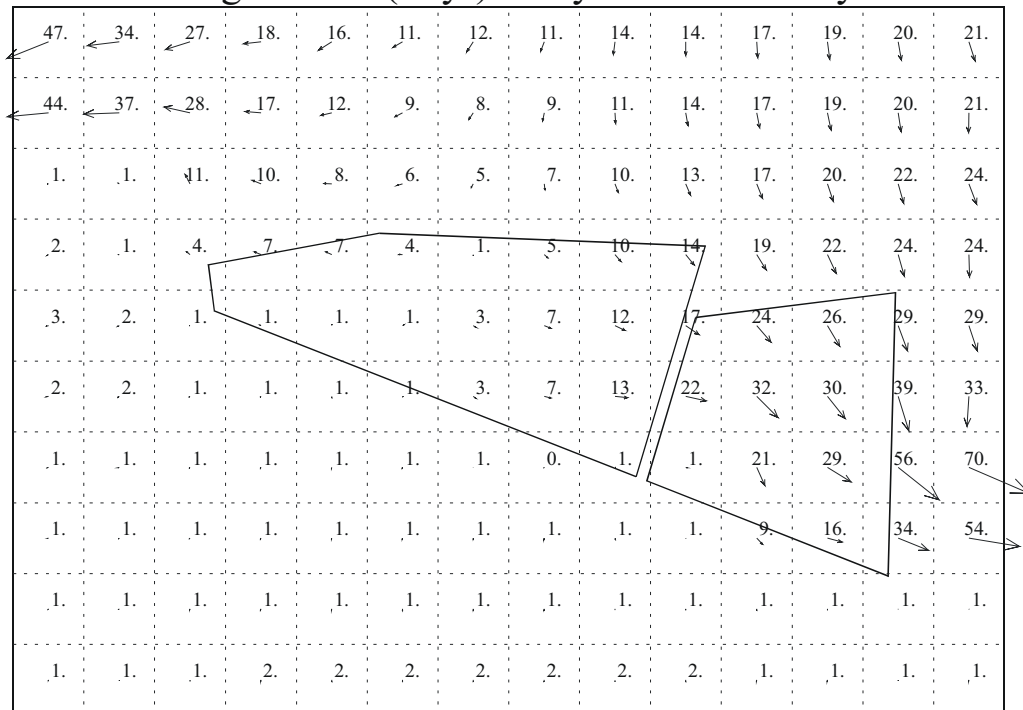


Figure C-6. Simulated aquifer velocities in the refined footprint beneath the Subsurface Disposal Area from the original Ancillary Basis for Risk Analysis model.

abra.GV: Avg Lin Vel (m/yr) in layer 1 at sim day = 15000.

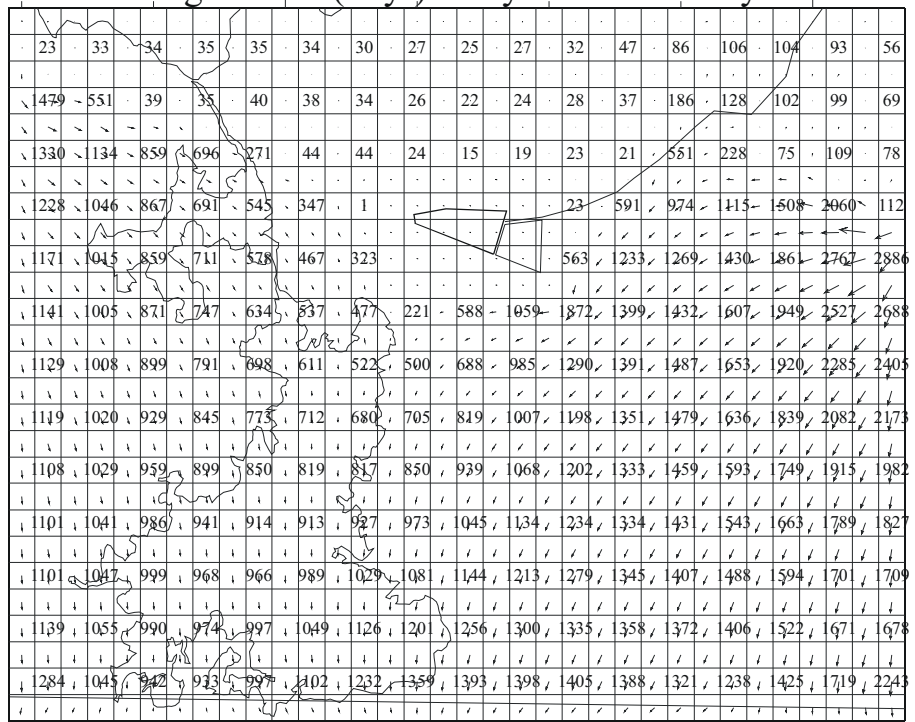


Figure C-7. Simulated aquifer velocities for the base domain from the original Ancillary Basis for Risk Analysis model.

vels1.GV1: Avg Lin Vel (m/yr) in layer 1 at sim day = 0.

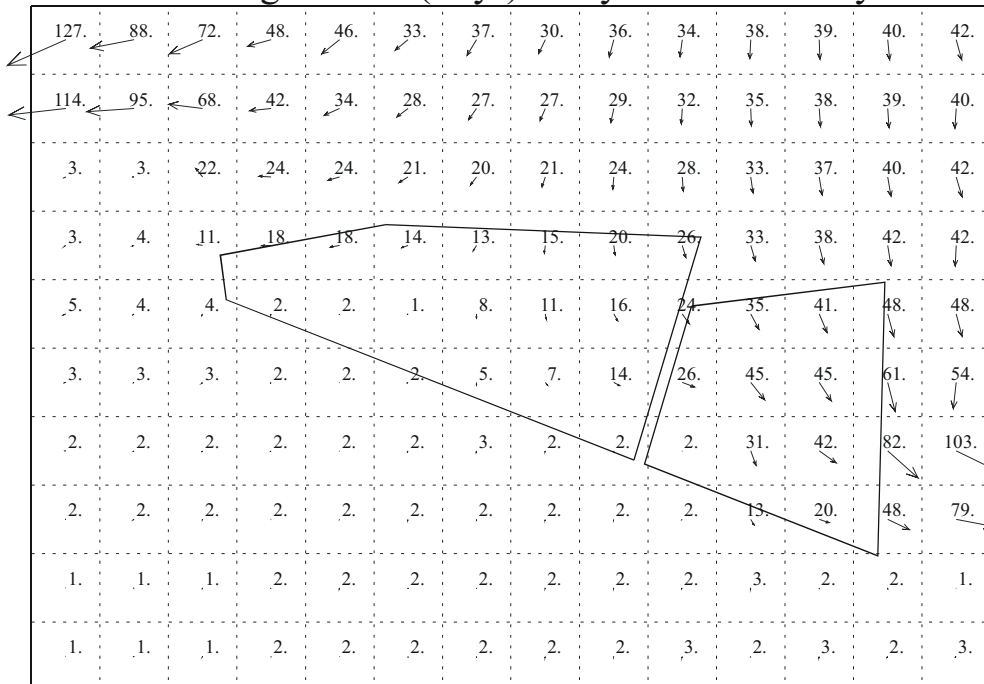


Figure C-8. Simulated aquifer velocities in the refined footprint beneath the Subsurface Disposal Area for uniformly assigned permeability of 712,000 mD in the extended domain.

yels1.GV: Avg Lin Vel (m/yr) in layer 1 at sim day = 0.

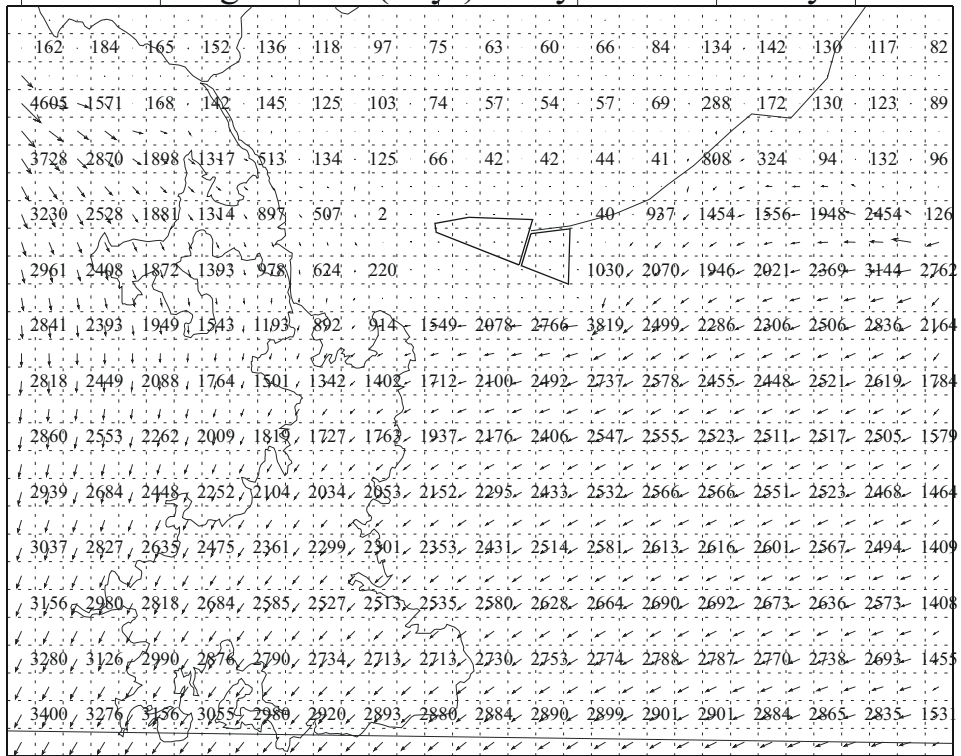


Figure C-9. Simulated aquifer velocities for the Ancillary Basis for Risk Analysis portion of the extended aquifer domain with uniformly assigned permeability of 712,000 mD in the extended domain.

vels2.GV1: Avg Lin Vel (m/yr) in layer 1

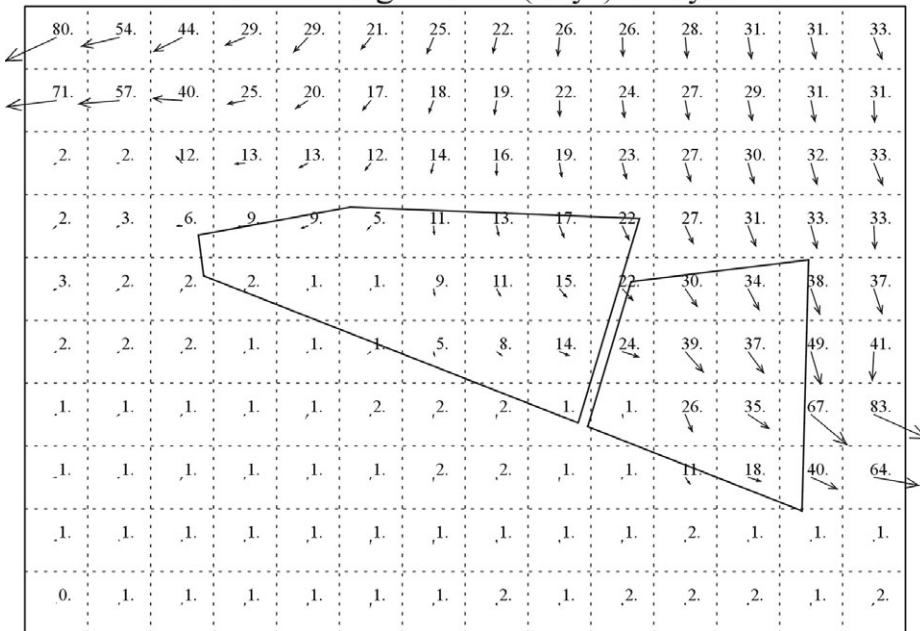


Figure C-10. Simulated aquifer velocities in the refined footprint beneath the Subsurface Disposal Area with permeabilities of 195,300 mD for Waste Area Group-10 Zone 12 and 1,666,350 mD for Waste Area Group-10 Zone 55 in the extended domain.

vels2.GV: Avg Lin Vel (m/yr) in layer 1

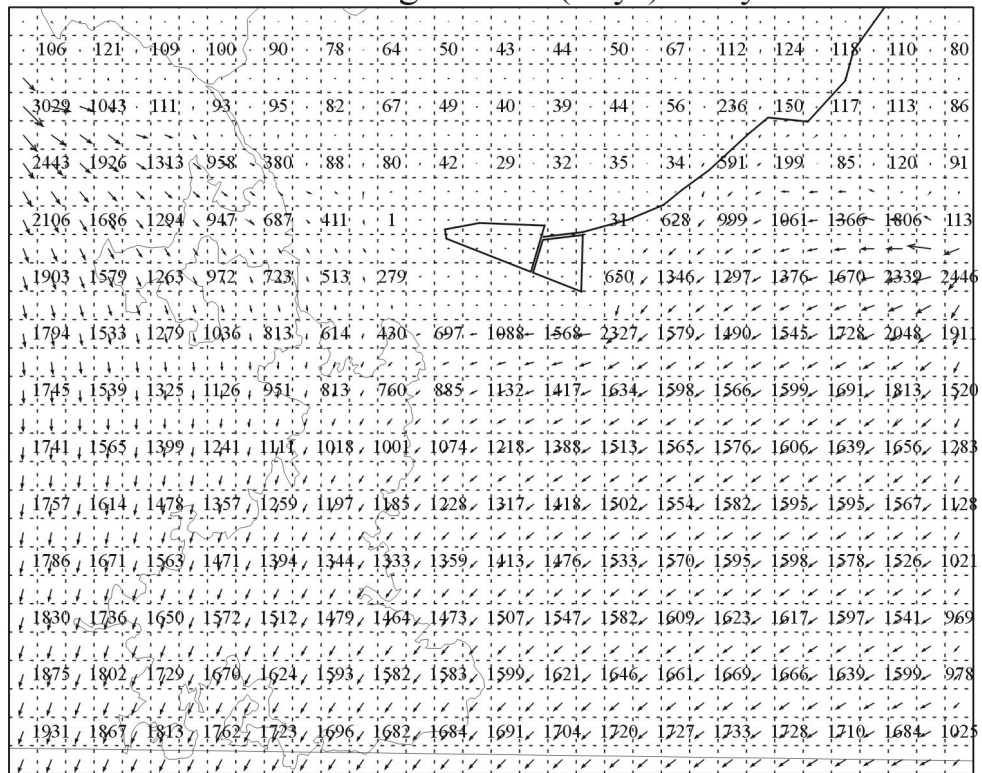


Figure C-11. Simulated aquifer velocities for the Ancillary Basis for Risk Analysis portion of the extended aquifer domain with permeabilities of 195,300 mD for Waste Area Group-10 Zone 12 and 1,666,350 mD for Waste Area Group-10 Zone 55 in the extended domain.

Figures C-6 and C-7 show average linear velocities calculated from the original ABRA model (original three permeability zones, original ABRA domain dimensions and boundary conditions). Figures C-8 and C-9 show the same refined area and original model domain but with the average linear velocities that result from expanding the domain to the new dimensions and using a uniform permeability of 712,000 mD for the entire expanded portion. Figures C-10 and C-11 show the effect on average linear velocity of incorporating the two Waste Area Group-10 permeability zones, Zones 12 and 55, with permeabilities of 195,300 and 1,666,350 mD, respectively.

The low permeability zone immediately downgradient of RWMC slows and refracts flow in the refined area. Resulting average linear velocities are approximately 1 to 2 m/yr in the refined area for all three cases (Figures C-6, C-8, and C-10). Figure C-6 shows velocities of less than 1 to 70 m/yr in the refined area of the original model. Figure C-7 shows the original modeled velocities range from 1 to 2,886 m/yr outside the refined area and is about 1,234 m/yr in the downgradient corner (southwest corner) of the original domain. The upper range of velocities, 2,886 m/yr (26 ft/d), is only slightly above the upper range of velocities (15 ft/d) predicted in earlier INL Site groundwater modeling (Robertson 1974).

Velocities increase in all locations as a result of expanding the domain with a relatively high uniform permeability of 712,000 mD and imposing a larger head drop across the domain (Figure C-8 and C-9). Figure C-8 shows a range of 1 to 127 m/yr in the refined area and Figure C-9 shows velocities more than doubling to 2 to 4,605 m/yr with about 3,400 m/yr in the downgradient corner of the original domain.

When the two additional Waste Area Group-10 permeability zones were incorporated into the extended domain, the velocities in Figures C-10 and C-11 are slowed somewhat relative to Figures C-8 and C-9 but are still higher than the original modeled velocities. This reduction results from a lower permeability of 193,500 mD that was assigned to the southwestern portion of the extended domain. Figure C-10 shows a range of 1 to 83 m/yr in the refined area and Figure C-11 shows a range of 1 to 3,029 m/yr outside the refined area with an average linear velocity of approximately 1,931 m/yr in the downgradient corner of the original model domain.

C-7. COMPARISON TO MEASURED WATER LEVELS

The simulated hydraulic heads from the extended domain model were examined for closeness of match to measured heads. Figure C-12 shows simulated contours and measured wells. A bilinear interpolation scheme was used in PV-Wave to determine simulated head at exact well locations since none of the actual wells are located exactly at a model grid centroid. Standard statistical summaries, such as mean error, mean absolute error, and root-mean squared error, are typically used to quantify simulation error (Anderson and Woosner 1992). These were calculated for the new model and are listed in Table C-1 for the set of 21 wells, common to both the original and extended models, that lies within the extended domain. Table C-1 also lists calculated residuals for these wells.

The original model was more closely calibrated to measured heads (root mean squared error = 1.57, mean average error = 1.08, and mean error = - 0.64; Holdren et al. 2002). The agreement of the new model is especially poor in locations furthest downgradient from RWMC (i.e., wells USGS-011 and USGS-125). This is the result of a large and non-uniform hydraulic gradient. The water-table elevation drops over 150-ft (46 m) across the extended domain. Though the original ABRA model was significantly better calibrated, it was only one-sixth the areal coverage with a total change in head of only 20 ft (6.1 m).

C-8. TRANSPORT SIMULATIONS

The extended model was used in TETRAD simulations with mass flux input from the ABRA vadose zone model (Holdren et al. 2002). Eight groups of contaminants were input to the model and a PV-Wave program was used to prepare resulting isopleths of equal cumulative risk for groundwater consumption. The resulting contour for 10^{-5} cumulative risk now barely crosses the INL Site southern boundary and is captured entirely within the extended domain. Figure C-13 shows the new cumulative risk isopleths resulting from this simulation. The most likely cause of the effective shorter extent of the 10^{-5} risk isopleth is greater dilution resulting from higher velocities in the extended domain.

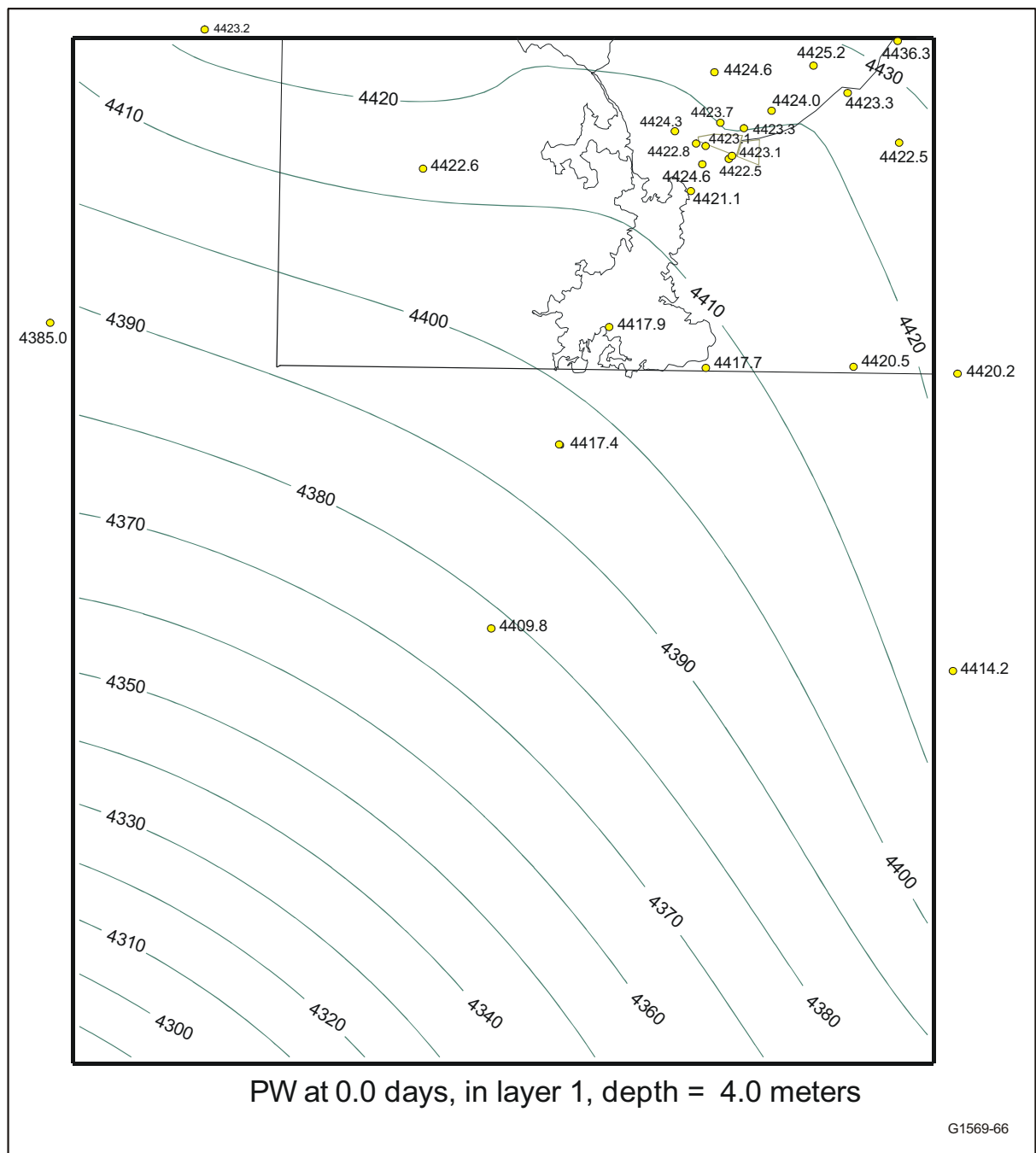


Figure C-12. Simulated water level contours and measured wells in extended domain.

Table C-1. Calculated residuals (simulated minus observed) and summary error statistics.

Well Name	Water-Table Elevation (ft, mean sea level)		Residual (ft)
	Observed	Simulated	
A11A31	4421.91	4413.95	-7.96
RWMC M1SA	4422.81	4417.2	-5.61
RWMC M3S	4423.34	4419.93	-3.41
M4D	4425.04	4414.21	-10.83
RWMC M7S	4424.02	4420.95	-3.07
RWMC M11S	4425.24	4424.08	-1.16
RWMC M13S	4423.31	4420.97	-2.34
RWMC M14S	4424.56	4423.68	-0.88
USGS-009	4417.91	4405.12	-12.79
USGS-011	4409.81	4377.9	-31.91
USGS-086	4422.61	4412.78	-9.83
USGS-087	4423.73	4420.1	-3.63
USGS-088	4424.58	4414.36	-10.22
USGS-089	4424.28	4414.22	-10.06
USGS-105	4420.47	4416.12	-4.35
USGS-106	4422.55	4423.52	0.97
USGS-109	4417.74	4407.63	-10.11
USGS-117	4423.07	4417.89	-5.18
USGS-119	4422.48	4417.41	-5.07
USGS-120	4421.08	4412.19	-8.89
USGS-125	4417.36	4396.02	-21.34

Error statistics	Mean error	-8.0
Mean absolute error	8.1	
Root-mean squared error	10.8	

b rad: Cumulative SCR Risk: CY 3432

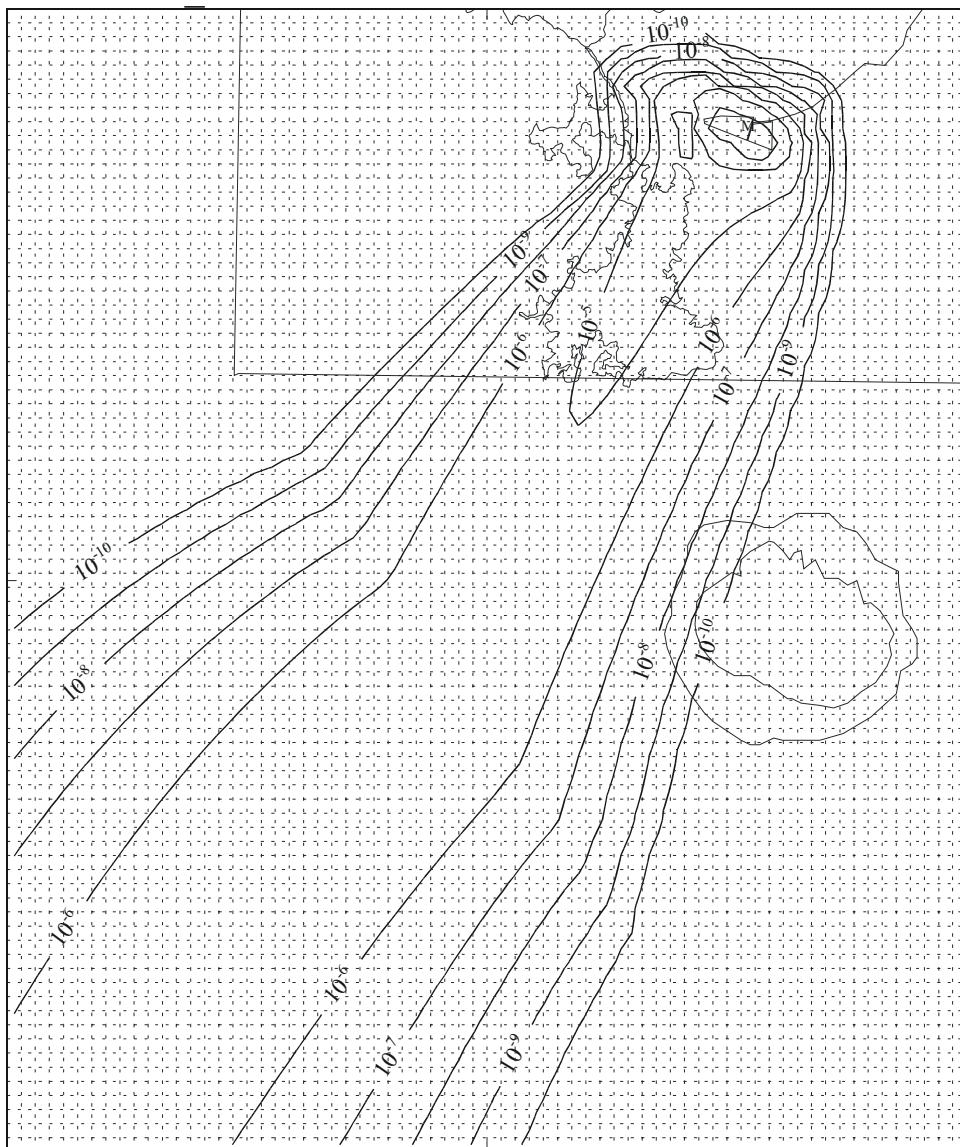


Figure C-13. Cumulative groundwater pathway risk contours from extended domain model.

C-9. CONCLUSION

The main objective of expanding the ABRA saturated model to fully encompass the 10^{-5} cumulative risk contour within the modeled domain was successfully accomplished. The model suffices for Operable Unit 7-13/14 risk modeling despite the water level error that resulted from significant changes in hydraulic head occurring over this new domain. These higher gradients increased the average linear velocity of groundwater throughout the saturated domain regardless of alternative permeability schemes. These higher velocities dilute cumulative risk thereby shrinking the overall risk contours relative to the original model results.

It should be noted that the extended domain prepared for this new model greatly exceeds Waste Area Group-7 boundaries. A model expanded to this degree may be more suited to Waste Area Group-10 modeling. Waste Area Group-10 includes miscellaneous and cumulative sitewide groundwater issues. The extended model and its subsequent water-table mapping and calibration issues represent work that may be best included in a new Waste Area Group-10 subregional-scale saturated groundwater model.

C-10. REFERENCES

- Anderson, M. P. and W. W. Woessner, 1992, "Applied Groundwater Modeling, Simulation of Flow and Advection Transport," *Academic Press*, San Diego, 1992.
- Golden Software, Inc., 2000, *Surfer Version 7.02 Surface Mapping System*, Golden, Colorado, 1993-2000.
- Holdren, K. Jean, Bruce H. Becker, Nancy L. Hampton, L. Don Koeppen, Swen O. Magnuson, T. J. Meyer, Gail L. Olson, and A. Jeffrey Sondrup, 2002, *Ancillary Basis for Risk Analysis of the Subsurface Disposal Area*, INEEL/EXT-02-01125, Rev. 0, Idaho National Engineering and Environmental Laboratory.
- McCarthy, J. M., R. C. Arnett, R. M. Neupauer, M. J. Rohe, and C. Smith, 1995, *Development of a Regional Groundwater Flow Model for the Area of the Idaho National Engineering Laboratory, Eastern Snake River Plain Aquifer*, INEL-95/0169, Rev. 1, Idaho National Engineering Laboratory.
- Robertson, J. B., 1974, *Digital Modeling of Radionuclide and Chemical Waste Transport in the Snake River Plain Aquifer at the National Reactor Testing Station, Idaho*, U.S. Geological Survey, IDO-22054.
- Vinsome, P. K. W. and G. M. Shook, 1993, "Multi-Purpose Simulation," *Journal of Petroleum Science and Engineering*, Vol. 9, pp. 29–38.
- Visual Numerics, Inc., 2001, *PV-WAVE User's Guide*, unpublished work, 1990–2001.

Appendix D

Analysis of Aquifer Hydraulic Gradient in the Radioactive Waste Management Complex Vicinity

Appendix D

Analysis of Aquifer Hydraulic Gradient in the Radioactive Waste Management Complex Vicinity

This appendix contains analyses on groundwater flow directions in the RWMC vicinity that were conducted by Michael Rohe for Operable Unit 7-13/14 in September 2003. Comparisons are made to simulated aquifer velocities from the ABRA model (Holdren et al. 2002). The resulting gradient analysis is compared to the draft RI/FS model aquifer velocities in Section 4.4.3 of this report.

D-1. INTRODUCTION

The purpose of this appendix is to examine, in detail, the aquifer water-table configuration in the Waste Area Group 7 vicinity. Groundwater flows as a result of some type of gradient, typically, hydraulic gradient, which is the difference between potential energy at various points in the aquifer. Usually, water moves in the direction of the maximum gradient at a rate proportional to magnitude. Various methods exist to determine direction and magnitude of hydraulic gradient, based on the measured potentiometric or water-table surface. The slope and direction of slope of this table infers the direction of groundwater flow, assuming an unconfined aquifer and limited refraction of flow.

The hydraulic gradient direction can be determined by mapping contour lines of equipotential hydraulic head that are based on measured aquifer well water levels. A large area can be covered with contouring if sufficient well data are available. However, this method requires well measurements that are taken within the same time frame where results are representative of that time instant only. Gradient direction is determined from lines perpendicular to contours; and the magnitude is determined from the distance between these contours. However, this method has often produced confusing results in the vicinity of RWMC.

Figure D-1 shows some possible contour lines of equal hydraulic head, based on aquifer well water levels measured in October 2002. Figure D-2 shows similar contours lines for a refined area near the SDA. In both figures, the contour lines were drawn by hand to reflect best judgment with regards to field data. The hand-drawn contours in Figures D-1 and D-2 give some general idea of the direction and magnitude of the hydraulic gradient in the Waste Area Group 7 vicinity. However, the hand-drawn contours are specific to the October 2002 time frame and do not consider temporal gradient changes or changes occurring at different spatial scales.

D-2. METHODOLOGY

A different method of determining hydraulic gradient direction and magnitude involves the use of three points of hydraulic head data and is well-documented in literature (Freeze and Cherry 1979, Fetter 1981). These three points form a plane surface that is representative of the water-table surface in the vicinity of these three wells. From the strike and dip of this surface, groundwater hydraulic gradient can be determined. A series of such triangles can be used to find the range in directions for RWMC.

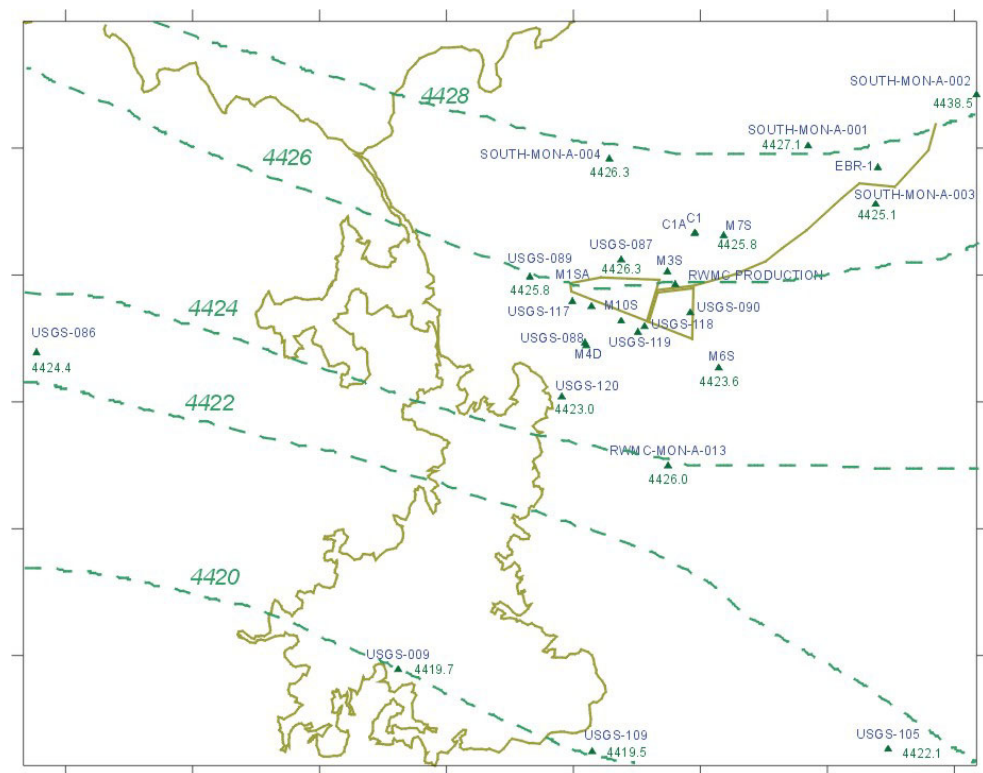


Figure D-1. Possible contour lines for October 2002 water level data.

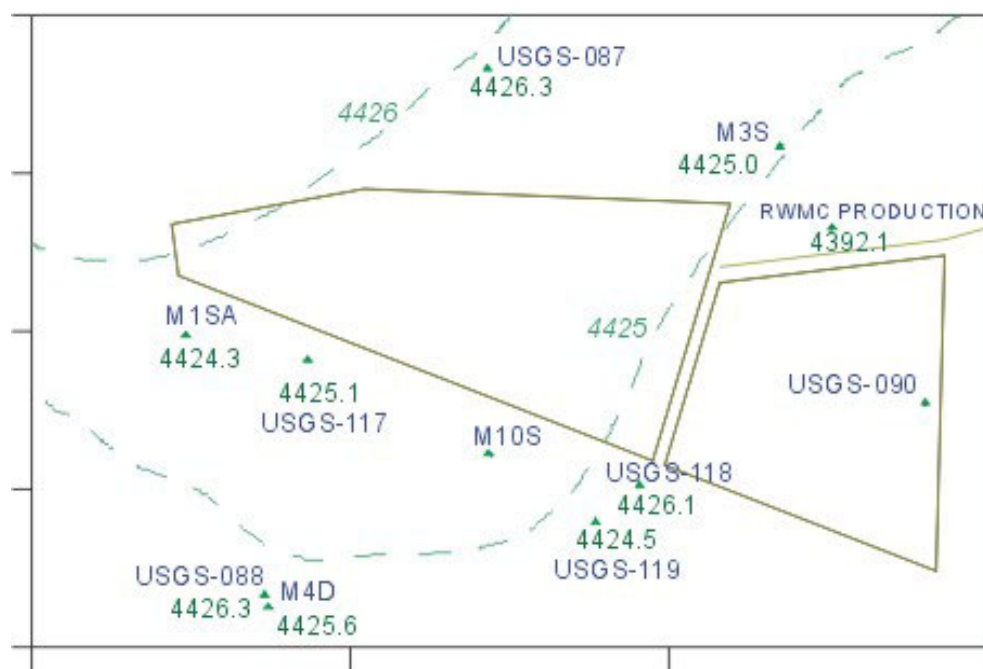


Figure D-2. Possible contour lines for water level data in the vicinity of the Subsurface Disposal Area based on October 2002 well measurements.

This method allows for examination of gradient at different well locations and over various size scales. More importantly, more time steps can be analyzed quickly and changes, if any, that can occur in gradient over time can be observed. Measurements must still be taken nearly simultaneously; however, long-term hydrograph records can be aligned between the three wells. Then, multiple calculations of gradient can be made.

Figure D-3 illustrates application of this method in the SDA area for Wells M3S, USGS-87, and USGS-117. Figure D-3 also includes directional frequency diagrams for the illustrated calculation and for the entire set of calculations using this combination of wells. The directional frequency histogram depicts calculated results of gradient direction. In these histograms, pie wedges are histogram bins with more frequent calculated directions extending pie wedges further from the center of the diagram. These histograms are similar to wind rose diagrams that are commonly used in atmospheric studies.

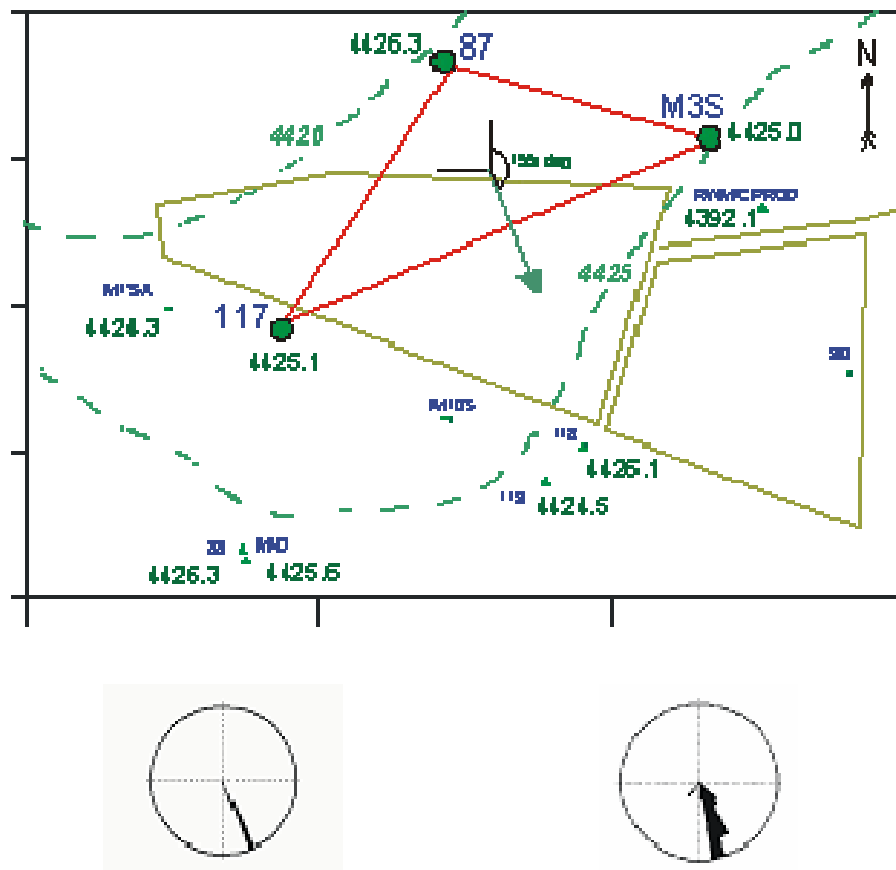


Figure D-3. Application of the three-point method (triangulation) for hydraulic gradient determination.

D-3. METHOD LIMITATIONS

Triangulation can be affected by errors in water-level measurements; these errors include errors in the manual measurement process, errors produced from well boreholes being deviated with respect to plumbness and straightness, errors in coordinate information for a given well, and errors associated with a time lapse between a given calculation's three water-level measurements.

The time-lapse error is often due to water levels changing over time in response to diurnal (daily) barometric pressure changes and synoptic weather effects (time scale of days and weeks). Several investigations at the INL Site have examined the response of aquifer wells to changing barometric pressure. Frederick and Johnson (1997) report typical diurnal barometric pressure changes of 3 cm (0.1 ft) (measured as water) and over 15.2 cm (0.5-ft) changes occurring at the synoptic time scale. They observed aquifer wells, such as USGS-059, in the Idaho Nuclear Technology and Engineering Center area respond to larger pressure changes with water level fluctuations of 9.1 cm (0.3 ft) or more. Hubbell et al. (2004) developed methods for minimizing barometric pressure changes on measured water levels. Their work in the RWMC area showed that 3-cm (0.1-ft) (as water) diurnal changes in barometric pressure have resulted in 6.1-cm (0.2-ft) water-level fluctuations in aquifer Well USGS-118.

The three-point solution for hydraulic gradient is especially sensitive to this barometric-induced error when applied to closely spaced wells. Figure D-4 illustrates the triangulation method at the SDA with “error bars” surrounding the individual well water elevations and are shown with respect to the hydraulic gradient field. These error bars extend 9.1 cm (0.3 ft) on either side of the elevation measurement and correspond to a possible error from barometric changes. The bars are only an approximation of the water-level error, but Figure D-4 shows that in a natural, low-hydraulic gradient of magnitude 5.0 ft/mi, the wells will need to be spaced sufficiently far apart so that these error bars do not overlap. Still, there exists at the INL Site the need to collect more accurate water level data that is unaffected by such barometric changes, which could be accomplished with methods such as those presented by Hubbell et al. (2004).

The corresponding hydrographs for these three wells are also provided in Figure D-4. For the most part, the water levels in Wells M3S and USGS-117 are approximately the same. Therefore, the line connecting these two wells forms a line of equipotential energy. The lines appear to separate and converge over time. Since these two wells are on the same equipotential line, the third well, Well 87, appears to strongly determine the direction and magnitude for these three wells. As a result, this combination may be less suitable than others due to this apparent bias.

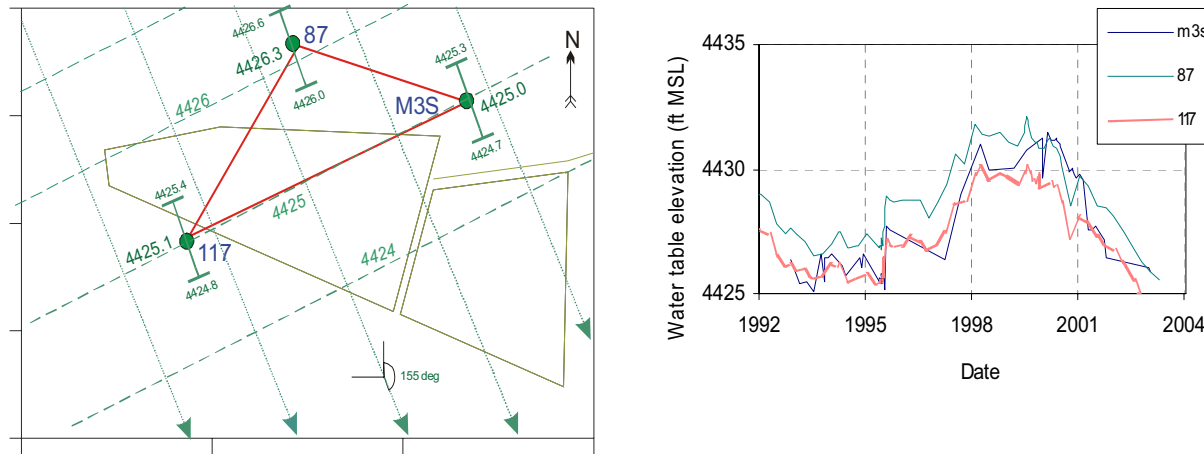


Figure D-4. Three-point solution and hydrographs for the M3S-87-117 combination.

D-4. SELECTING WELL COMBINATIONS

Many combinations are possible when selecting groups of three wells from a larger set of wells. The number of possible nonordered (i.e., listing each combination only once regardless of the order of wells in the combination) can be found from the following expression (from Devore and Peck 1990):

$$n!/(x!(n-x!)) \quad (D-1)$$

where:

- n = number of wells in set
x = number to be combined.

The set of wells examined includes 25 aquifer wells ($n = 25$) with three wells required per each combination. Therefore, the possible combinations is

$$\begin{aligned} n &= 25 \\ x &= 3 \\ n! &= 1.55E+25 \\ x!(n-x)! &= 6.74E+21 \\ n!/(x!(n-x!)) &= 2,300 \end{aligned}$$

Out of only 25 wells, over 2,000 three-well combinations are possible. Some criteria must be used in applying this method so that a manageable number of combinations can be identified that best reflects real gradient conditions. When combining these wells, it is important that certain factors be observed, which may indicate some wells should not be compared together. These factors include significant differences in completion depths and borehole diameters. In particular, the size and shape of the resulting triangle has a strong effect on whether the calculated gradients reflect reality or not. In this analysis, these factors were considered in developing a set of 40 different well combinations.

For each comparison, hydrograph records were aligned so that contemporaneous comparisons of water-table elevation data could be made. Borehole deviation correction factors were also applied. Prudent use of available groundwater elevation data also requires a high-level of confidence in well reference point elevations (i.e., land surface, measuring point, and brass cap monument).

D-5. RESULTS

Results of triangulation indicate that groundwater gradient in the vicinity of Waste Area Group 7 generally is south-southeast (approximately 159 degrees from north). Results for the entire set of 3,100 hydraulic-gradient calculations are shown in Table D-1. These results indicate that there is a great deal of variability in the hydraulic gradient (i.e., a standard deviation of 66 degrees for the entire set). The mean gradient magnitude (6.3 ft/mi) shows a similar high variance (10 ft/mi standard deviation). In general, water-level measurements were chosen to minimize the spread in measurement dates for each calculation of hydraulic gradient. Approximately 1 week (i.e., 8.6 days) is the average time between measurements for the entire set of calculations.

Table D-1. Summary of entire set of 3,100 three-point gradient calculations for the Radioactive Waste Management Complex covering 1972 through 2003.

Statistic	Direction (degrees)	Magnitude (ft/mi)	Number of days ^a
Minimum	0.2	0.1	0.0
Maximum	359	328	28
Mean	159	6.3	8.6
Standard Deviation	66	10.1	6.1

a. Number of days between each water-level measurement used in a particular gradient calculation.

Figure D-5 shows histograms for the results of all 3,100 calculations considered as a single set. The directional frequency histogram shows a large portion (i.e., approximately 31%) of the calculated gradients has an azimuth between 155 to 185 degrees (from north). The magnitude histogram shows over 50% are in the 3 to 7 ft/mi range. The histograms appear to be bimodal. A small portion (i.e., 11%) is in the range of 40 to 60 degrees and suggests some flow reversal occurs at RWMC.

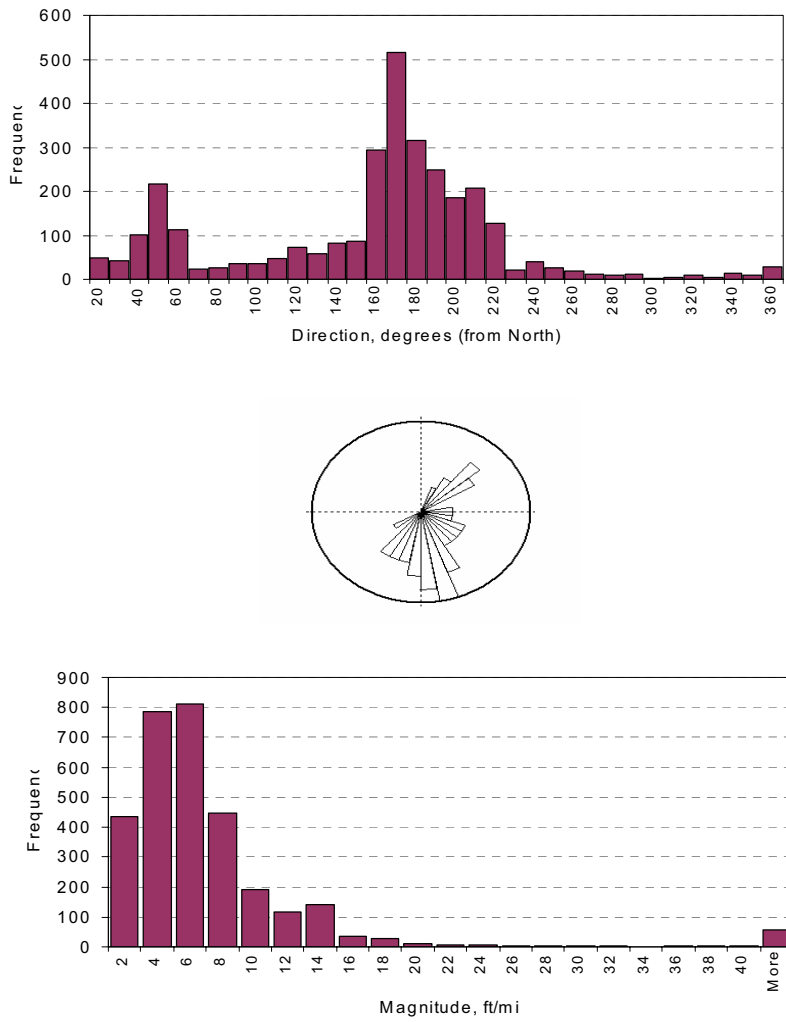


Figure D-5. Histograms for entire set of 3,100 gradient calculations.

Table D-2 lists results for the 40 three-well combinations. The table lists the individual wells in each combination, summary statistics for gradient direction and magnitude, the area covered by each combination of wells, the number of calculations performed for each combination, and the range in dates represented by these calculations. Also shown in Table D-2 is the range of screening depths represented by each three-well combination. This range was the difference between the least and greatest screened interval depth below the water table and was believed to be an indicator of how compatible a given set of wells is for comparing water-level measurements.

Figure D-6 shows mean gradient directions on a large scale. Each arrow is plotted at the centroid of the triangle formed by the three wells and represents the mean gradient direction. The arrow size is proportional to the area covered by the three-well combination. Larger area combinations produce results that appear consistent with the generally accepted south-southwestern gradient. For instance, combination “m12s-86-105” (i.e., Wells M12S, USGS-086, and USGS-105) covered 41.4 km² (16 mi²) and produced gradient results of 199 ± 1 degree mean direction and 3.5 ± 0.1 ft/mi mean magnitude. Smaller combinations, such as “m14s-m7s-89” (1.4 km² [0.55 mi²]), produce highly variable results (168 ± 50 degrees; 1.5 ± 1.1 ft/mi) that are fairly inconsistent with the regional concept.

Figure D-7 shows the hydraulic gradient calculation results for a smaller region that matches the refined domain used in the ABRA (Holdren et al. 2002). As indicated in Tables D-1 and D-2, the directional frequency histograms for most of the three-well combinations show a great deal of variability. Very small combinations produce highly variable results (i.e., m1s-m4d-89), and are, perhaps, affected by barometric pressure or other sources of error that can cause the well hydrographs to cross each other frequently. These results may not be representative of the general movement of water in the RWMC vicinity.

Systematic errors, such as error in a land surface reference datum, may cause other small area combinations to produce unexpected results, even if those results have less variability. Otherwise, smaller triangulations that produce less variable results may reveal local-scale flow anomalies. In general, flow in the Eastern Snake River Plain aquifer is in a direction along the axis of the Snake River Plain (northeast to southwest). However, on local scales, such as at RWMC, flow may occur predominantly in directions parallel to vent corridors, fissures, and fracture orientations, which are, in general, perpendicular to the axis of the plain and parallel to the tectonic faulting of the Basin and Range geologic province. Larger triangulations generally yield gradients that point in the direction of regional flow, parallel to the axis of the plain, which follows a water-table shape that is similar to the regional topography, sloping from northeast to southwest.

Figure D-8 is the same as Figure D-7, except the results of the ABRA-simulated velocity are superimposed (arrows). These aquifer velocity simulations were prepared using a numerical groundwater model and reflect permeability distributions in the RWMC vicinity. The hydraulic head measurements, collected in the field from RWMC aquifer wells and used to triangulate gradient, show some agreement with these simulations. In particular, there is agreement between calculated gradient (based on field measurements) and simulated velocity in the significant southeastern flow that appears beneath the eastern portion of the SDA.

Table D-2. Summary of three-point gradient calculations (sorted by number of calculations).

Well 1	Well 2	Well 3	Number of Calculations	Area (mi ²)	Range in Penetration Depths (ft)	Gradient Direction		Magnitude		
						Mean (degrees from N)	Standard Deviation (degrees)	Mean (ft/mi)	Standard Deviation (ft/mi)	Date Range
A11A31	M11S	M14S	24	1.72	25	225	29	0.7	0.3	1999–2003
A11A31	M13S	USGS-89	10	2.12	15	172	19	1.7	0.4	1999–2003
A11A31	M7S	USGS-89	18	1.13	15	170	23	2.0	0.4	1999–2003
M10S	USGS-88	USGS-117	11	0.03	17	162	129	7.9	3.0	1992–2000
M10S	USGS-118	USGS-119	7	0.005	78	191	10	22.7	5.2	1994–2000
M11S	M12S	M13S	28	0.36	22	207	2	13.7	5.0	1999–2003
M12S	USGS-86	USGS-105	9	16.72	63	199	1	3.5	0.1	1999–2003
M12S	USGS-89	USGS-105	13	7.69	95	220	3	4.7	2.2	1999–2003
M13S	M14S	USGS-109	12	4.43	147	169	5	1.7	0.2	1999–2003
M13S	USGS-86	USGS-109	11	11.88	138	177	4	1.7	0.2	1999–2003
M13S	USGS-105	USGS-109	9	4.88	147	209	9	2.4	0.5	2000–2003
M1S	M3S	USGS-87	300	0.07	44	173	16	7.4	1.7	1992–2003
M1S	M4D	USGS-89	241	0.04	181	87	84	6.9	4.1	1992–2003
M1S	M6S	M7S	14	0.55	25	191	30	1.8	0.2	2001–2003
M1S	USGS-87	USGS-119	292	0.12	48	203	12	5	1	1992–2002
M3S	M10S	USGS-117	8	0.06	24	237	60	4.2	2.0	1992–2000
M3S	M11S	M14S	26	0.65	25	191	7	1.8	0.3	1999–2003
M3S	M4D	M6S	16	0.32	204	166	56	1.5	0.6	1992–2003
M3S	M6S	M7S	116	0.20	23	200	31	1.9	0.8	1992–2003
M3S	M6S	USGS-88	17	0.32	24	114	32	1.9	0.5	1992–2002
M3S	M7S	USGS-87	134	0.07	44	169	27	5.6	2.7	1992–2003
M3S	M7S	USGS-90	106	0.09	7	180	21	2.7	0.9	1993–1999

Table D-2. (continued).

Well 1	Well 2	Well 3	Number of Calculations	Area (mi ²)	Range in Penetration Depths (ft)	Gradient Direction		Magnitude	
						Mean (degrees from N)	Standard Deviation (degrees)	Mean (ft/mi)	Standard Deviation (ft/mi)
M3S	USGS-87	USGS-117	296	0.07	44	159	12	5.4	1.2
M3S	USGS-117	USGS-118	20	0.09	46	240	55	2.9	1.3
M4D	M10S	USGS-117	9	0.03	178	250	152	9.6	10.0
M6S	M13S	M14S	6	1.43	15	166	2	1.3	2001-2001
M6S	M7S	M13S	10	0.56	23	154	2	2.0	2001-2002
M6S	M7S	USGS-89	4	0.71	23	157	4	1.9	0.2
M6S	USGS-87	USGS-120	18	0.55	63	184	17	2.9	0.4
M6S	USGS-90	USGS-119	23	0.10	73	187	68	1.4	1992-2003
M7S	M14S	USGS-89	12	0.55	17	168	50	1.5	2001-2002
USGS-87	USGS-88	USGS-89	190	0.19	37	122	95	12.8	1993-1999
USGS-87	USGS-88	USGS-90	167	0.21	41	114	39	10.4	19
USGS-87	USGS-89	USGS-90	163	0.17	41	110	53	7.1	1999-2003
USGS-87	USGS-89	USGS-117	221	0.10	37	193	29	5.5	21
USGS-87	USGS-90	USGS-118	7	0.10	66	146	22	3.5	1972-1999
USGS-88	USGS-89	USGS-90	172	0.24	5	103	57	15.6	4
USGS-88	USGS-89	USGS-117	203	0.07	18	44	23	14.3	1987-2003
USGS-89	USGS-90	USGS-120	70	0.49	43	167	26	2.4	1.5
USGS-117	USGS-119	USGS-120	132	0.14	32	171	21	2.7	0.8
									1987-2003

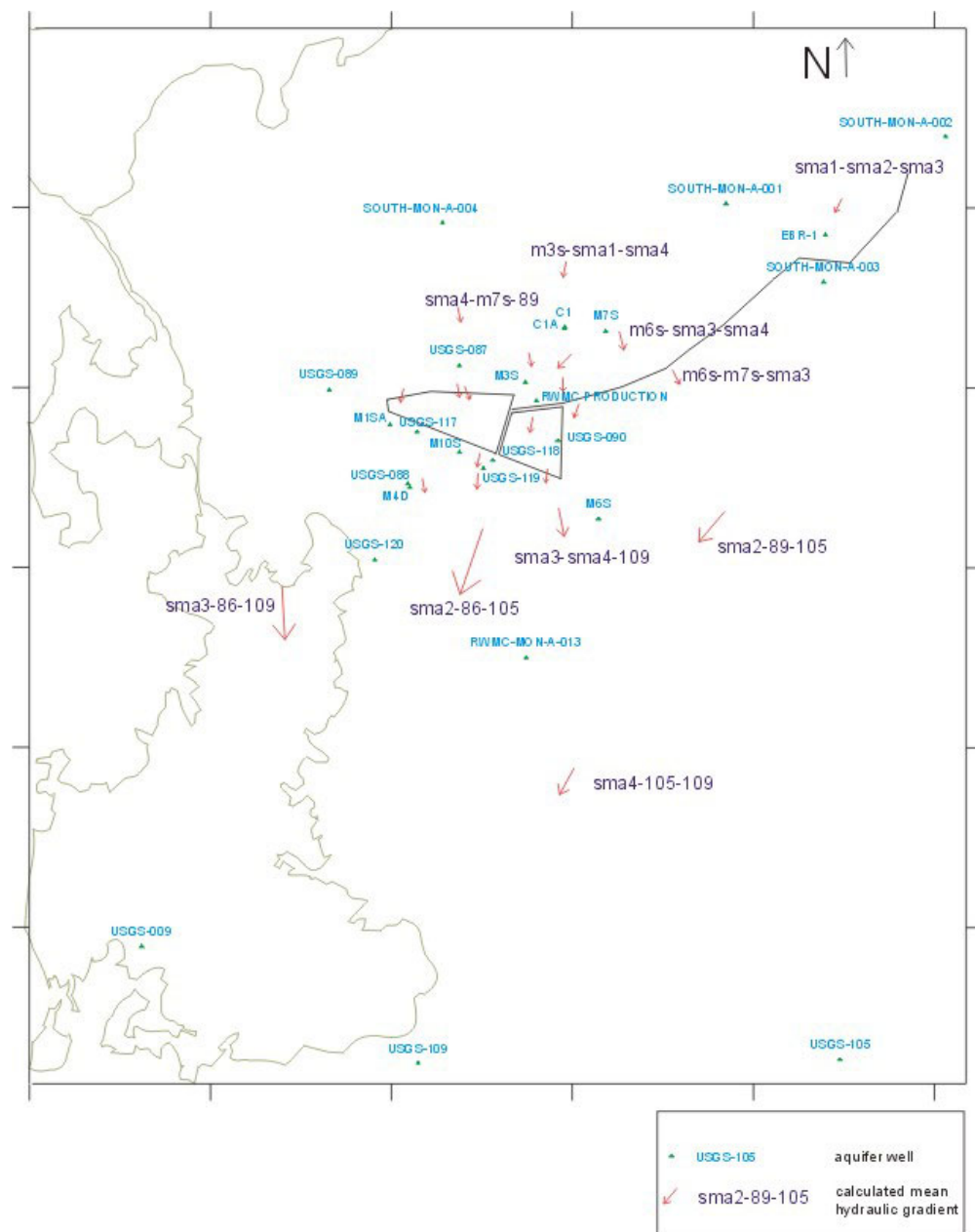


Figure D-6. Results of the mean hydraulic gradient direction for the Radioactive Waste Management Complex vicinity. Arrows are proportional to area represented by each three-well set.

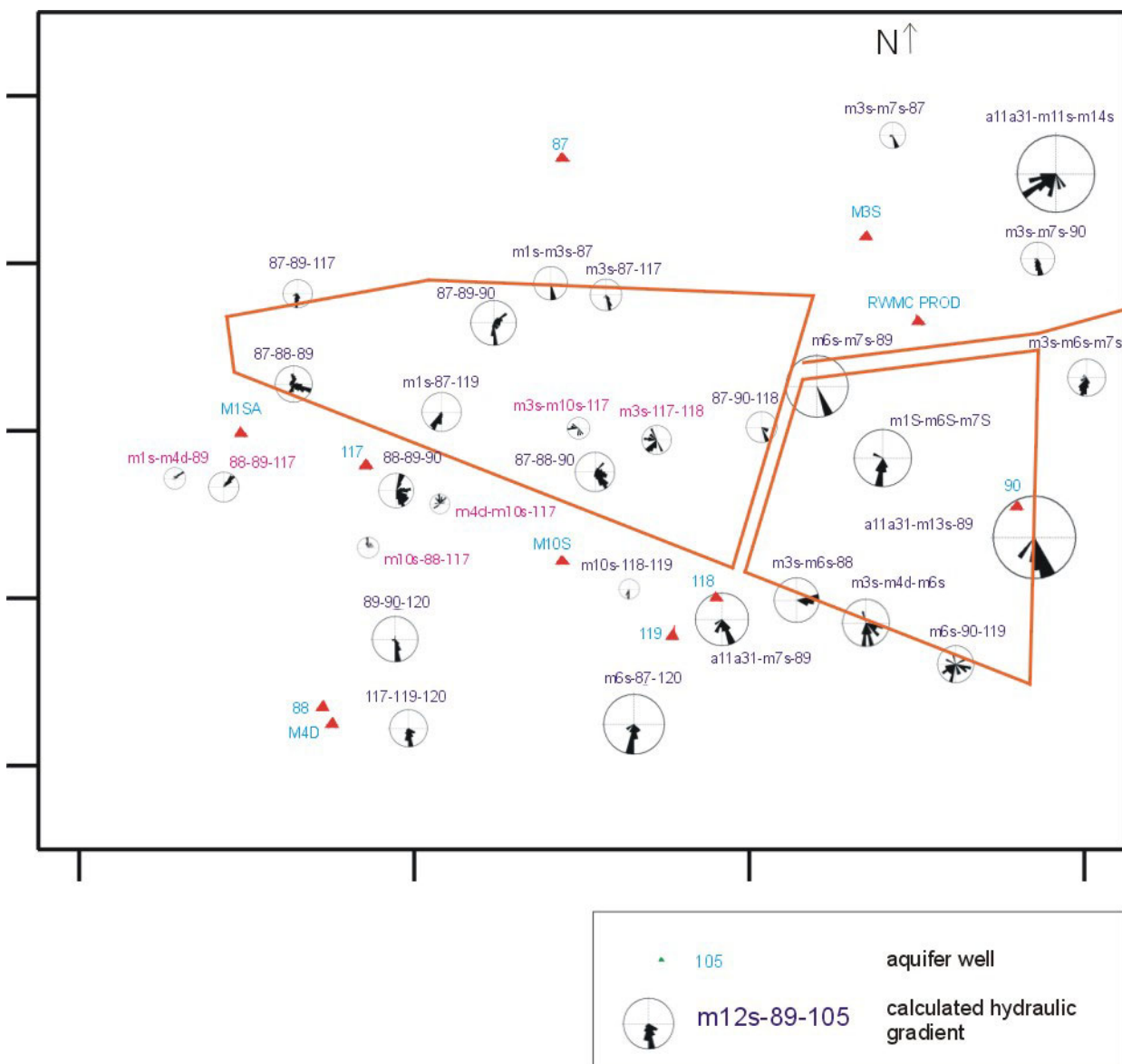


Figure D-7. Hydraulic-gradient directional frequency diagrams (i.e., rose diagrams). Rose diagrams are proportional in size to the area covered by the three-well combination (red font indicates very small combinations [i.e., < 0.10 mi²]).

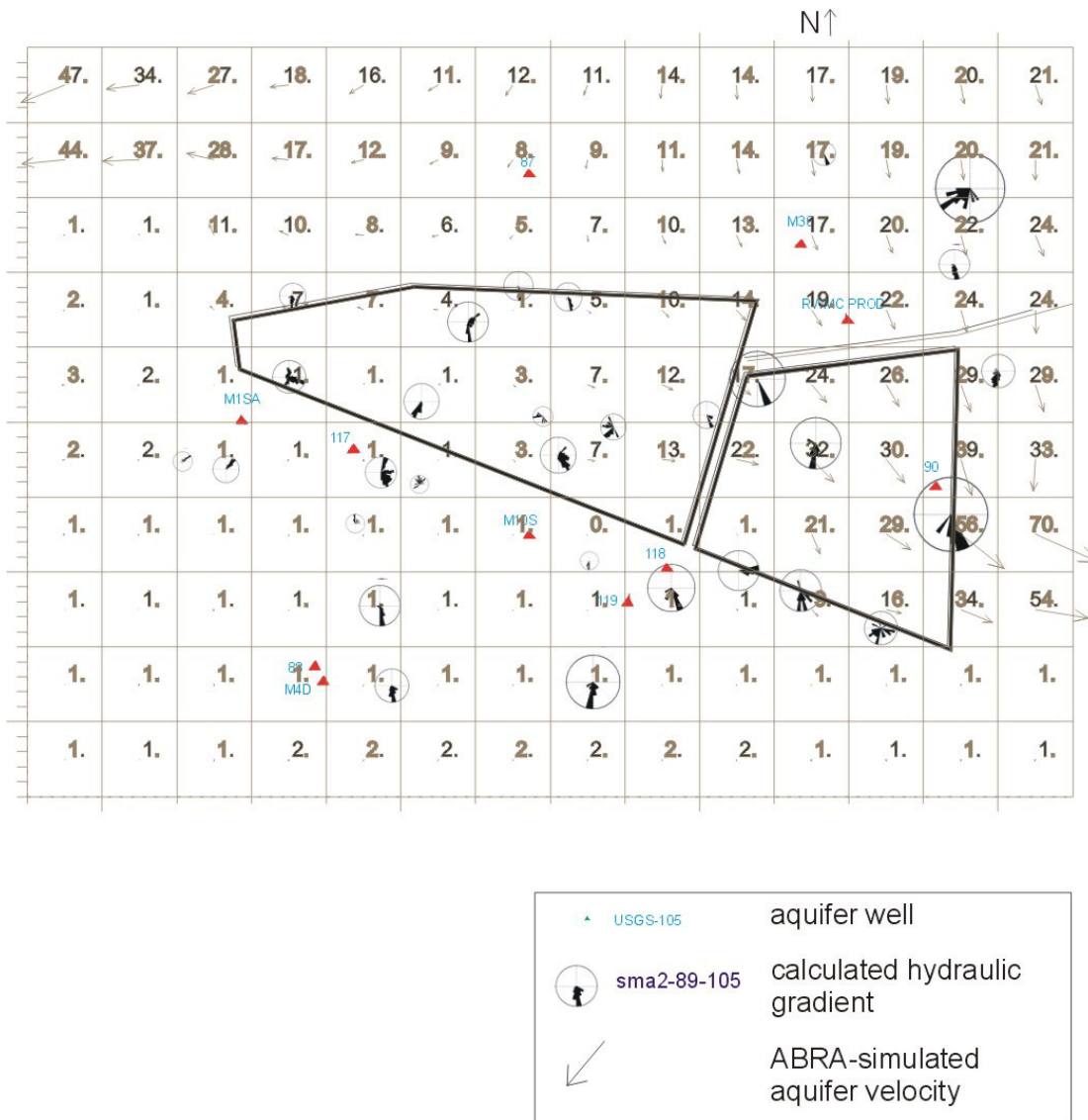


Figure D-8. Comparison of diagrams for the calculated, hydraulic-gradient directional frequency and the results of velocity simulations for the Ancillary Basis for Risk Analysis.

D-6. EFFECTS OF SEPARATION SCALE AND TEMPORAL CHANGES

It was discussed earlier that if the error associated with the measurement is greater than the difference in water-table elevation between two wells used to calculate hydraulic gradient, then the results of this calculation may be suspect. As mentioned, that can be the case for a three-well combination that covers a small area. Figure D-9 shows the effect that closely-spaced wells have on calculated gradients. These three wells cover an area less than 0.26 km^2 (0.10 mi^2) and, as a result, their hydrographs appear to cross one another. When the hydrographs change order (as to which one has the highest elevation), the calculated gradient dramatically changes direction but the relative magnitude may change only little. The resulting directional frequency diagram can be highly variable. This may be the result of barometric fluctuations or even pumping of the RWMC production well (note the well's water elevation in Figure D-2).

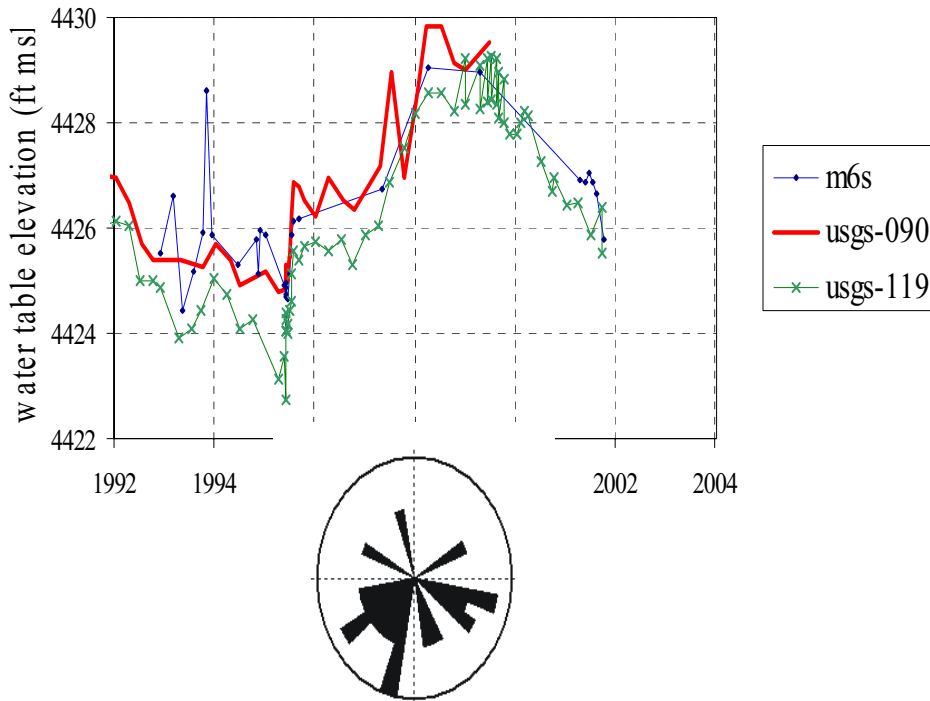


Figure D-9. Hydrograph and resulting rose diagram on the effect of closely-spaced wells on the calculated hydraulic gradient.

Localized recharge from surface waters in the vicinity of RWMC can also cause hydrographs to cross despite well separation distance. Several RWMC-area aquifer wells appear to be affected by flow in the Big Lost River. Some of these wells are located sufficiently far enough from each other such that their hydrograph separation exceeds typical barometric-induced fluctuations; however, their hydrographs have crossed each other in the past in response to stages of the Big Lost River. Figure D-10 depicts hydrographs for three wells used in a particular triangulation (i.e., Wells USGS-87, -88, -89). Also included in Figure D-10 is the river hydrograph for a station near Arco, Idaho. Although other gaging stations on this river are located closer to the INL Site, the Arco station has a much longer and complete record than closer stations; therefore, the Arco station is used in Figure D-10. Flow into the RWMC spreading areas (designed for Big Lost River diversion) appears to effect some groundwater flow reversal.

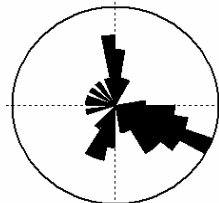
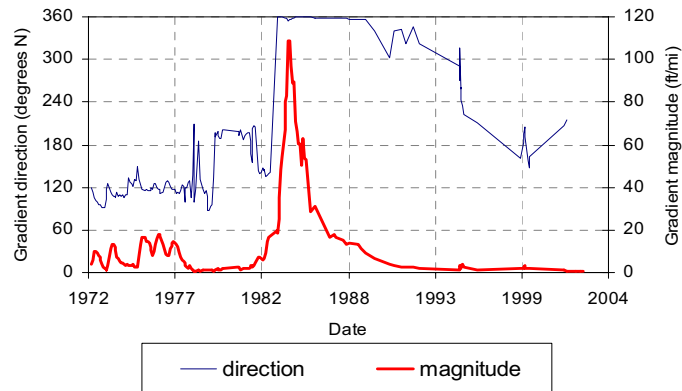
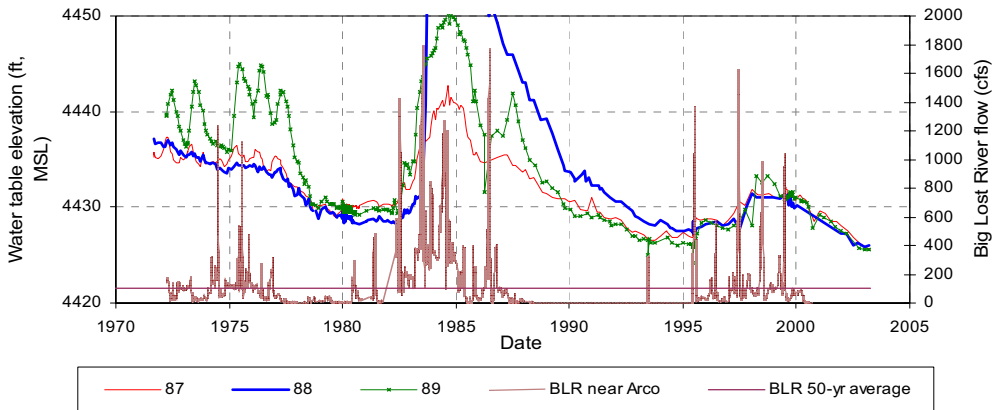


Figure D-10. Hydrographs for the 87-88-89 combination and Big Lost River near Arco, Idaho. The resulting gradient directional histogram is also shown.

The directional histogram shows three different major directions of gradient (approximately 120, 180, and 360 degrees from north), corresponding to different flows in the Big Lost River. Table D-3 summarizes flow conditions in the river and corresponding changes in hydraulic gradient as observed in Wells USGS-87, -88, and -89. Although Well USGS-88 may have a casing leak somewhere between land surface and the aquifer water table that results in spurious high-water levels in this well, other combinations show similar gradient reversals (see the -87-88-89 combination in Figure D-7). The RWMC spreading areas are located southwest of the SDA; groundwater mounding southwest of RWMC would cause gradient direction to point northeast.

Table D-3. Effects of the Big Lost River near Arco on hydraulic gradient (triad -87-88-89).

Period	Flow Type	Big Lost River Near Arco,		
		Mean Discharge (cfs)	Mean Direction (degrees)	Mean Magnitude (ft/mi)
1971–1978	High	125	117	7
1979–1982	Low	29	186	5
1983–1988	High	306	356	48
1989–1995	Low	3	256	2

Finally, the hydraulic gradient in the RWMC area appears to change with time. Large changes in water availability, resulting from long-term (i.e., about 10-year) drought cycles, affect the water-table elevation. It appears that not all wells have the same response to these long-term cycles. As a result, the hydraulic gradient, as determined from aquifer well water-level measurements, appears to change in direction and magnitude over time. Figure D-11 shows directional changes of up to 90 degrees over the course of monitoring from 1993 to 2003 for the m3s-97–117 well combination.

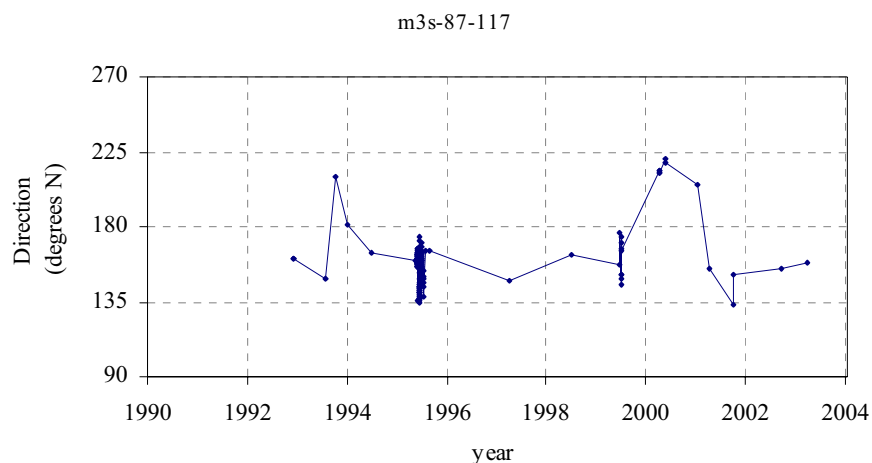


Figure D-11. Change in hydraulic gradient direction over time for one three-well combination (i.e., Wells RWMC-m3s, USGS-087, and USGS-117).

An outcome of this analysis is that there should be a certain minimum area required for using water-table elevation data to determine hydraulic gradient direction and magnitude. At RWMC, like other facilities at the INL Site, there appears to be highly variable local hydraulic gradients that are inconsistent with the regional gradient.

The water table beneath RWMC, and elsewhere at the INL Site, is not a flat, uniform surface. The water table has undulations, ridges, and bumps caused by local heterogeneity. Quite possibly the water is moving in a direction counter to regional gradient over small distances. Figures D-12 and D-13 show the effects of scale on calculated hydraulic gradient. These figures suggest that variance is minimal after an area of about 5.2 km^2 (2 mi^2) is exceeded.

D-7. CONCLUSIONS

Although there are practical limitations to application of the triangulation method for calculating hydraulic gradient (i.e., well separation scales of 5.2 km^2 [2 mi^2] or more, error-free water level data, and accurate land surface reference data), this method can be used to examine gradients at different spatial and temporal scales. The hydraulic gradient in the RWMC vicinity appears to be mostly 160 to 190 degrees (from north) at about 3 to 7 ft/mi magnitude. Variance is quite high in this area (up to 150 degrees and 32 ft/mi for direction and magnitude, respectively). These may be associated with data error, spatial scaling, or recharge from the Big Lost River. Localized heterogeneities in the aquifer matrix may affect gradients at smaller spatial scales. However, when examined at different time scales, flow in the Big Lost River (and to the RWMC spreading areas) appears to contribute to gradient reversals.

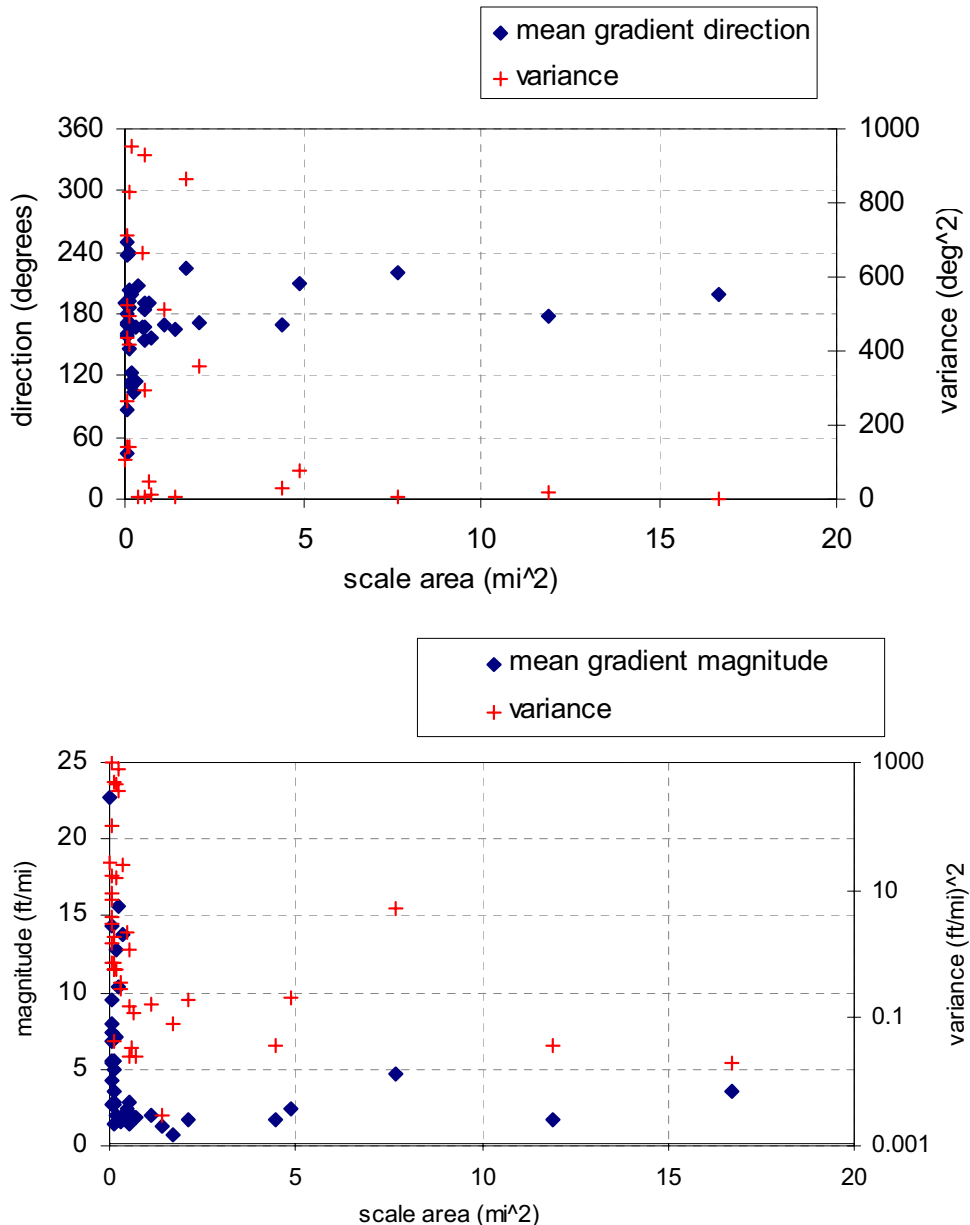


Figure D-12. Effect of scale size on the calculated hydraulic gradient direction and magnitude. (Note the use of logarithmic scale for magnitude variance.)

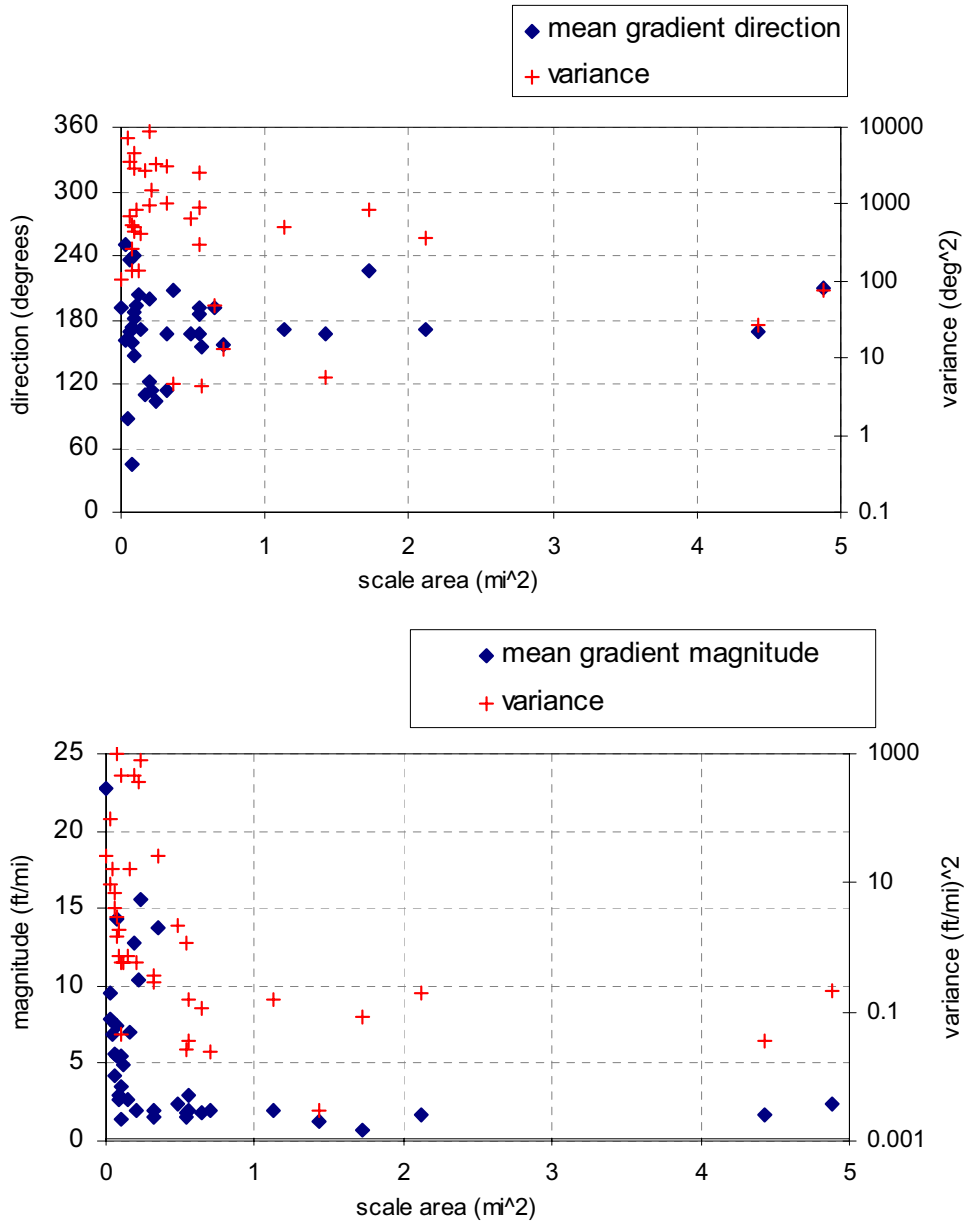


Figure D-13. Detailed view of the effect of scale size on the calculated hydraulic gradient direction and magnitude. (Note the use of logarithmic scale for variance.)

D-8. REFERENCES

- Devore, J. L. and R. Peck, 1990, *Introductory Statistics*, West Publishing Co., St. Paul.
- Fetter, C. W., Jr., 1981, "Determination of the Direction of Groundwater Flow," *Ground Water Monitoring Review*, Fall 1981.
- Frederick, D. B. and G. S. Johnson, 1997, Depth and Temporal Variations in Water Quality of the Snake River Plain Aquifer in Well USGS-59 near the Idaho Chemical Processing Plant at the Idaho National Engineering and Environmental Laboratory, Research Technical Note 97-1, Idaho Water Resources Research Institute, Moscow, Idaho.
- Freeze, R. A. and J. A. Cherry, 1979, *Groundwater*, Englewood Cliffs, New Jersey: Prentice-Hall.
- Holdren, K. Jean, Bruce H. Becker, Nancy L. Hampton, L. Don Koeppen, Swen O. Magnuson, T.J. Meyer, Gail L. Olson, and A. Jeffrey Sondrup, 2002, *Ancillary Basis for Risk Analysis of the Subsurface Disposal Area*, INEEL/EXT-02-01125, Rev. 0, Idaho National Engineering and Environmental Laboratory.
- Hubbell, J. M., M. J. Nicholl, J. B. Sisson, and D. L. McElroy, 2004, "Application of a Darcian Approach to Estimate Liquid Flux in a Deep Vadose Zone," *Vadose Zone Journal*, Vol. 3, pp. 560–569.

Appendix E

Comparison of Additional Interbed Hydrologic Properties to Estimated Values

Appendix E

Comparison of Additional Interbed Hydrologic Properties to Estimated Values

This appendix presents a comparison of measured interbed hydrologic properties to those estimated in the Leecaster (2002) kriging, which is implemented in the RI/FS model. Additional data are presented first and are followed by comparison data. This material comes from a draft report prepared by Larry Hull, Cheryl Whitaker, and Joel Hubbell with contributions from Molly Leecaster and Larry Blackwood. The material in this appendix provides substantiation for properties assigned in the RI/FS model.

E-1. ADDITIONAL RESULTS FOR HYDROLOGIC ANALYSES OF INTERBED SAMPLES

Hydrologic analysis results found in this section are documented in Schaffer (2004). Interbed core samples were recovered during well-drilling activities in Fiscal Year 2003 by the Operable Unit 7-08 Project. Figure E-1 shows well locations where additional core samples were taken for hydrologic property analyses.

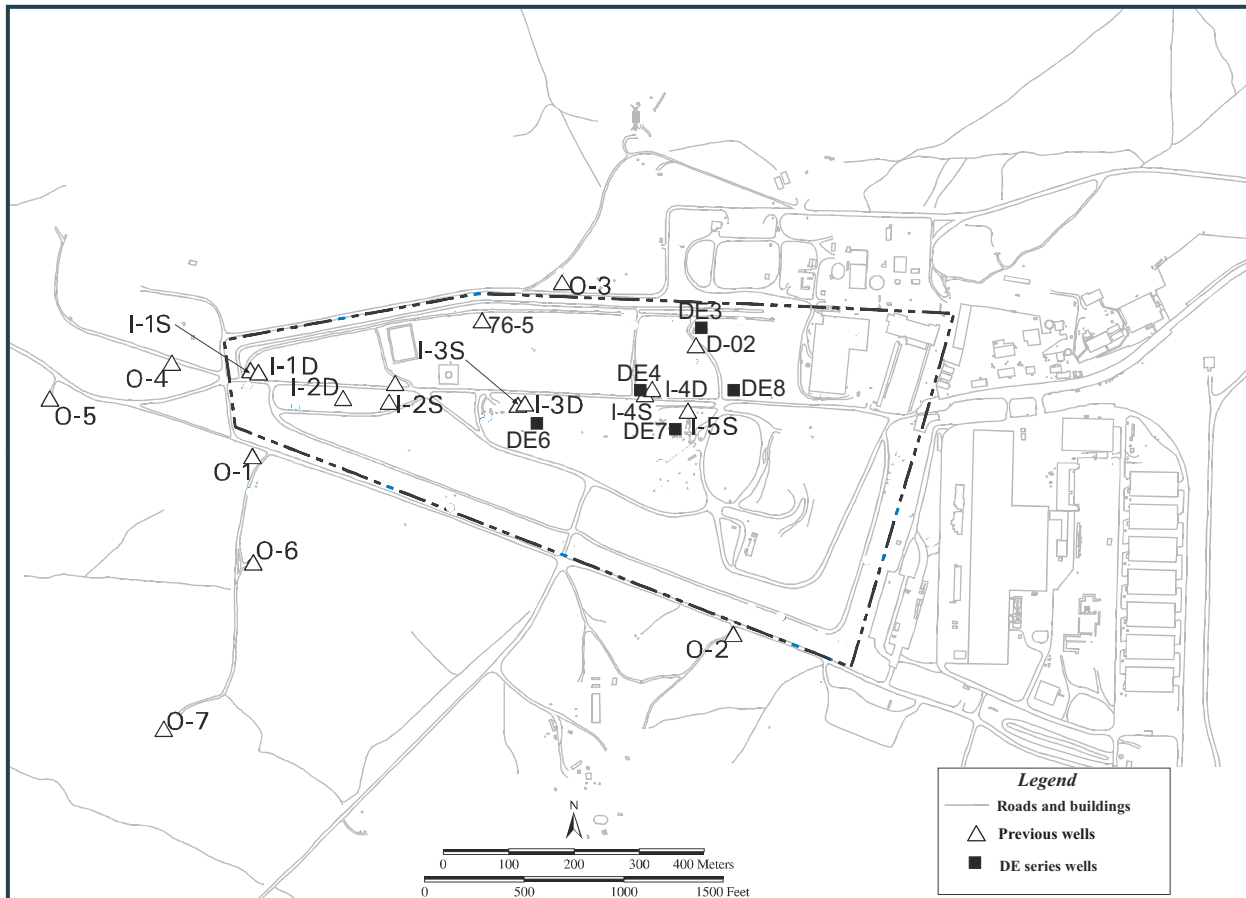


Figure E-1. Current and previous well locations for interbed core hydrologic properties analysis.

Samples for analysis of hydrologic properties were taken from the uppermost section of the core interval, nearest the basalt layer above the interbed and from a distinct coarse-to-fine (e.g., sand to silt or clay) sediment interface, when available. Samples for analysis of hydrologic properties required an intact sample approximately 15 cm (5.9 in.) long.

Samples were analyzed for saturated hydraulic conductivity, porosity, moisture characteristics (i.e., seven-point moisture release curve), grain size, initial volumetric water content, and dry bulk density (Table E-1). Results (Table E-2) were compared with previous analyses of hydrologic properties done on core and interbed material at RWMC to assess the degree of continuity within the interbeds. The data were also compared to hydrologic parameters used in the TETRAD model for Operable Unit 7-13/14 to determine whether the model is conservative or not with respect to these properties.

Table E-1. Sampling of core hydrologic properties and analysis approach for the Subsurface Disposal Area.

Objective	Data Use	Measurement	Method	Detection Level
Obtain samples from stored interbed cores for analyses of hydrologic properties.	Determine spatial variation of interbed layers underlying the Subsurface Disposal Area.	1. Saturated hydraulic conductivity	1. ASTM D2434-68 and <i>Methods of Soil Analysis</i> (Chapter 28, Klute 1986)	1. $\pm 1 \times 10^{-7}$ cm/s
	Support Waste Area Group 7 modeling.	2. Porosity	2. <i>Methods of Soil Analysis</i> (Chapter 18, Klute 1986)	2. ± 0.01
	Provide additional characterization to update and test correlation ranges present in Leecaster (2002) in support of the Ancillary Basis for Risk Analysis (Holdren et al. 2002).	3. Moisture characteristic (seven points)	3. ASTM D2325-68 and <i>Methods of Soil Analysis</i> (Chapter 26, Klute 1986)	3. $\pm 0.01\%$
		4. Particle size analysis (standard sieves [wet] #4-200/hydrometer analysis)	4. ASTM D422-63	4. $\pm 1 \mu\text{m}$
		5. Initial volumetric water content	5. ASTM D2216-98/D4643-00 (ASTM 2000b)	5. Not applicable
		6. Dry bulk density	6. ASTM D2937-00e1 and <i>Methods of Soil Analysis</i> (Chapter 13, Klute 1986)	6. Not applicable
		7. Calculated unsaturated hydraulic conductivity	7. Not applicable	7. Not applicable

ASTM = American Society for Testing and Materials (now known as ASTM International)

Table E-2. Hydrologic properties of interbed sediment.

Well Name	Well Alias	Sample Depth (ft bsl)	Bulk Density (g/cm ³)	Moisture Content (%)	Total Porosity (%)	Saturated Hydraulic Conductivity (cm/s)
RWMC-1810	DE-3	243.3	1.67	17.3	29.8	1.30E-03
RWMC-1813	DE-4	233.1	1.59	25.7	34.6	2.62E-04
RWMC-1813	DE-4	239.3	1.64	22.9	31.1	7.27E-05
RWMC-1816	DE-6	240.2	1.67	19.4	30.7	5.13E-04
RWMC-1819	DE-7	242.5	1.61	20.9	32.1	7.99E-04
RWMC-1819	DE-7	247.5	1.64	18.8	31.7	1.32E-03
RWMC-1819	DE-7	249	1.79	18.1	23.2	4.54E-04
RWMC-1822	DE-8	233.4	1.60	4.4	35.2	8.33E-02
RWMC-1822	DE-8	240.7	1.50	17.9	37.2	3.04E-03
RWMC-1822	DE-8	242	1.82	12.6	21.6	1.29E-05

E-2. CURRENT RADIOACTIVE WASTE MANAGEMENT COMPLEX RESULTS FOR ANALYSES OF INTERBED HYDROLOGIC PROPERTIES AND PREVIOUS HYDROLOGIC PROPERTIES

Results of current hydrologic properties were compared with previous work by Leecaster (2002). The analytical approach is given below.

Porosity and hydraulic conductivity were measured in ten samples from five new locations in 2004. Permeability was calculated by multiplying hydraulic conductivity by 9.66E + 07. The measurements were taken from C-D interbed soil and were located close to previous sample sites (see Figure E-1). New porosity and permeability results were compared with predicted values derived by universal kriging and inverse distance weighting, respectively. Discussion of these methods and rationale for use are presented and described by Leecaster (2002). Table E-3 lists the new wells, the closest well from Leecaster (2002), measured values for porosity and permeability, predicted values, prediction intervals, and the values at the nearest well.

Table E-3. Comparison of new C-D interbed core porosity and permeability to model predictions and near-well values.

New Interbed Core	RWMC-1810 (DE-3)	RWMC-1813 (DE-4)	RWMC-1816 (DE-6)	RWMC-1819 (DE-7)	RWMC-1822 (DE-8)
Closest well (distance ft)	D02 (202.2)	I4-D (57.2)	I3-D (174.8)	8801D (37.5)	D02 (454.5)
Observed porosity (%)	29.8	34.6 31.1	30.7	32.1 31.7 23.2	35.2 37.2 21.6
Predicted porosity	45.20	30.98	42.10	47.07	48.43
Prediction interval porosity	(37.4-53.0)	(26.6-35.3)	(35.1-49.1)	(43.6-50.6)	(38.4-58.5)
Closest observed porosity	43.02	29.88	44.2	48.86	43.02

Table E-3. (continued).

New Interbed Core	RWMC-1810 (DE-3)	RWMC-1813 (DE-4)	RWMC-1816 (DE-6)	RWMC-1819 (DE-7)	RWMC-1822 (DE-8)
Observed permeability (mD)	737.36	271.22 75.26	39.89	827.12 1,366.46 469.98	86,231.88 3,147.00 13.35
Predicted permeability	476.18	290.74	504.63	230.34	498.98
Prediction interval permeability	(169.3-783.0)	(0-616.1)	(145.9-863.3)	(0-524.0)	(161.6-836.4)
Closest observed permeability	321.27	3.00	339.23	10.80	321.27

All porosity values, except those from Well RWMC-1813 (DE-4), were lower than porosities measured nearby and were less than the lower-bound of the prediction intervals.

Four of ten permeability values were within the predictions intervals. For those outside, two were below the lower limit and four were greater than the upper limit. Eight of the ten permeability values were greater than permeability values measured nearby. Small sample size makes analysis of results more uncertain, but, given that condition, the data do not suggest significant bias in the model.

In general, predictions were not very close to new data values. For both permeability and porosity, sample size was small and small-scale variability was large compared with the overall variance, making spatial modeling difficult and highly uncertain. The porosity variogram was modeled with a 0 nugget, indicating that the small-scale variance is negligible. This may be a shortcoming of the model. Setting the nugget to 33% of the total variance (sill) did not improve the correspondence between the new porosity results and the prediction intervals. Therefore, although a zero nugget may be a shortcoming of the model, increasing the nugget alone does not improve correspondence between the new values and the predictions.

An easting trend was originally fit to the porosity data, owing to a couple of large values on the east and small values on the west. However, the effect of this seems to be small because predictions at the new 2004 locations vary little if the trend is removed.

Spatial modeling with so few sample locations and large small-scale variability is difficult. However, it is an improvement from predicting an overall mean or median for the whole area. Although the new data do not match the model very well, the new results are closer to the model predictions than to the overall median (68 mD). Therefore, we conclude that modeling spatial distribution of permeability is an improvement from predicting an overall mean or median for the whole area.

E-3. REFERENCES

- ASTM D422-63, 2002, "Standard Test Method for Particle-Size Analysis of Soils," ASTM International.
- ASTM D2325-68, 2000, "Standard Test Method for Capillary-Moisture Relationships for Coarse- and Medium-Textured Soils by Porous-Plate Apparatus," ASTM International.
- ASTM D2937-00e1, 2000, "Standard Test Method for Density of Soil in Place by the Drive-Cylinder Method," ASTM International.

ASTM D2434-68, 2000, "Standard Test Method for Permeability of Granular Soils (Constant Head)," ASTM International.

ASTM D4643-00, 2000, "Standard Test Method for Determination of Water (Moisture) Content of Soil by the Microwave Oven Method," ASTM International.

Holdren, K. J., H. B. Becker, N. L. Hampton, L. D. Koeppen, S. O. Magnuson, T. J. Meyer, G. L. Olson, and A. J. Sondrup, 2002, *Ancillary Basis for Risk Analysis of the Subsurface Disposal Area*, INEEL/EXT-02-01125, Rev. 0, Idaho National Engineering and Environmental Laboratory.

Klute, A., 1986, "Methods of Soil Analysis Part 1 Physical and Mineralogical Methods," 2nd Edition, eds. G. S. Campbell, R. D. Jackson, M. M. Mortland, D. R. Nielsen, and A. Klute, Madison: American Society of Agronomy, Inc., Soil Science Society of America, Inc.

Leecaster, M. K., 2002, *Geostatistic Modeling of Subsurface Characteristics in the Radioactive Waste Management Complex Region, Operable Unit 7-13/14*, INEEL/EXT-02-00029, Rev. 0, Idaho National Engineering and Environmental Laboratory.

Schaffer, J. M., INL, to Katie Hain, DOE, September 24, 2004, "Contract No. DE-AC07-99ID13727—Transmittal of Limitations and Validations Report for Interbed Core Sampling Conducted in November 2003 for Waste Area Group 7," CCN 52247.

Appendix F

Reanalysis of B-C Interbed Porosity Spatial Variability

Appendix F

Reanalysis of B-C Interbed Porosity Spatial Variability

This appendix contains the reanalysis of the B-C interbed porosities for the variogram and kriging results. Leecaster (2002) used minimum instead of average porosities from each location where core samples were evaluated for the B-C interbed.

The values (i.e., mean porosity) used in the analysis are given in Table F-1 and are seen in Figure F-1. There was no evidence of a spatial trend based on a regression of locations (all p-values were greater than 0.15). The incorrect data did show a trend. Because the data were not significantly different from normal (Shapiro-Wilk p-value = 0.57), the raw data were used to determine the variogram and kriging predictions. Because of the small number of sample locations, anisotropy was assumed without verification and an omni-directional variogram was used. The variogram cloud (Figure F-2) suggests spatial correlation at short lags; however, the empirical variogram (Figure F-3) with at least five pairs of points used for each value plotted does not suggest spatial correlation at short lags. Based on previous work and the variogram cloud, a spherical model with range = 1,000 ft, sill = 38, and nugget = 0 (Figure F-3) was used in ordinary kriging. The resulting kriging predictions on the four grids (Table F-2) are presented in Figures F-4 through F-7. Grids 1, 2, and 3 correspond to the base and refined grids for the RI/FS model shown in Figure 4-2 of this document.

Table F-1. Mean porosity for the B-C interbed.

Well	Mean Porosity
I1-S	25.6
I2-S	29.4
I3-S	26.4
I4-S	47.5
O-1	32.5
O-2	28.4
O-3	33.8
O-5	29.9
O-6	39.8
O-7	34.9
O-9	35.5
BG-91	35.5
BG-94	36.5
BG-95	32.7
BG-96	43.2
D15	37.9
UZ98-2	46.1

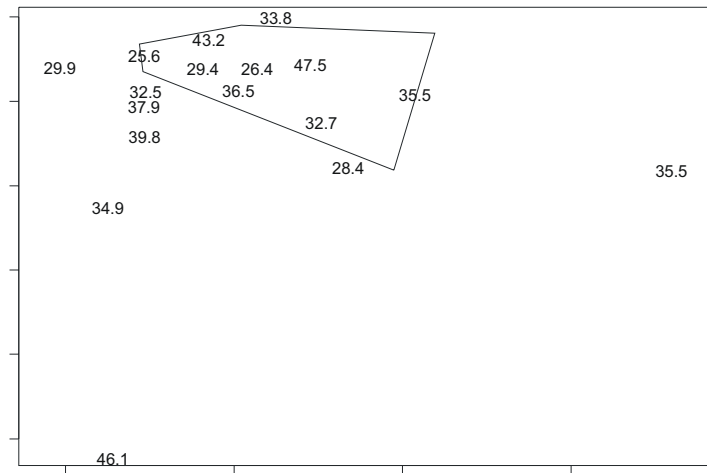


Figure F-1. Mean porosity value for the B-C interbed. Sampling locations shown relative to the Subsurface Disposal Area.

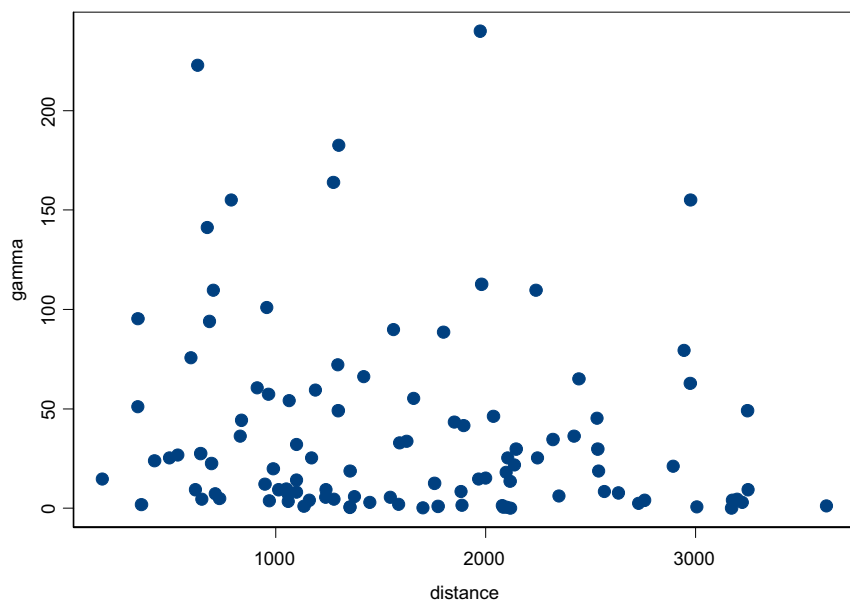


Figure F-2. Variogram cloud for mean porosity from the B-C interbed.

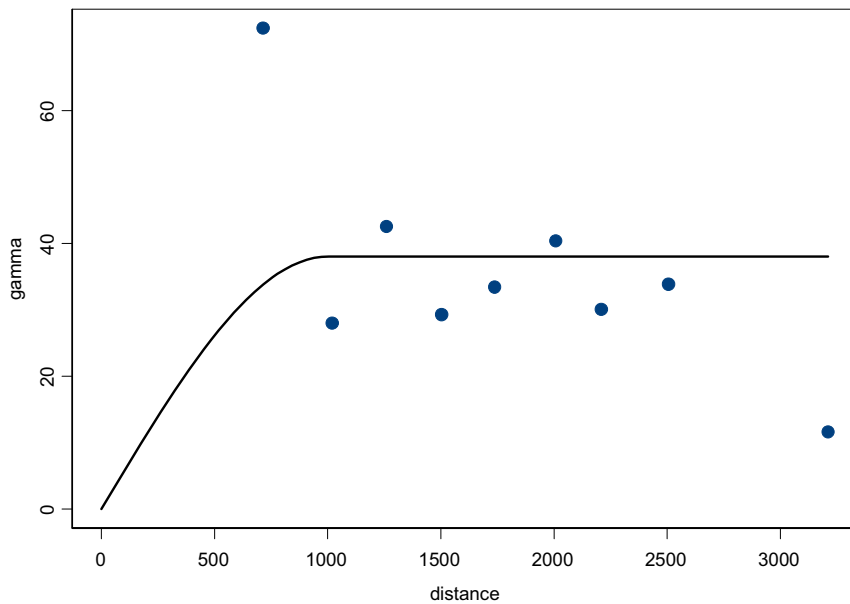


Figure F-3. Empirical variogram for mean porosity from the B-C interbed with spherical model (range = 1,000 ft, sill = 38, and nugget = 0).

Table F-2. Prediction grids.

Grid	East-West		North-South	
	Interval (ft)	Number	Interval (ft)	Number
0	1,000	17	1,000	13
1	500	14	500	10
2	250	18	250	12
3	125	28	125	14

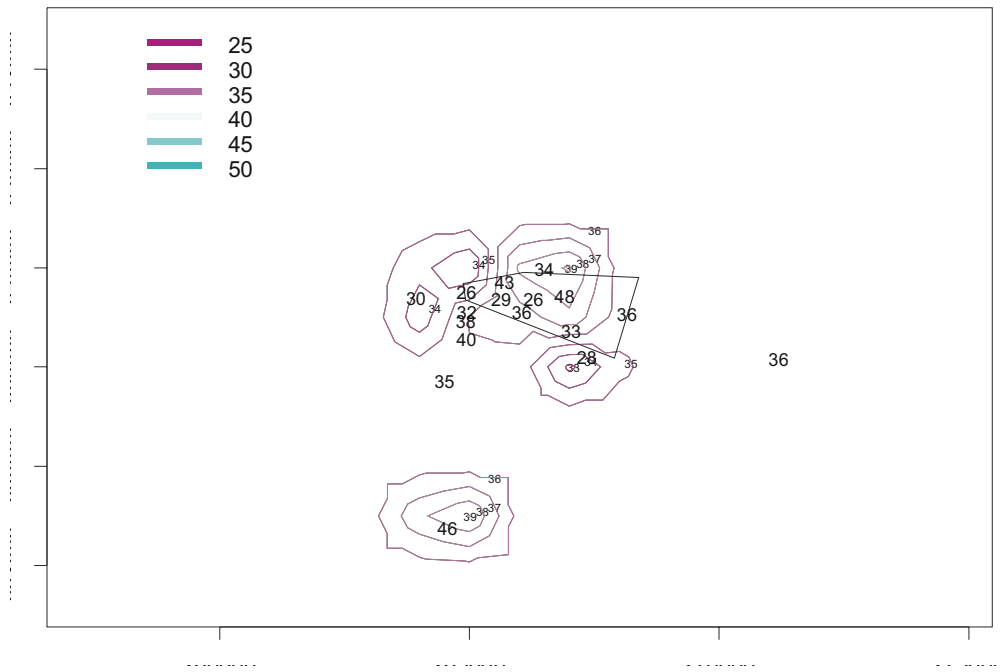


Figure F-4. Ordinary kriging predictions for mean porosity from the B-C interbed for grid 0.

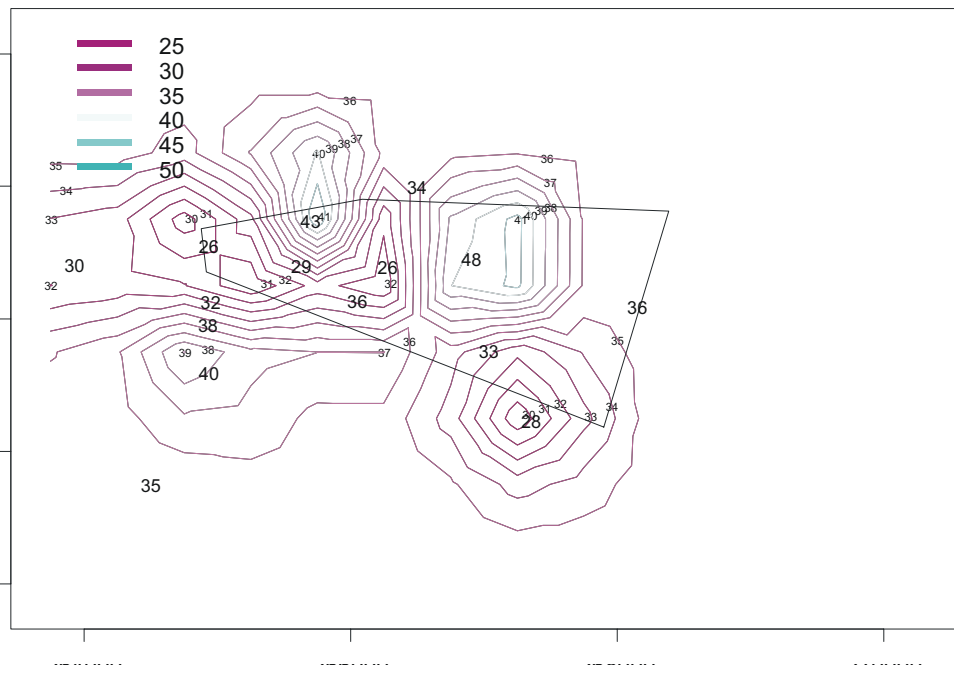


Figure F-5. Ordinary kriging predictions for mean porosity from the B-C interbed for grid 1.

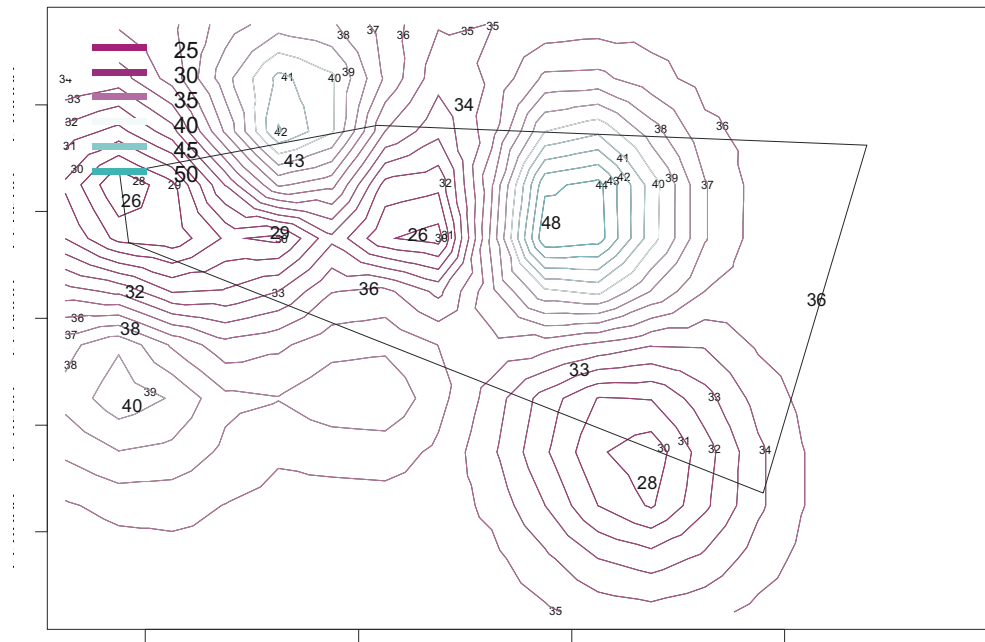


Figure F-6. Ordinary kriging predictions for mean porosity from the B-C interbed for grid 2.

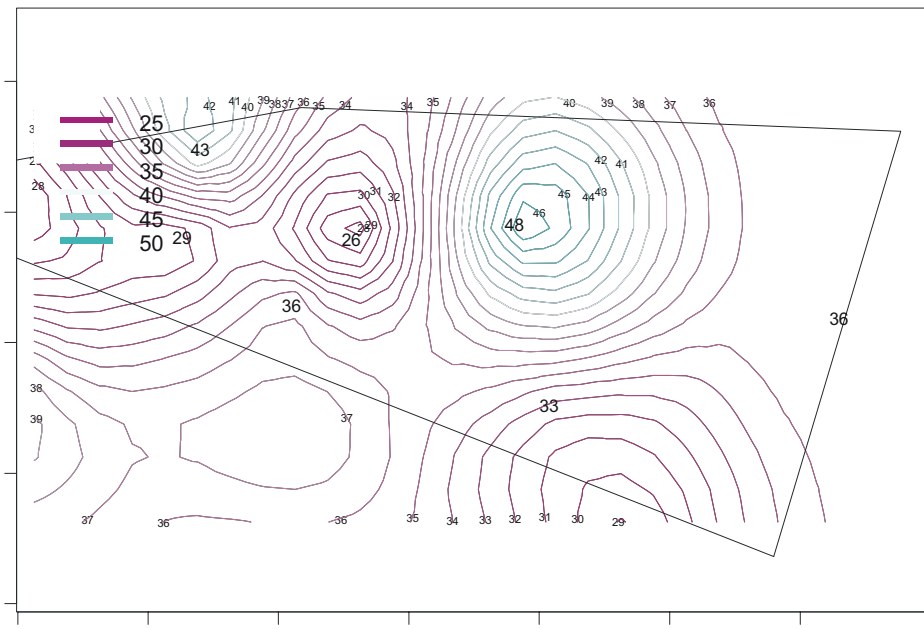


Figure F-7. Ordinary kriging predictions for mean porosity from the B-C interbed for grid 3.

REFERENCES

Leecaster, Molly K., 2002, *Geostatistic Modeling of Subsurface Characteristics in the Radioactive Waste Management Complex Region, Operable Unit 7-13/14*, INEEL/EXT-02-00029, Rev. 0, Idaho National Engineering and Environmental Laboratory.

Appendix G

Complete Carbon Tetrachloride Vapor-Phase Model Calibration Results

Appendix G

Complete Carbon Tetrachloride Vapor-Phase Model Calibration Results

This appendix contains the complete set of final CCl₄ vapor-phase model calibration results. Figure G-1 contains time-history comparisons of model results to observed data at each vapor port. Figure G-2 contains comparisons of time-averaged vertical profiles at each vapor monitoring well.

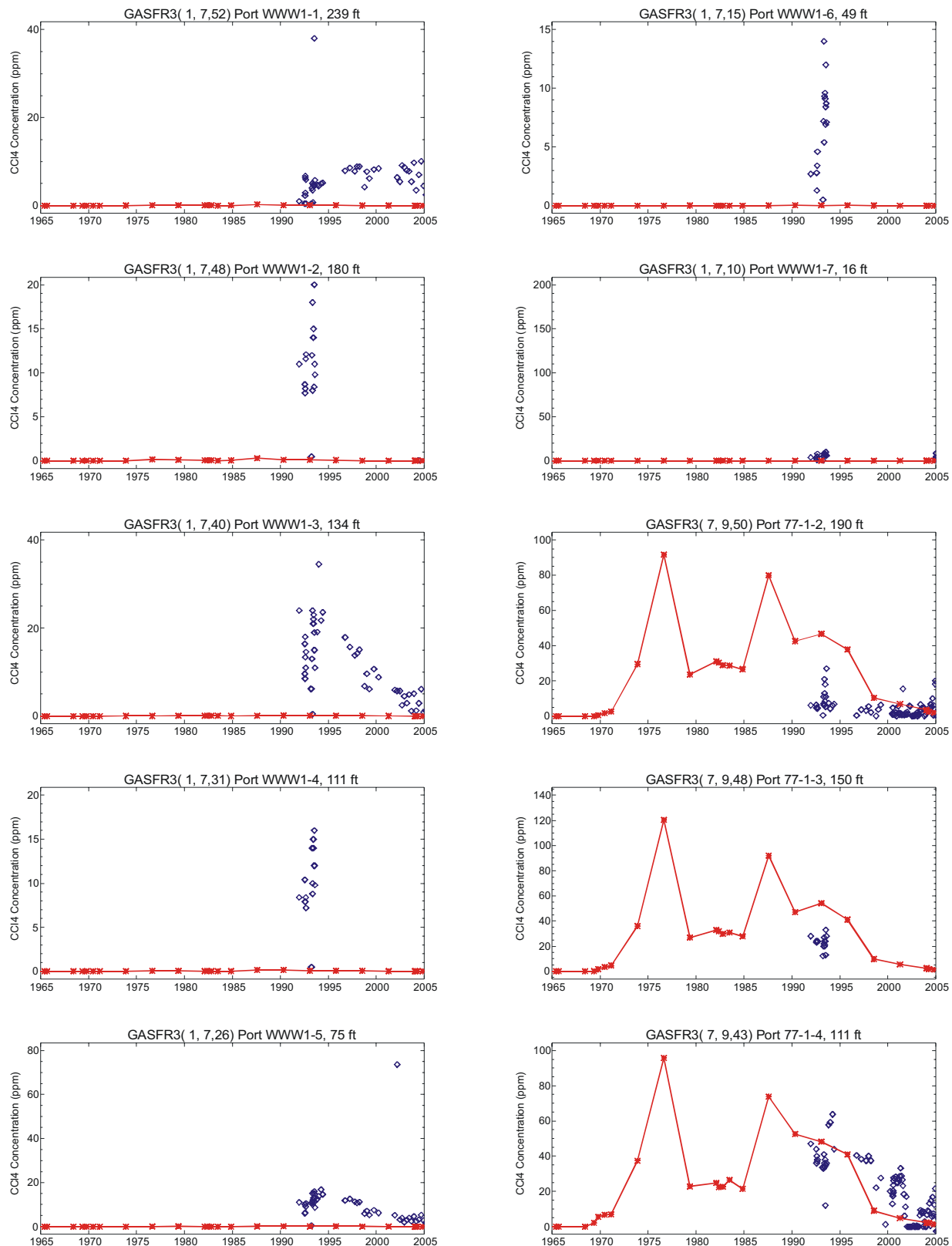


Figure G-1. Comparison of simulated (stars) and measured (diamonds) time histories of carbon tetrachloride vapor concentrations through the year 2005 for each vapor monitoring port. The port name and depth in feet below land surface are indicated above each graph.

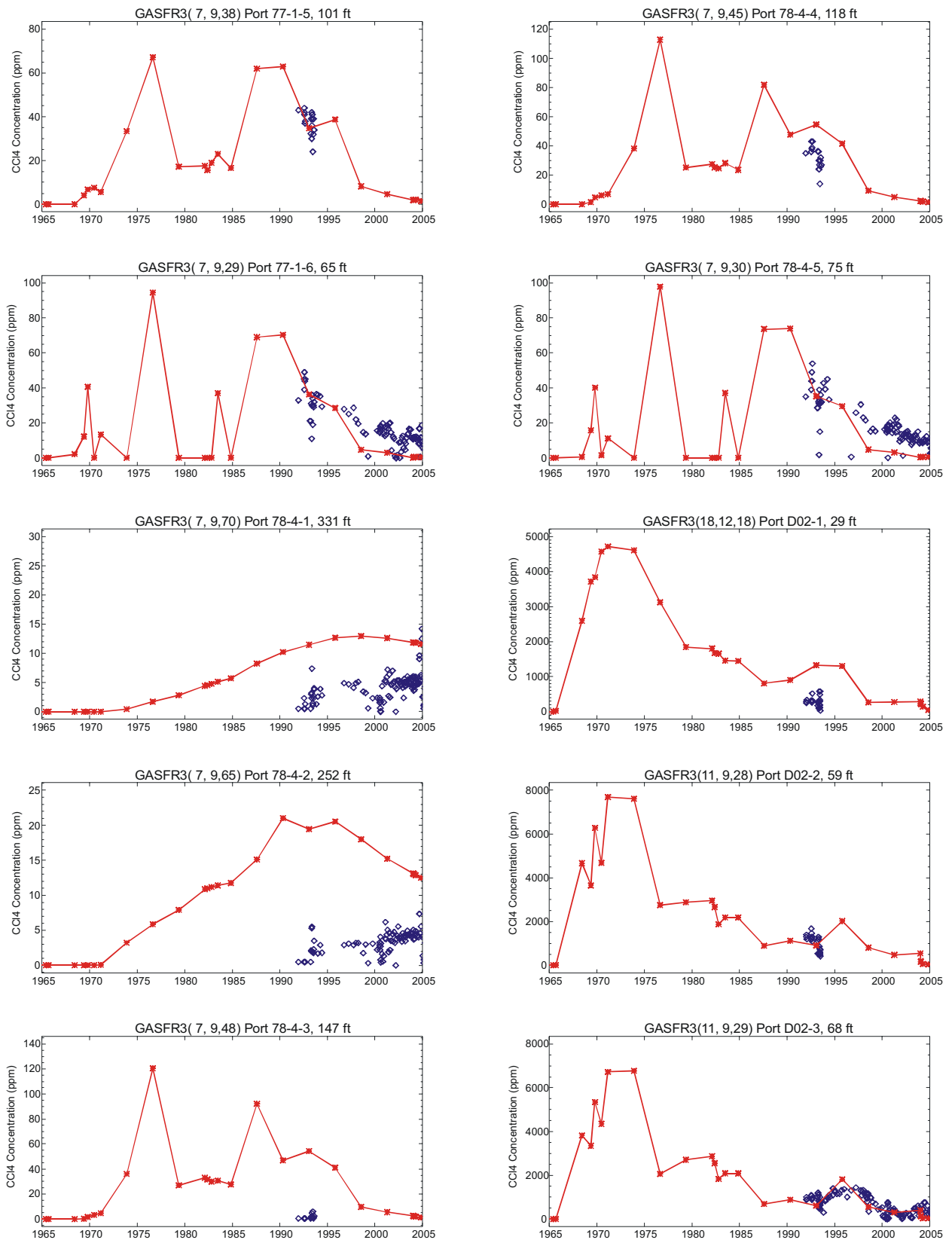


Figure G-1. (continued).

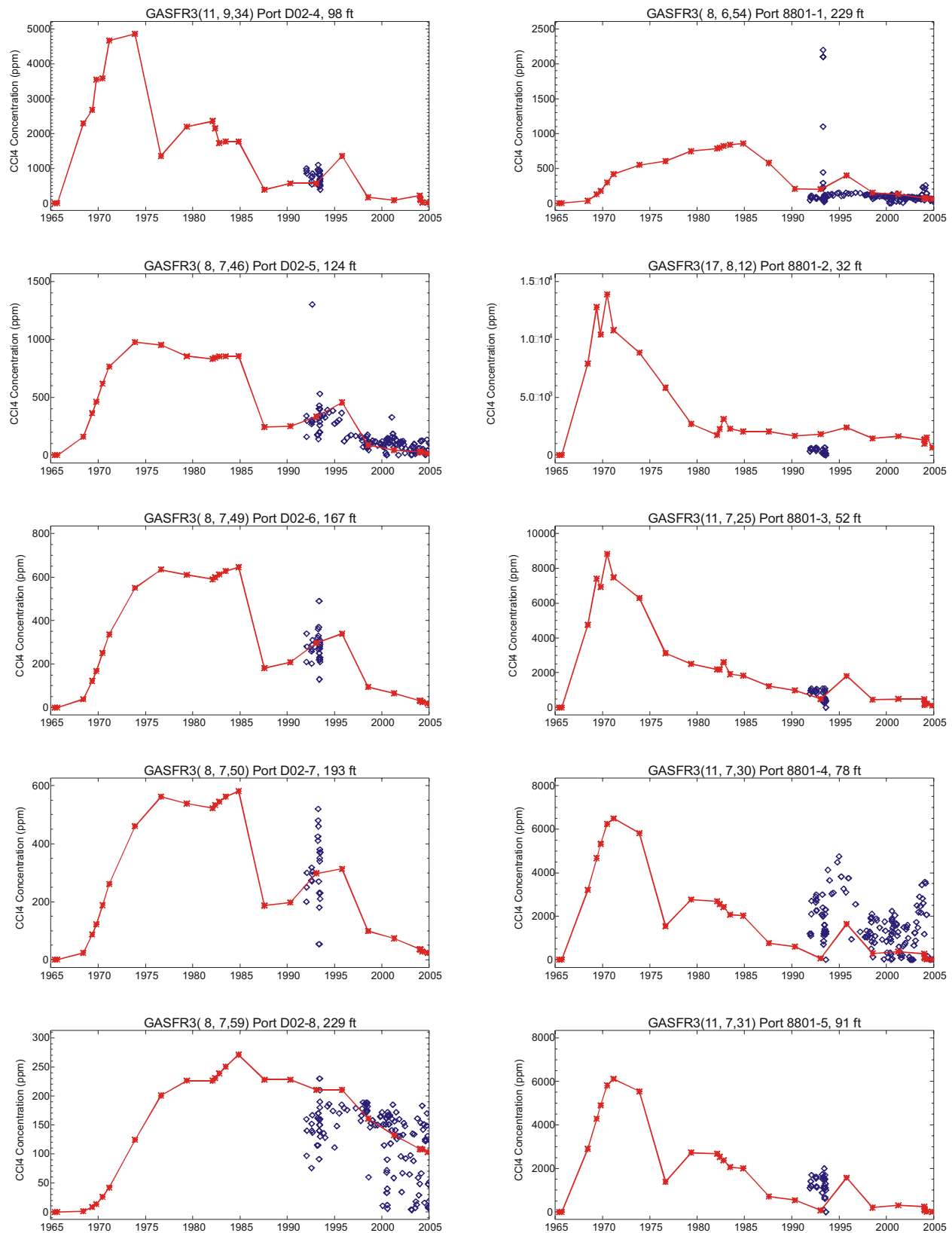


Figure G-1. (continued).

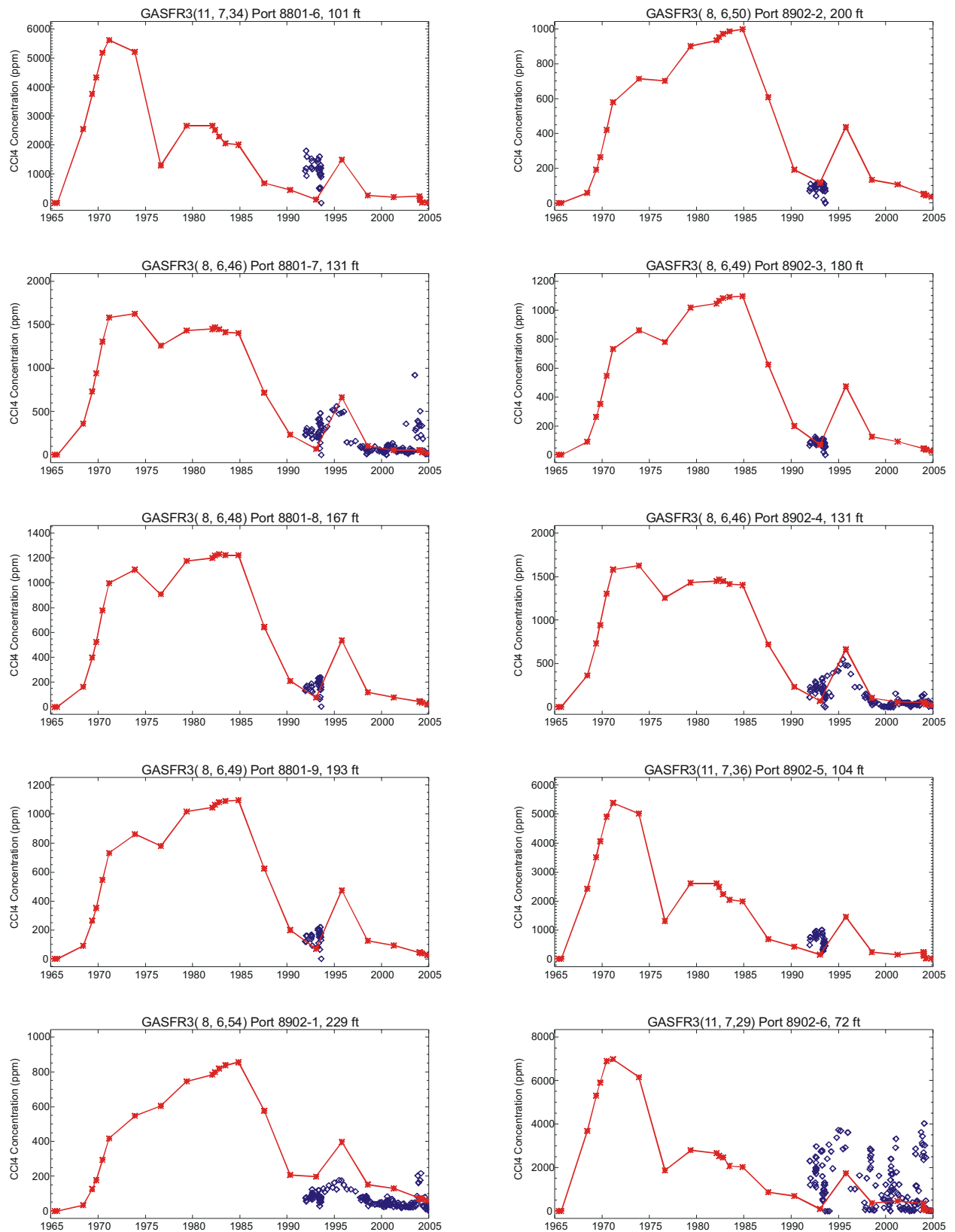


Figure G-1. (continued).

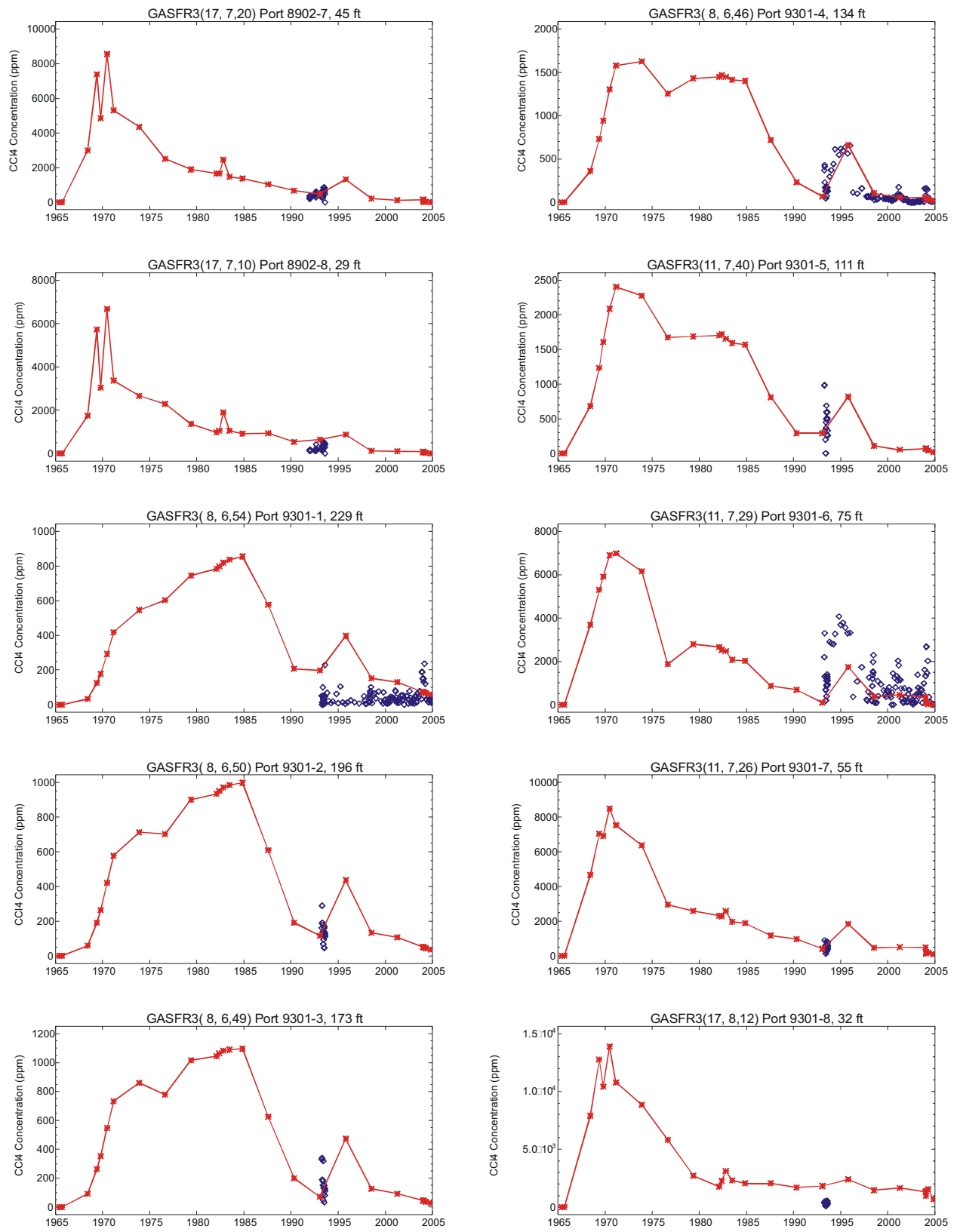


Figure G-1. (continued).

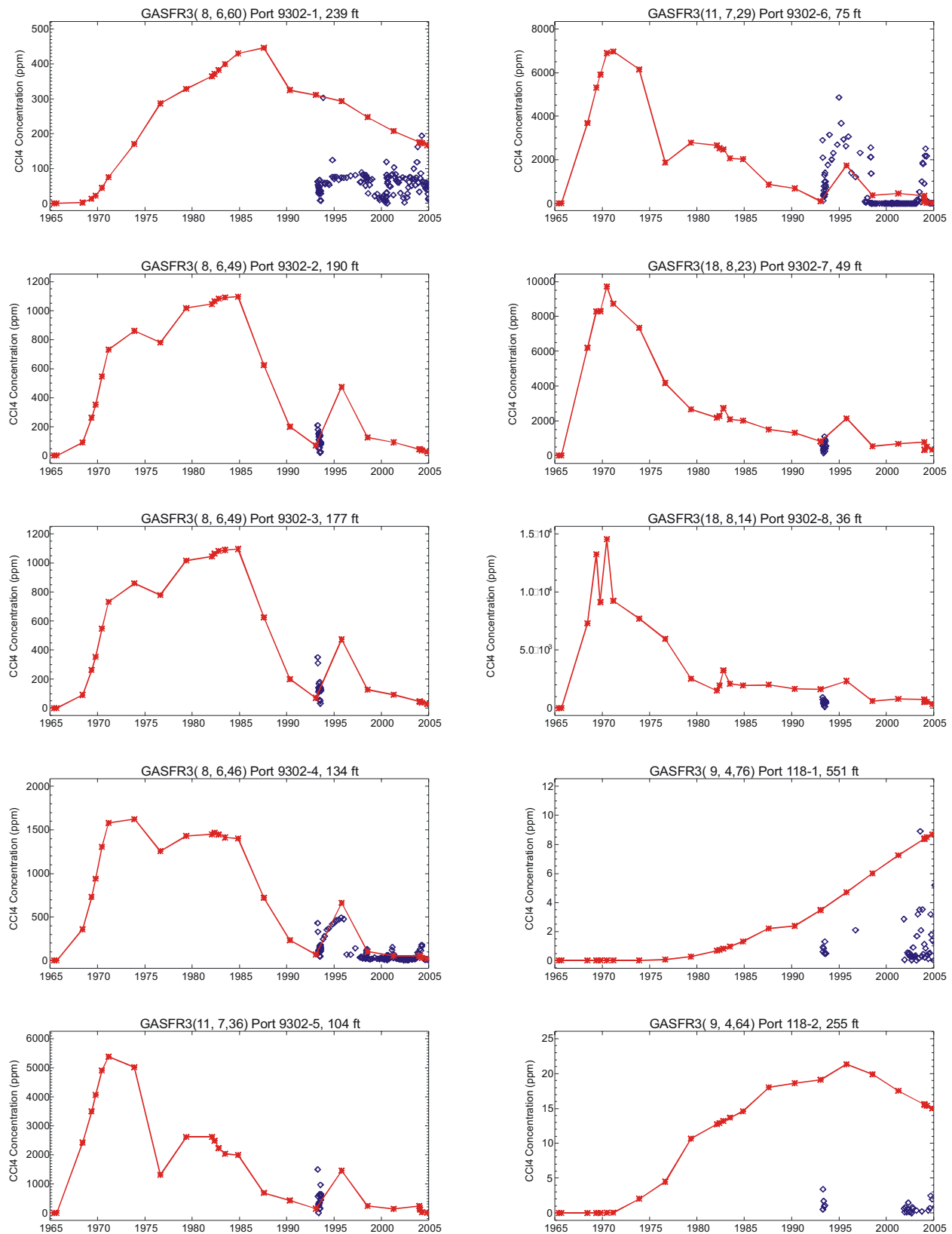


Figure G-1. (continued).

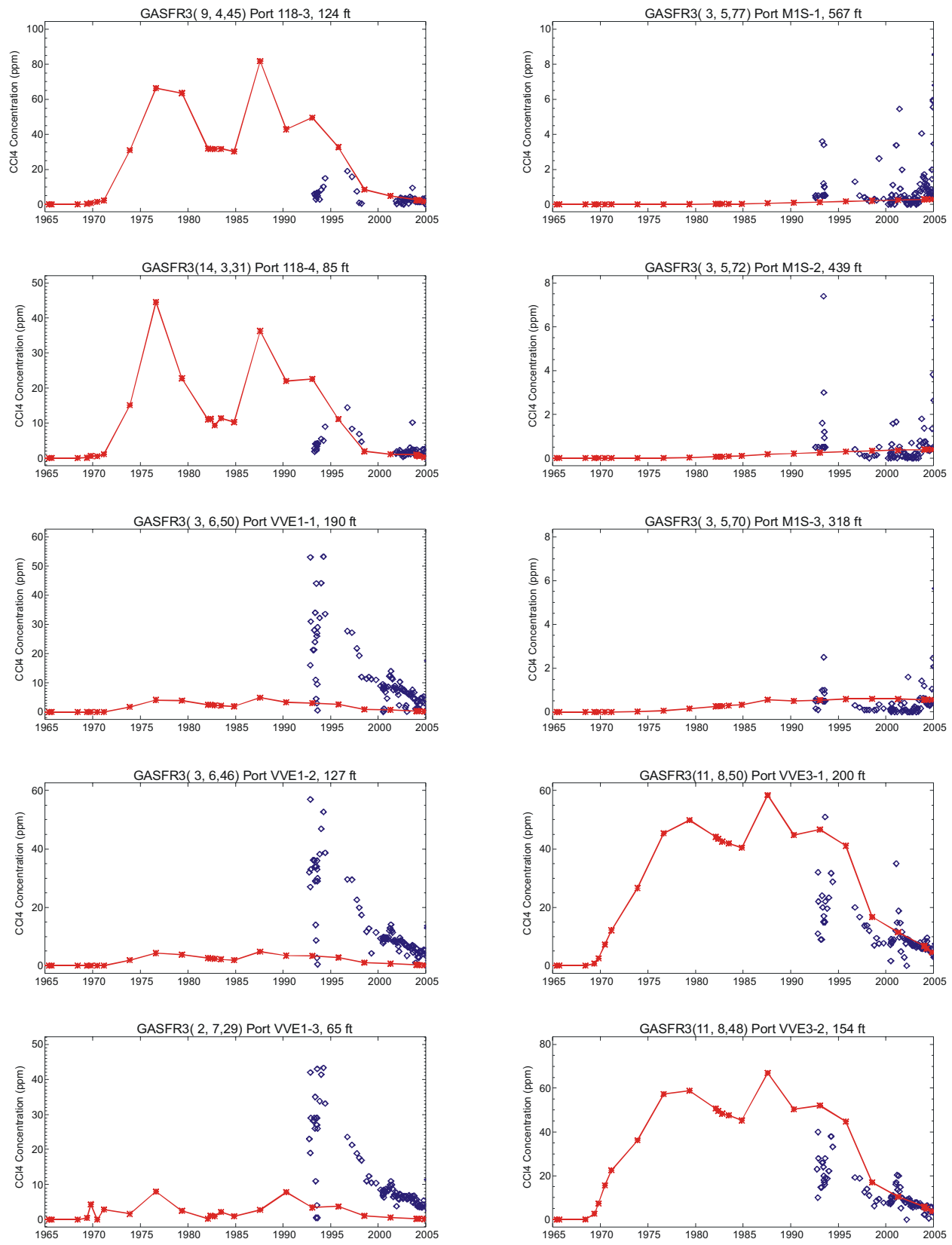


Figure G-1. (continued).

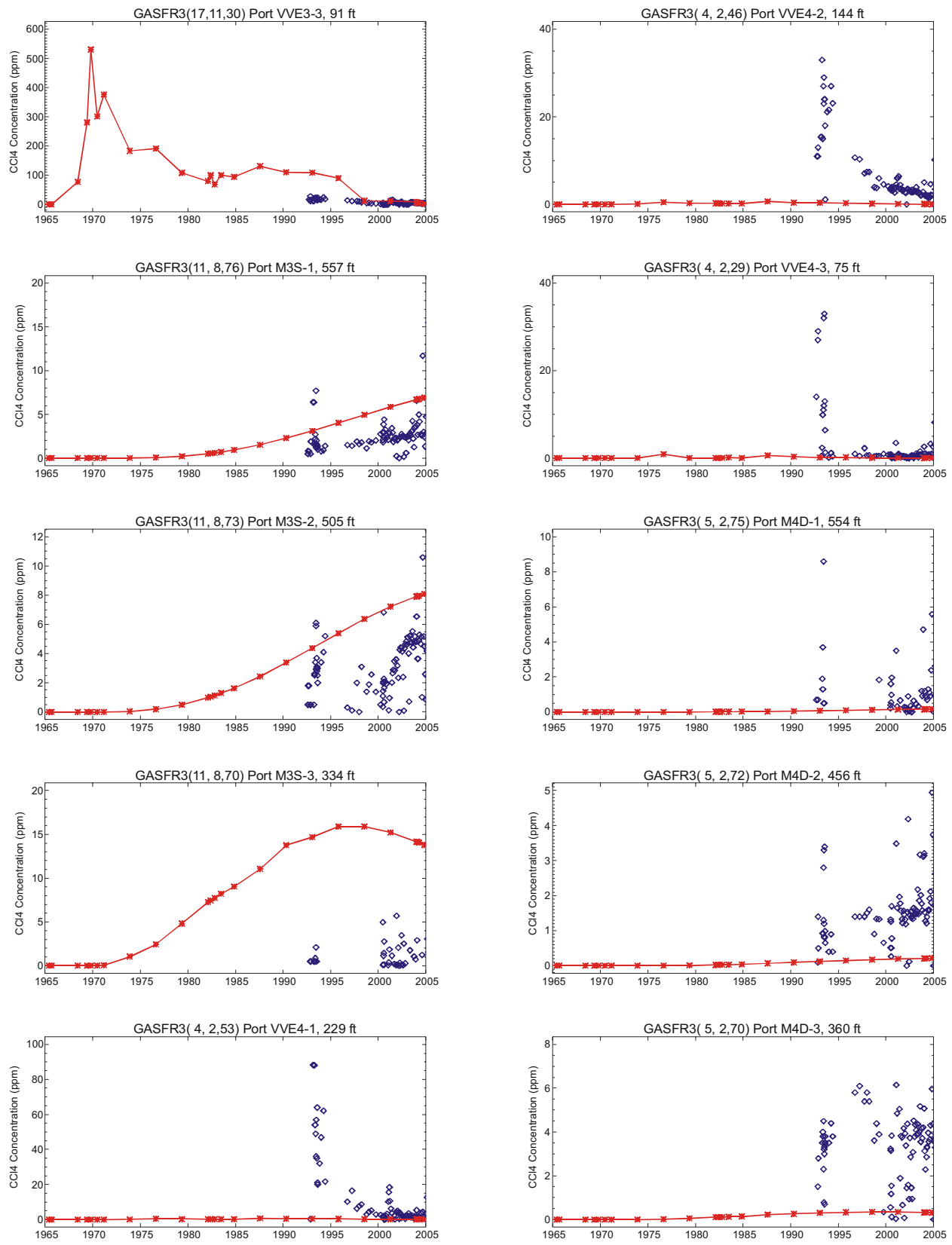


Figure G-1. (continued).

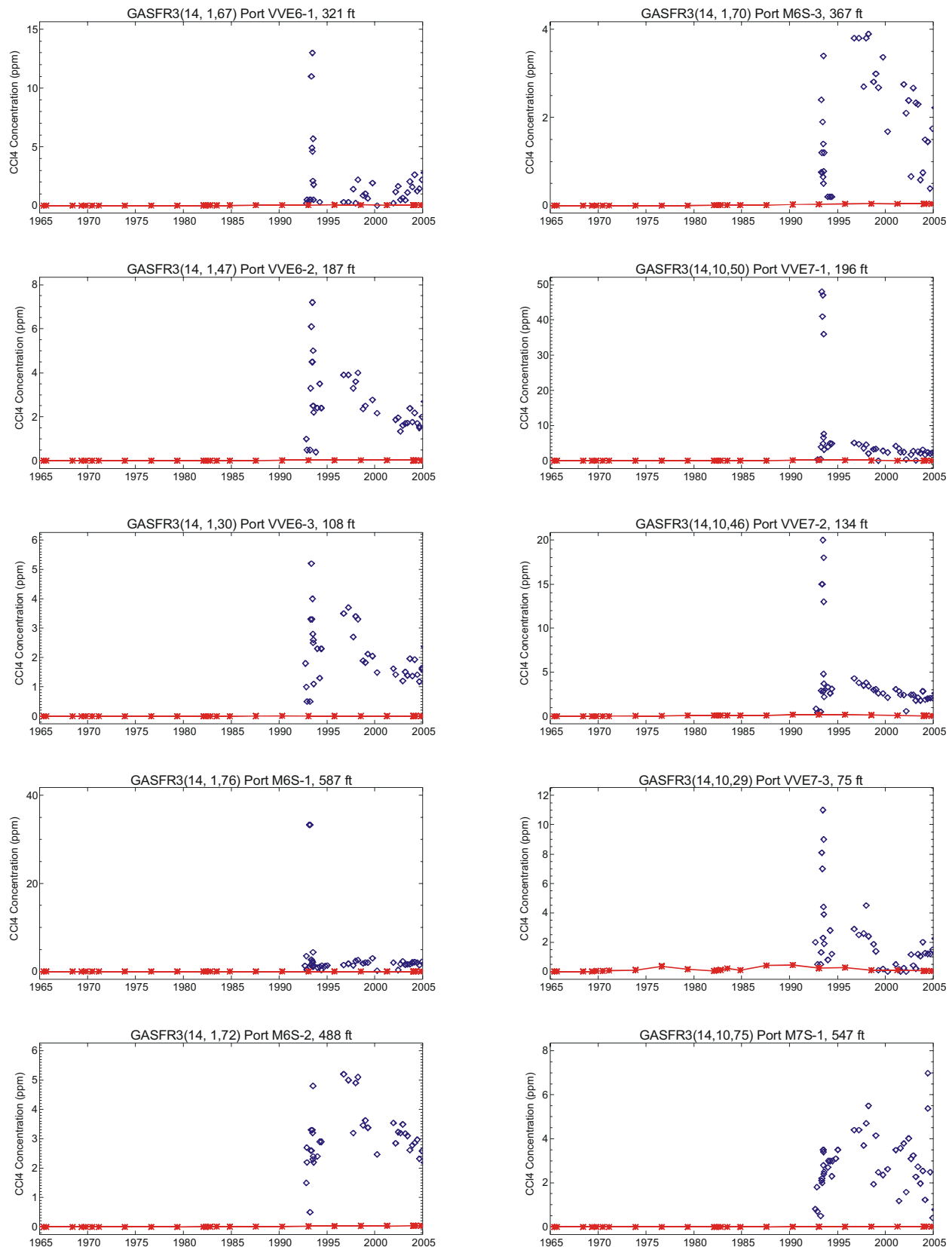


Figure G-1. (continued).

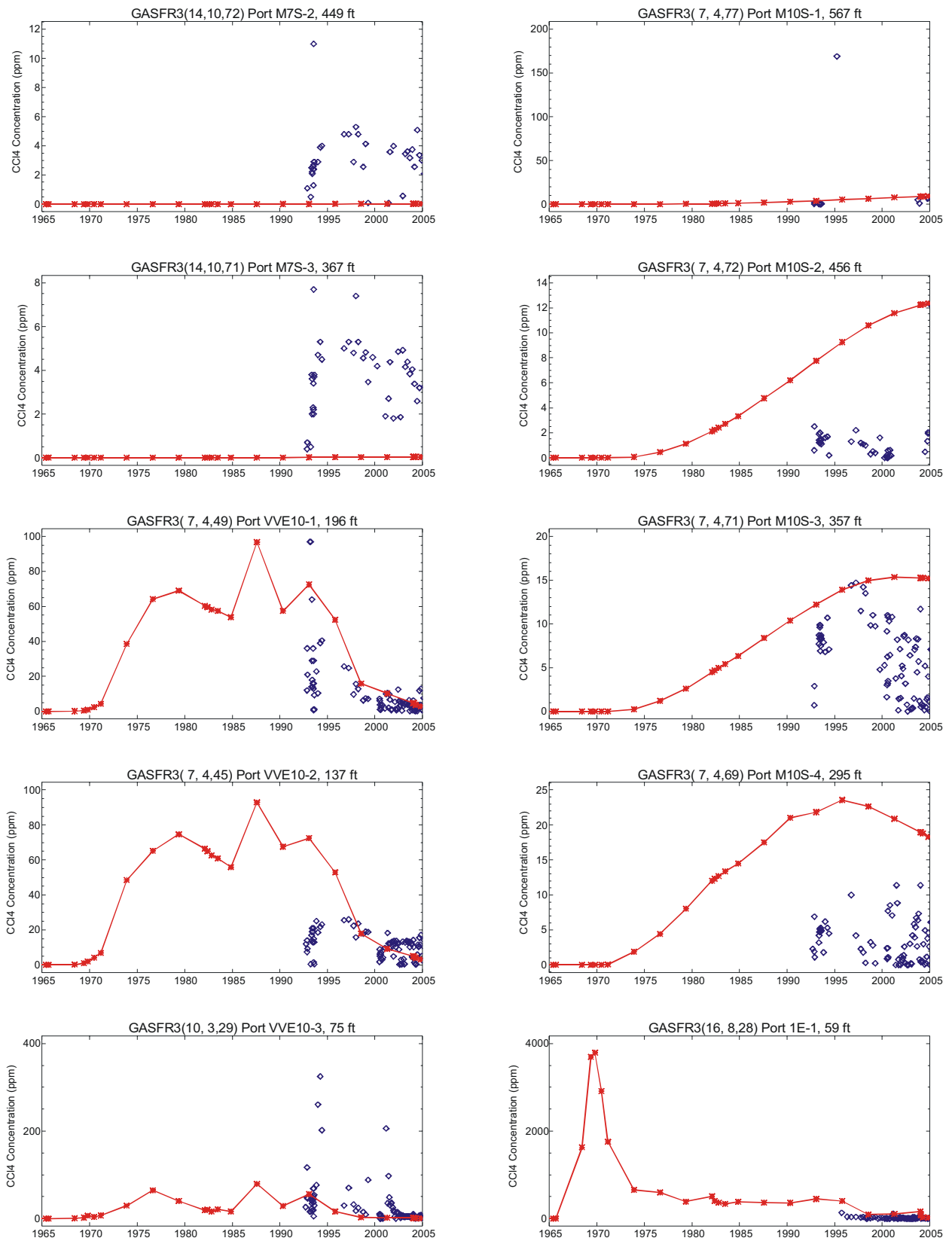


Figure G-1. (continued).

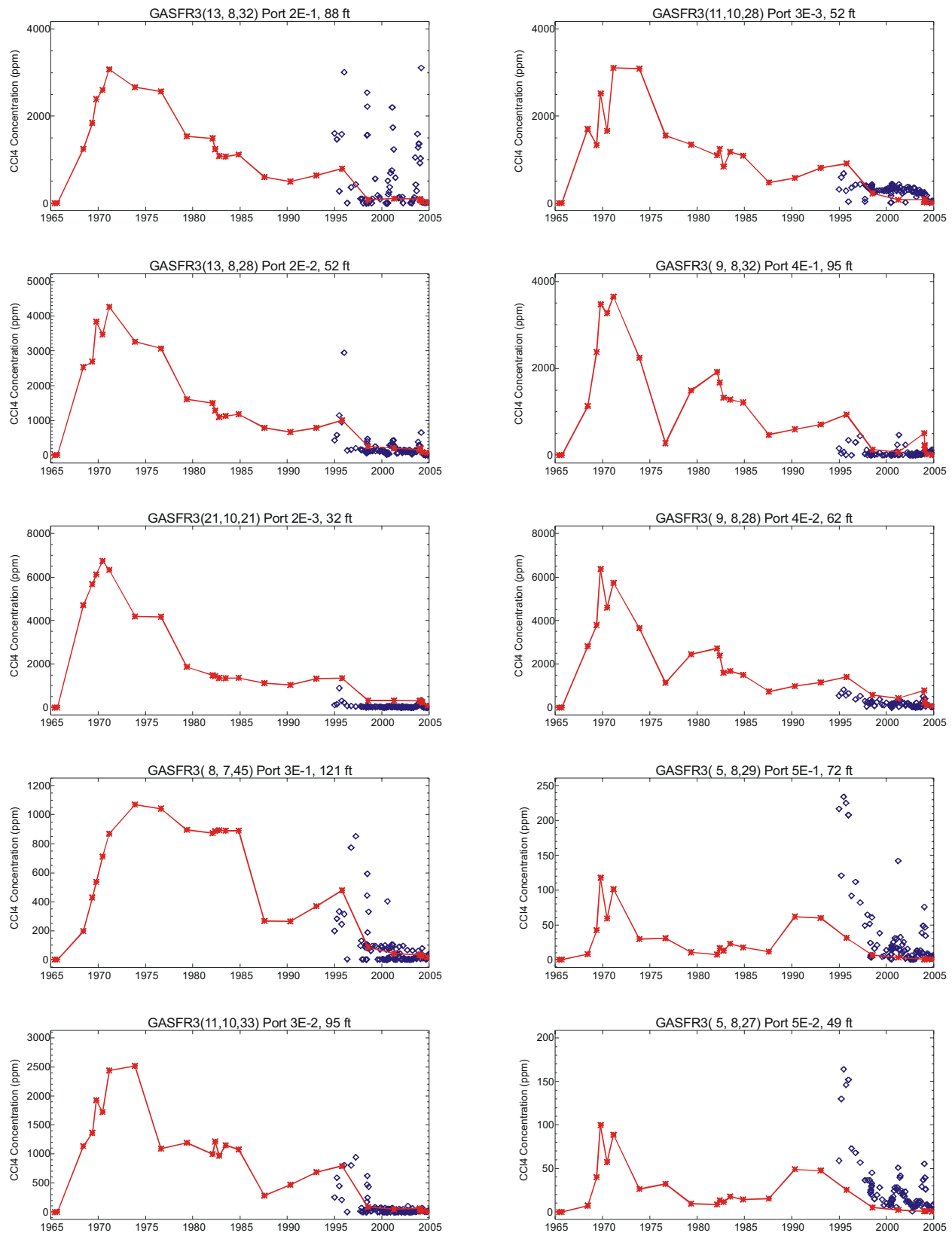


Figure G-1. (continued).

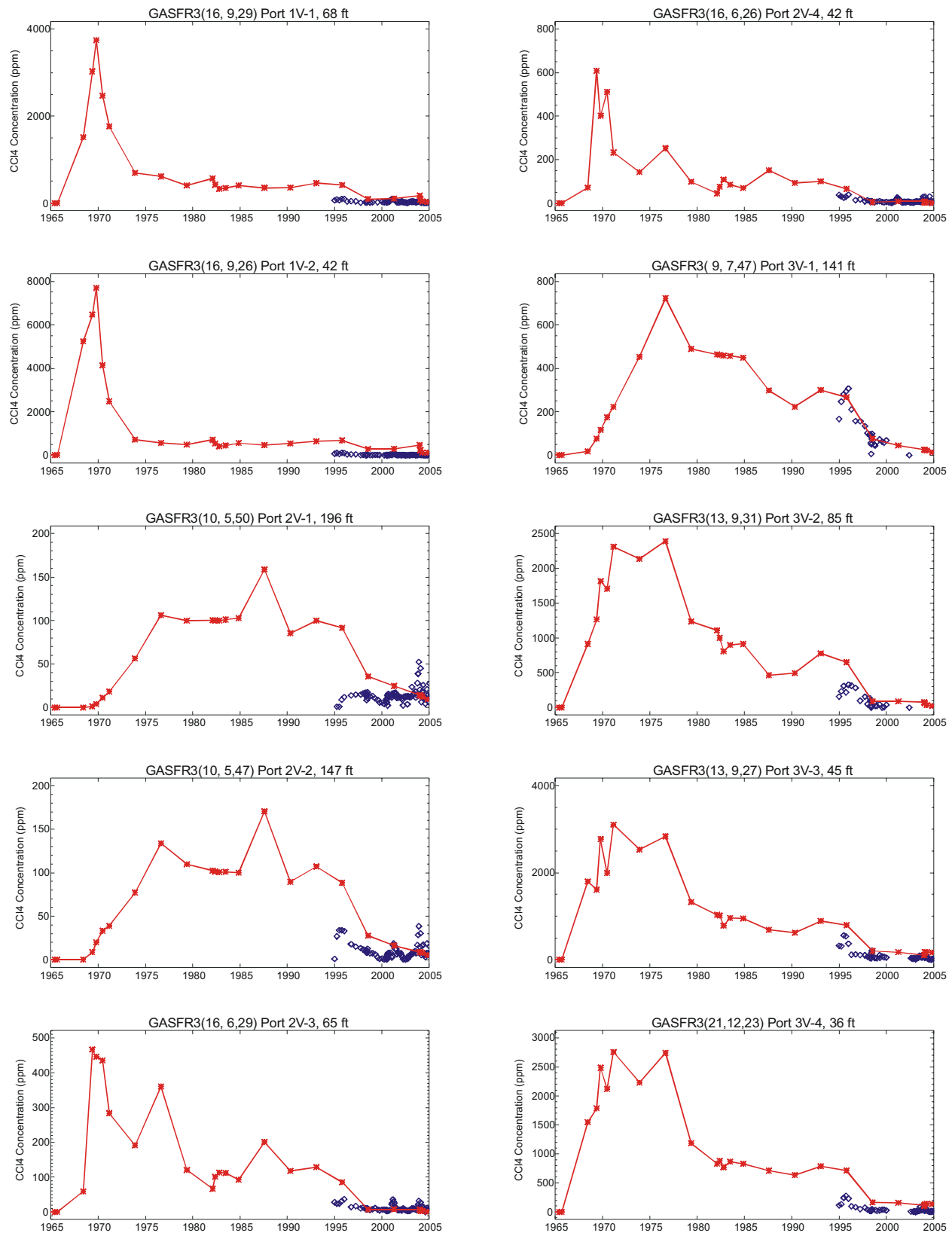


Figure G-1. (continued)

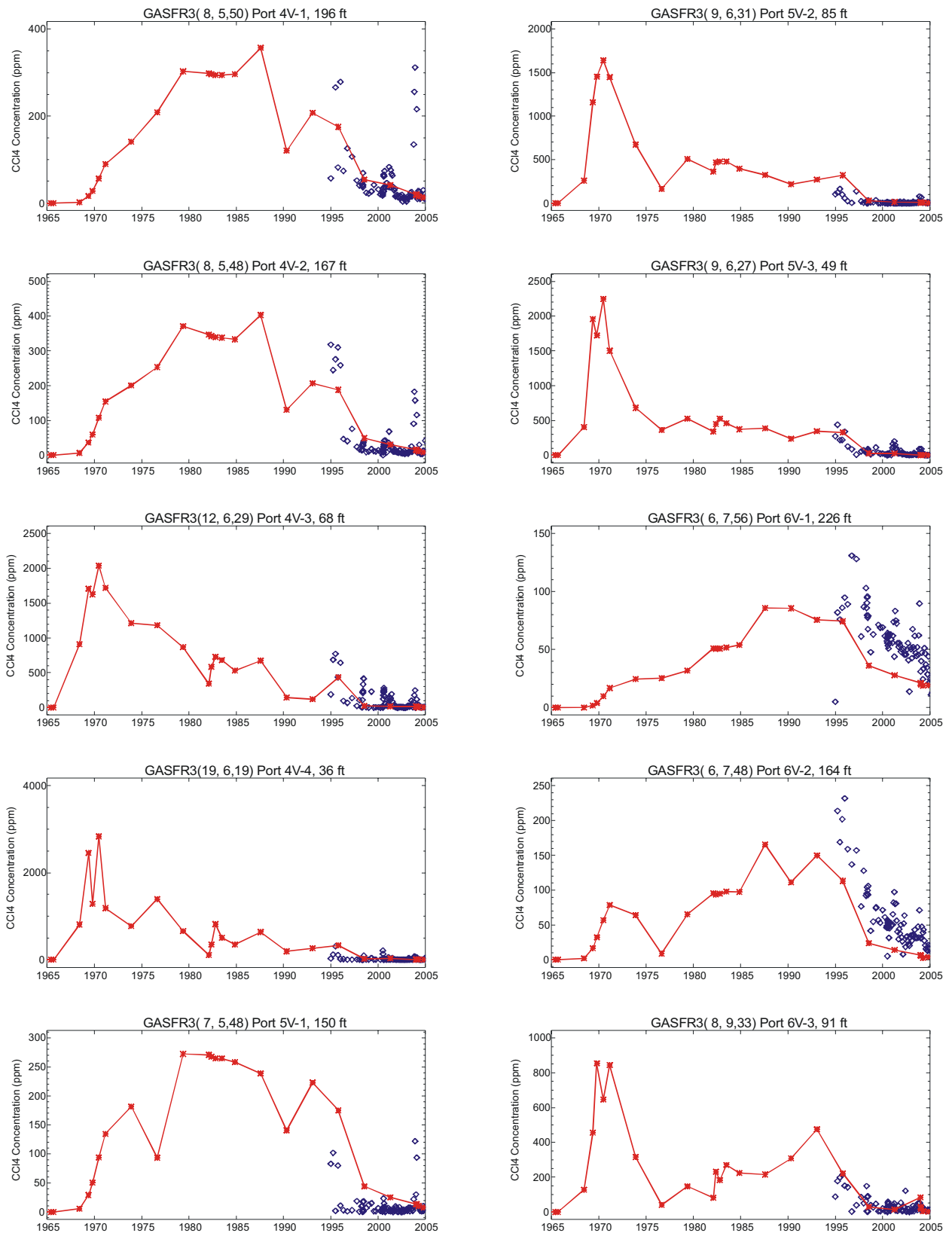


Figure G-1. (continued)

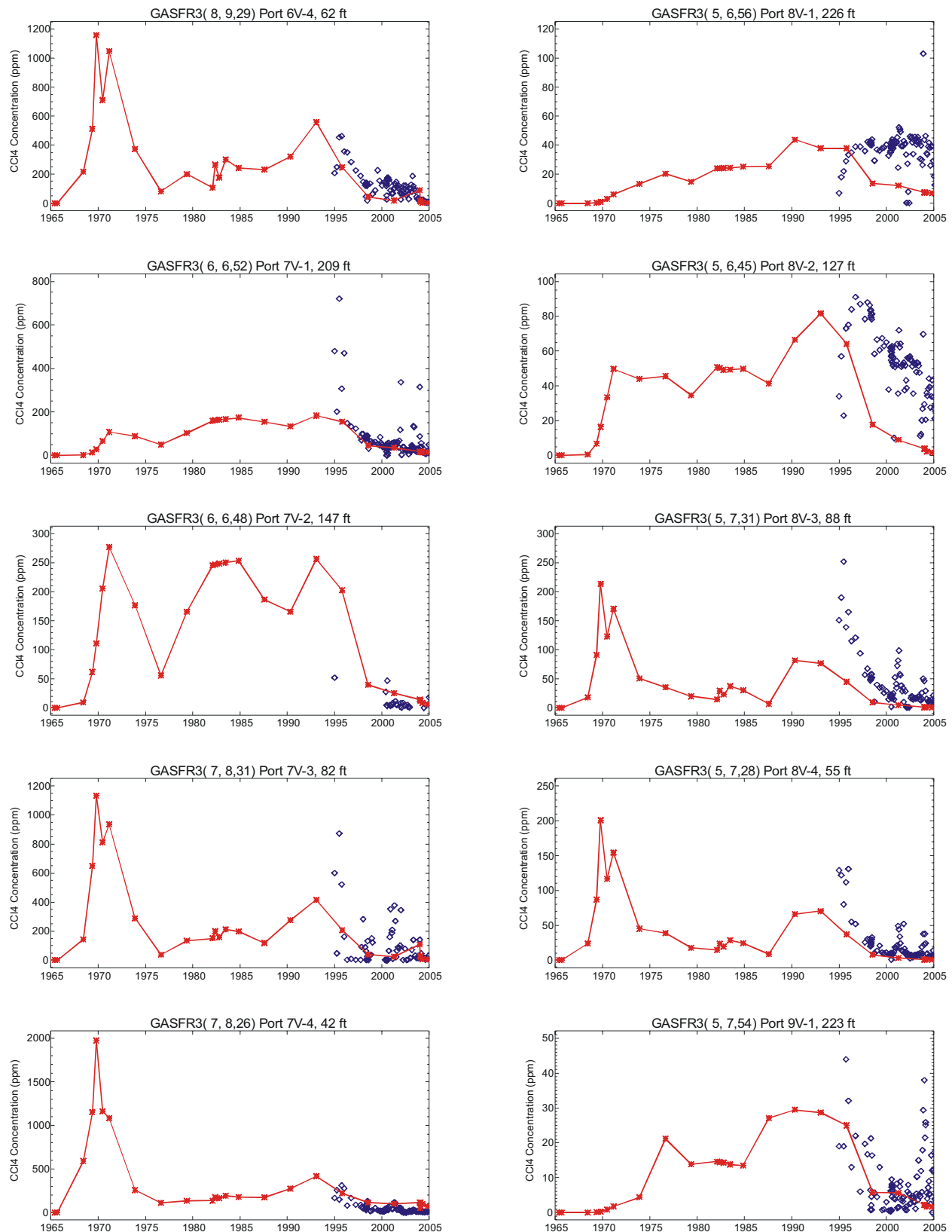


Figure G-1. (continued).

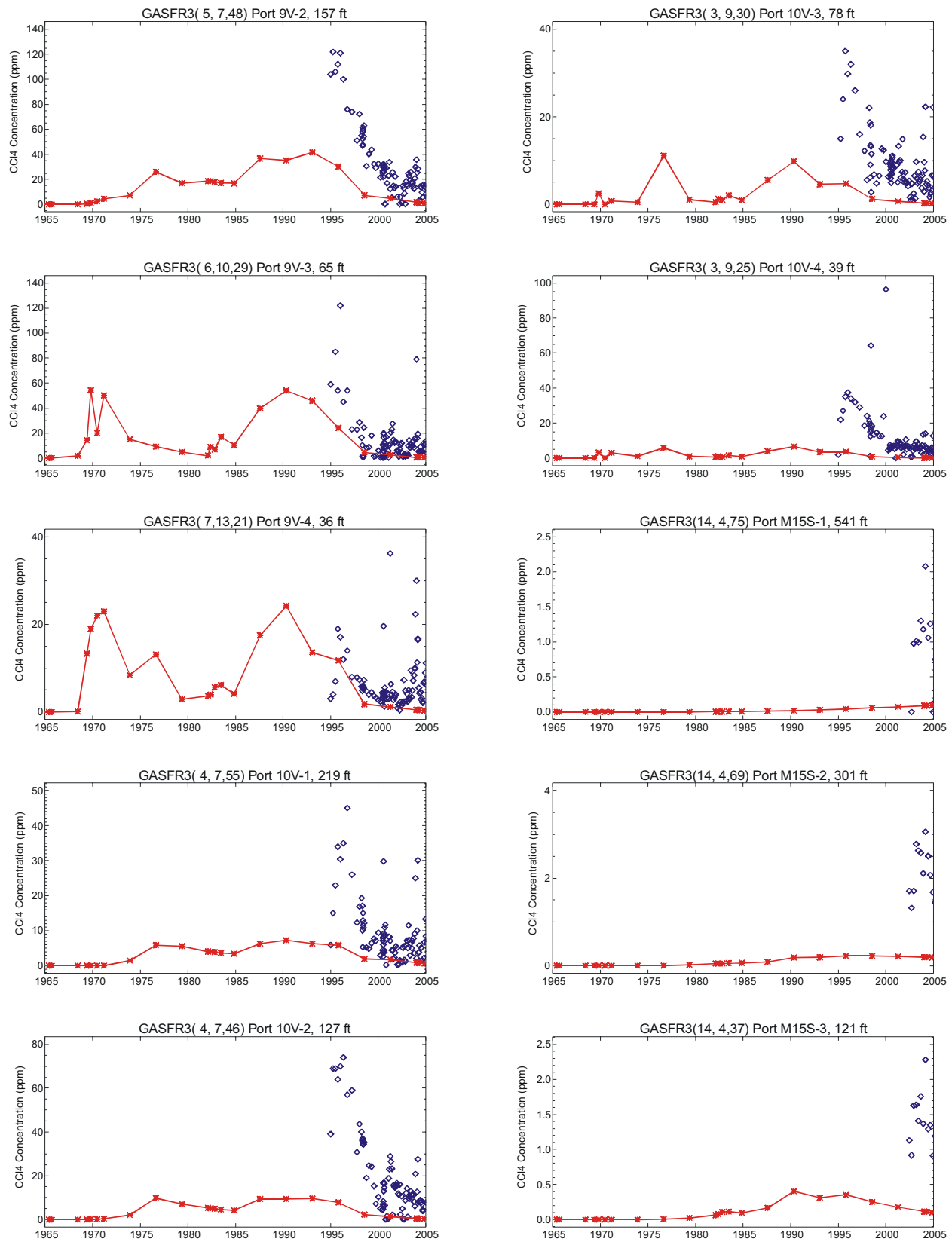
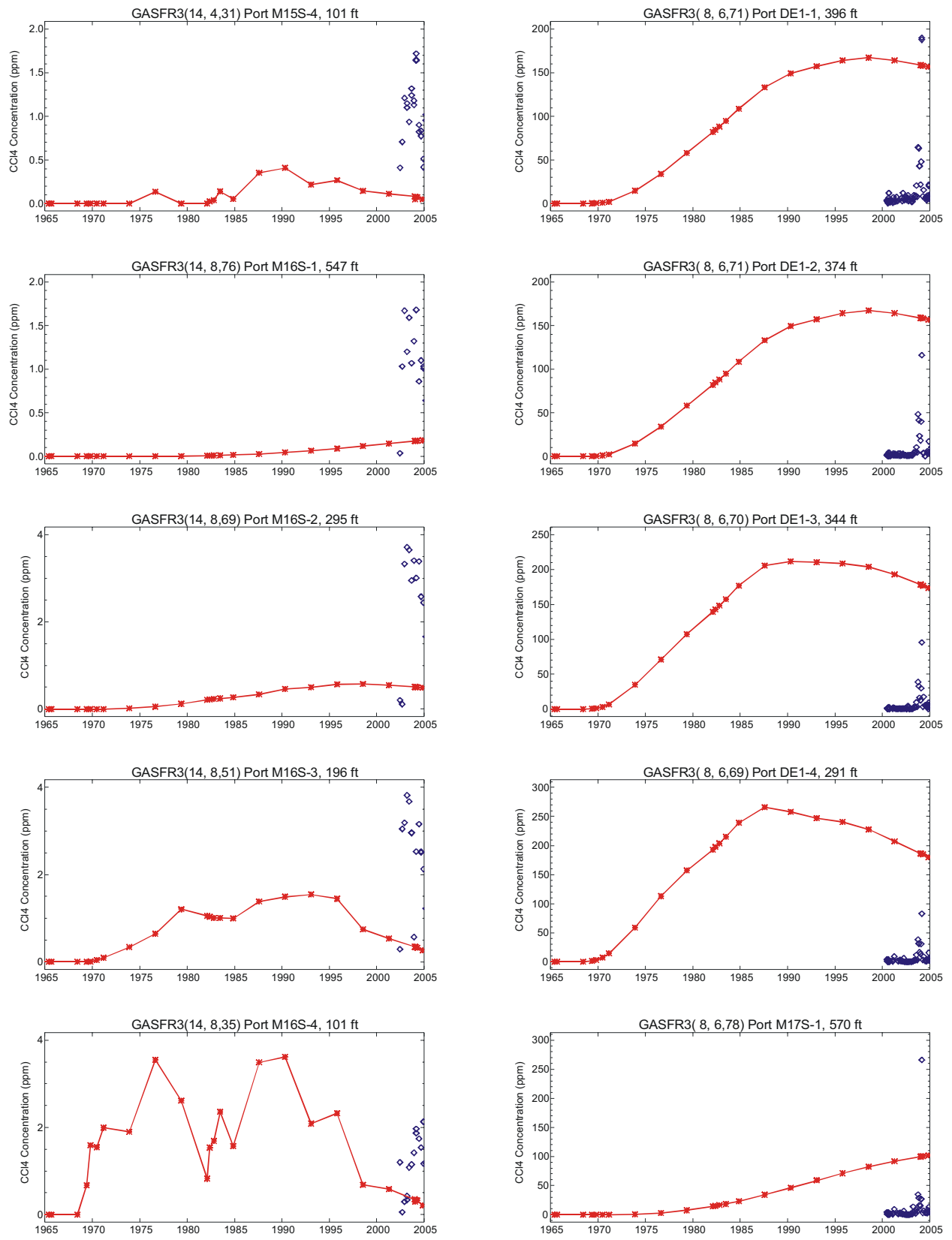


Figure G-1. (continued).



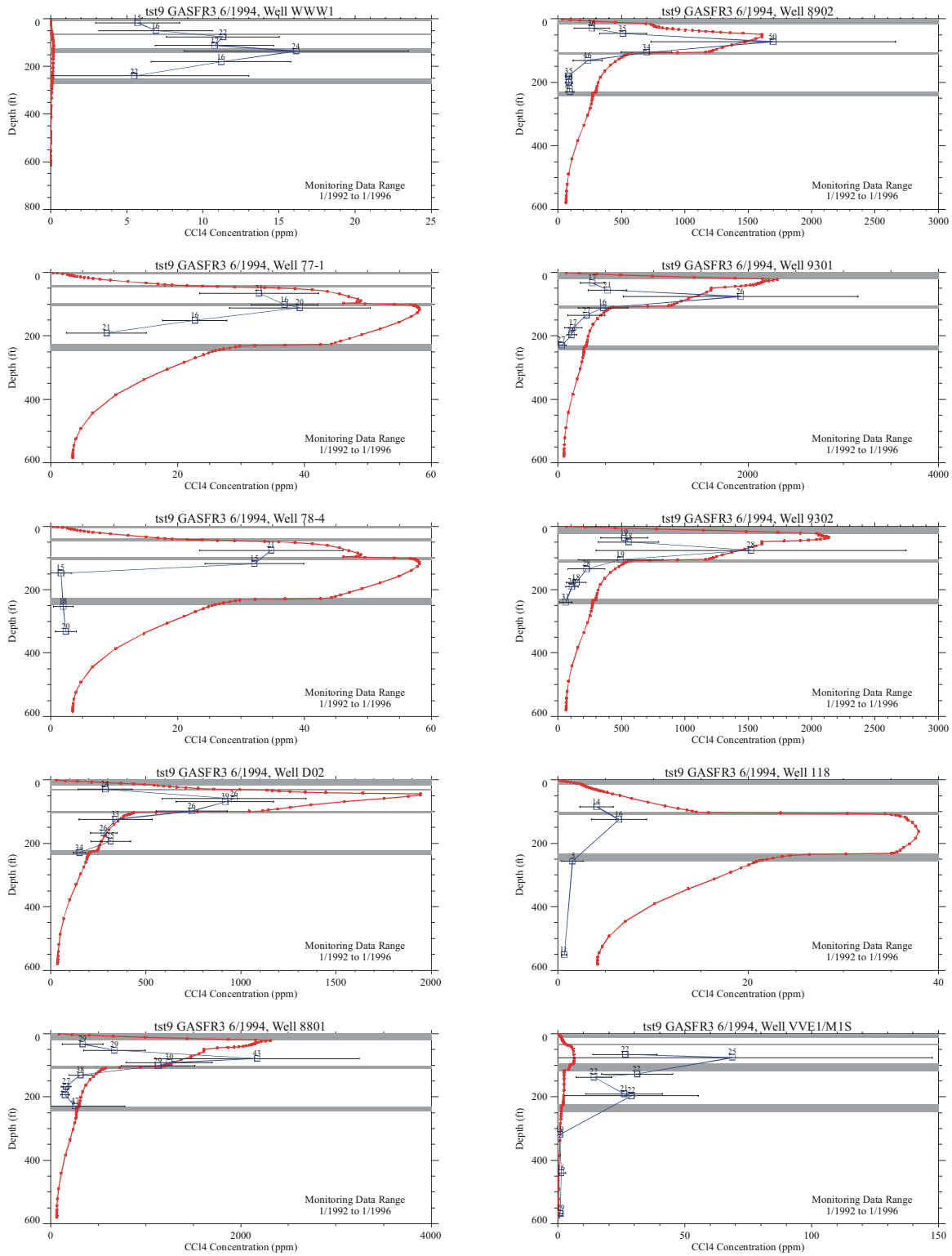


Figure G-2. Comparison of simulated and measured vertical profiles of carbon tetrachloride vapor concentrations at each vapor monitoring well. The well name is indicated above each graph. The simulated data is from June 1994. The measured data was averaged over a 4-year period (i.e., 1992 to 1996). The number above each measured data point is the number of data points used to calculate the average.

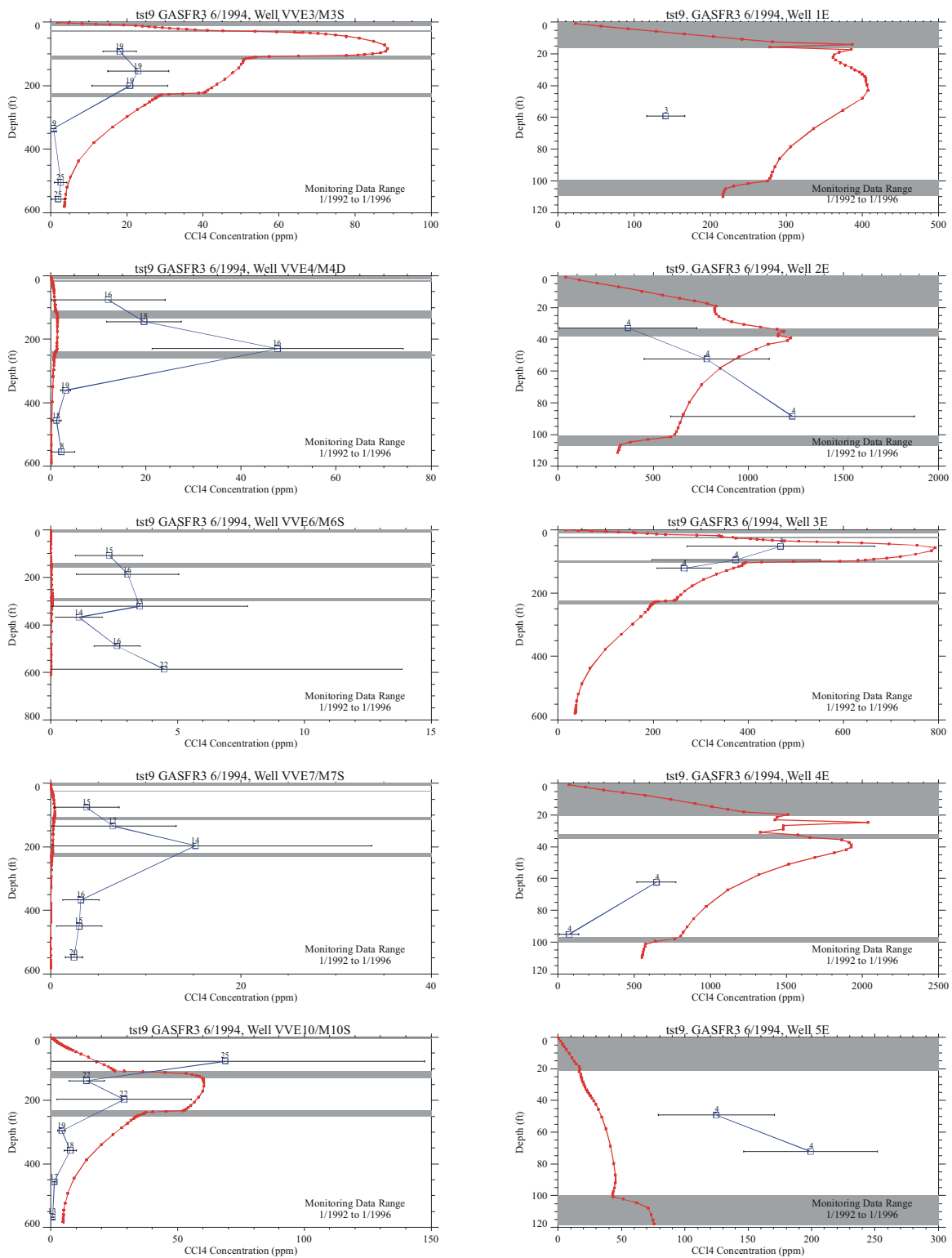


Figure G-2. (continued).

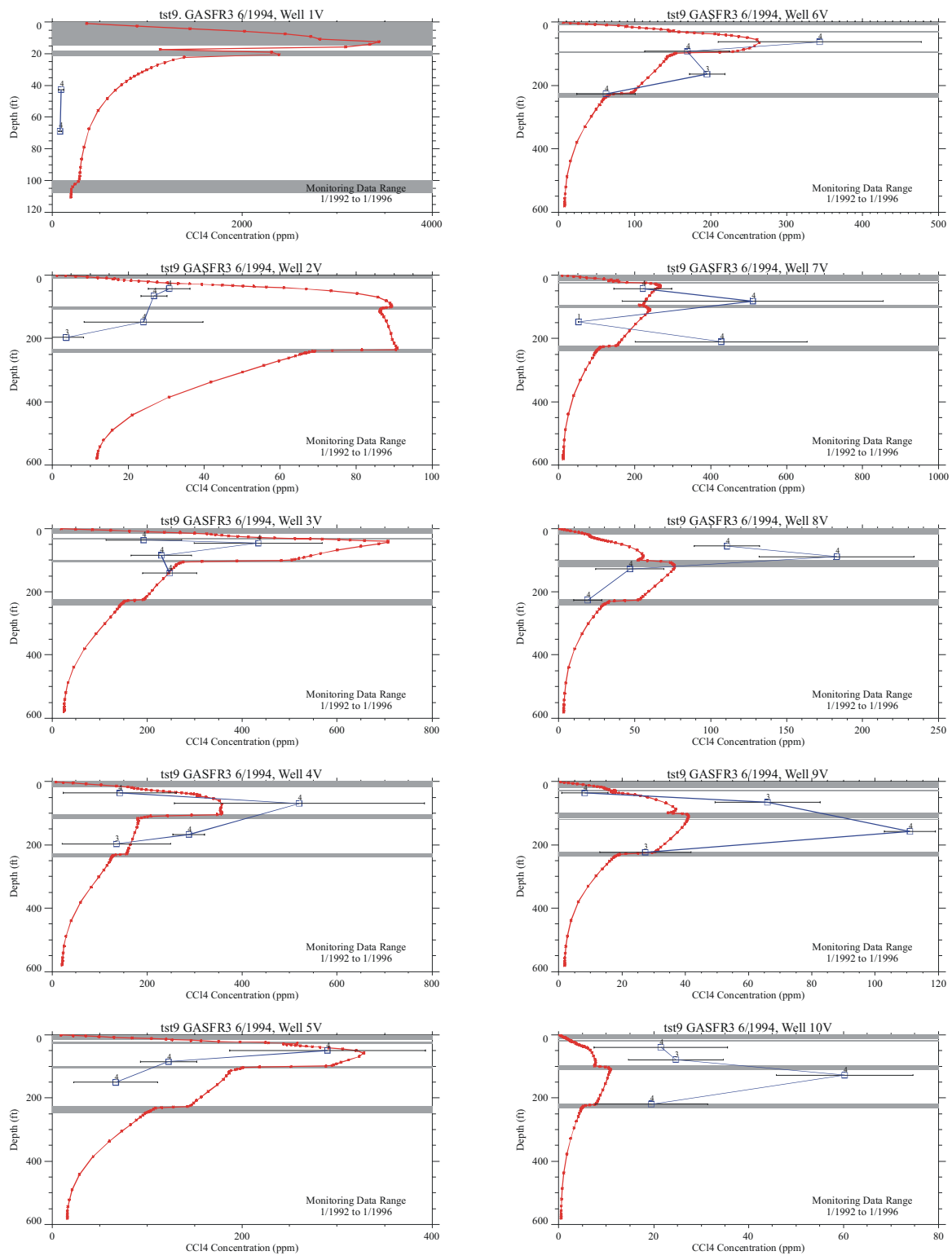


Figure G-2. (continued).

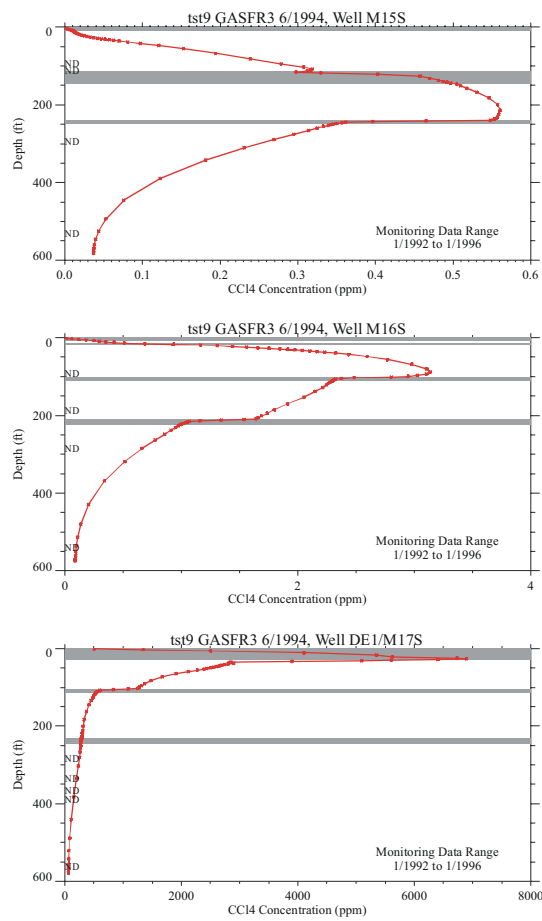


Figure G-2. (continued).

